UNIVERSITY OF CALIFORNIA
RIVERSIDE

# Astrocytic Ephrin-B1 Controls PV Synapse Formation Through Regulating EphB2 in PV Boutons

A Dissertation submitted in partial satisfaction
of the requirements for the degree of

Doctor of Philosophy

in

Biomedical Science

by

Samantha Nicole Sutley

March 2024

Dissertation Committee:
Dr. Iryna M. Ethell, Chairperson
Dr. Peter W. Hickmott
Dr. Vijayalakshmi Santhakumar

The Dissertation of Samantha Nicole Sutley is approved:

_____

_____

_____

Committee Chairperson

University of California, Riverside

ACKNOWLEDGEMENTS

First and foremost, I would like to acknowledge my mentor, Dr. Iryna Ethell. I consider myself to be very lucky to have been trained by such a brilliant, enthusiastic, and passionate scientist as yourself. I would like to thank you for your constant support and guidance, for giving me the freedom to pursue my passions and interests, and for all of the time and energy that you invested in my training. Thank you for believing in me, encouraging me, and pushing me to be the best I can be. Lastly, thank you for being a role model to me and such an excellent example of what it means to be a good mentor.

I would also like to thank my committee members Dr. Peter Hickmott and Dr. Viji Santhakumar. Thank you both for all the helpful discussions about my project and for all of the technical support when I was learning the whole cell recordings. I really could not have done the electrophysiology without both of your help! I would like to say a special thanks to Dr. Hickmott who trained me to blind-patch. Thank you for your guidance and especially for your patience and encouragement during my training. I would also like to thank the Hickmott and Santhakumar lab members Sarah Maples, Laura Dovek, and Andrew Huang for their technical support.

I would like to thank everyone in the Ethell lab for all of the support. I would like to say a special thanks to Dr. Anna Kulinich. Thank you for always being there for me. I have learned so much about science and life in general from you. Thank you for always being willing to help me out, listen to me vent, and for always being so supportive and encouraging. Thank you to Tori Wagner for all of our fun philosophical discussions and for making the last couple of years of my PhD so fun! I would also like to thank all of the

rotating PhD students, medical students, and undergraduate students who assisted with my projects.

I am also endlessly grateful to my family including my parents, sister, aunt Pam and Uncle Steeve, and to my parents in-law and my new brothers! First, thank you to my parents for supporting me through this (very long) educational journey. Thank you for all of the sacrifices you both made to make this possible for me. Thank you to my Dad, from whom I inherited my logical way of thinking, my curiosity, and my passion for science. Thank you to my Mom, from whom I inherited my ability to find creative solutions to my problems. You would be surprised how many times my inherited ability to MacGyver something came in handy when I had to fix my Ephys rig. Thank you to my sister, Tabitha, for your friendship and for supporting me and encouraging me through all of this. Your silly jokes and our Fortnite dates really kept me going when times were tough. I genuinely could not have done this without you.

Thank you to all the friends I made during this time who became family, especially Jeff, Stefanie, Aman, Rebecca, Troy, Courtney, and Bryant! I am so thankful to have met you all and I could not have done this without your support and encouragement.

# DEDICATION

I dedicate this work to my husband, Jeffrey Koury. Thank you for always believing in me even when I did not believe in myself and for your constant support and encouragement during this time of my life. You were my rock throughout this entire PhD and even when things were tough you always found a way to make things a little better. This dissertation truly would not have been possible without you!

ABSTRACT OF THE DISSERTATION

Astrocytic Ephrin-B1 Controls PV Synapse Formation Through Regulating EphB2 in PV Boutons

by

Samantha Nicole Sutley

Doctor of Philosophy, Graduate Program in Biomedical Sciences

University of California, Riverside, March 2024

Dr. Iryna M. Ethell, Chairperson

Although once thought of as simply supportive cells of the brain, astrocytes are now understood to be active participants in maintaining neuronal homeostasis through their glial-neuronal and glial-glial interactions. Indeed, astrocytes are exquisitely equipped to sense and respond to their environment, allowing them to perform a diverse array of essential activities such as ion and neurotransmitter homeostasis, and regulation of synaptogenesis, synapse elimination, and synapse plasticity. Developing and maintaining the proper number of synapses as well as an appropriate balance of excitatory and inhibitory synapses is critical for proper brain function. Indeed, excitatory-

inhibitory (E/I) imbalance and impaired inhibition are hypothesized to underlie the development of hyperactive neuronal networks, driving the pathological phenotypes and behavioral impairments observed in neurodevelopmental disorders (NDDs) such as autism spectrum disorder (ASD) and epilepsy. Dysfunctions in parvalbumin (PV) expressing inhibitory interneurons including reduced numbers and hypofunction of PV interneurons have been observed in several NDDs, prompting investigation into the mechanisms involved in regulating the formation, maintenance, and function of PV connections with excitatory pyramidal cells (PCs). The work presented in this thesis investigates the role of astrocytic ephrin-B1 in glial-neuronal interactions, with a particular focus on the development of inhibitory PV->PC synapses and glial-glial interactions, investigating the role of astrocytic ephrin-B1 in astrocyte-oligodendrocyte communications.

Ephrin-B/EphB trans-synaptic signaling at excitatory synapses is well studied and has been shown to be critical for regulating excitatory synapse development and maturation, however the role of ephrin-B/EphB signaling in inhibitory synapses is less clear. Astrocytic ephrin-B1 was previously demonstrated to negatively regulate excitatory synapse development and positively regulate inhibitory synapse development, however the mechanism behind this regulation was unclear. My studies delineate a mechanism in which astrocytic ephrin-B1 facilitates the development of PV->PC inhibitory synapses through regulating the expression of its EphB receptor in PV boutons. My work also identifies a previously undescribed negative regulatory role of trans-synaptic EphB2/ephrin-B signaling at PV->PC inhibitory synapses. My work demonstrates that

EphB2 expression in PV interneurons disrupts PV->PC inhibitory synapse development and that astrocytic ephrin-B1 positively regulates PV->PC synapse formation by interfering with EphB receptor signaling in PV boutons. Disruption of this regulatory mechanism by removal of astrocytic ephrin-B1 during development led to impaired inhibition in vivo as evidenced by increased seizure susceptibility and repetitive behaviors. My work also investigated astrocyte-oligodendrocyte interactions during development and suggests that astrocytic ephrin-B/EphB receptor signaling positively regulates oligodendrocyte development and myelination. Loss of astrocytic ephrin-B1 during development impaired oligodendrocyte and myelin gene expression, leading to impaired myelination and reduced numbers of oligodendrocytes in the corpus callosum, as well as the presence of a clasping phenotype. Together, these studies implicate astrocytic ephrin-B1 as an important regulator of several neurodevelopmental processes, including inhibitory PV->PC synaptogenesis and oligodendrocyte development.

TABLE OF CONTENTS

LIST OF FIGURES

**Chapter One**



**Chapter Two**

**Chapter Three**



LIST OF TABLES

**Chapter Two**



**Chapter Three**

# CHAPTER ONE:

# Introduction to "Astrocytic Ephrin-B1 Controls PV Synapse Formation Through Regulating EphB2 in PV Boutons"

## 1.1 Astrocytes Regulate Synapse Formation, Elimination, and Function

Astrocytes, the star-shaped cells of the CNS, are one of the major glial cells in the brain. Although astrocytes were once considered to be nothing more than the "glue" of the CNS, serving supportive roles for neuronal functions, it is now well recognized that astrocytes perform many essential functions which are critical for proper CNS function (Volterra and Meldolesi, 2005). Some of these essential functions include neuronal development, synaptogenesis and synapse elimination, synaptic plasticity, buffering the extracellular space, ion homeostasis, neurotransmitter uptake and metabolism, gliotransmission, and regulation of the blood-brain barrier (Barres, 2008; Khakh and Deneen, 2019; Gradisnik and Velnar, 2023). Additionally, astrocytes regulate both the innate and adaptive immune response, playing important roles in neuroinflammatory diseases (Liddelow and Barres, 2017; Khakh and Deneen, 2019; Sofroniew, 2020). Thus, astrocytes are essential regulators of neuronal development and function.

### *1.1.1 Astrocytes in Synapse Formation*

Astrocytes are well positioned to influence synapses as their projections contact over half of synapses in the hippocampus, ensheathing the entire synapse and forming intimate associations with them (Ventura and Harris, 1999; Verkhratsky and Nedergaard, 2018). During development, astrocytes regulate synaptogenesis and synapse refinement through both secreted and contact dependent mechanisms (Barres, 2008; Allen and Eroglu, 2017; Tan and Eroglu, 2021). For example, the astrocyte-secreted extracellular matrix (ECM) proteins thrombospondin (TSP) 1 and 2 (Christopherson et al., 2005)

promote the development of post-synaptically silent excitatory synapses through interacting with the gabapentin receptor α2δ–1 (Eroglu et al., 2009), integrins (DeFreitas et al., 1995), and neuroligin-1 (Xu et al., 2010). Astrocytes also secrete hevin and SPARC, both of which play antagonizing roles in excitatory synapse development. Whereas hevin promotes excitatory synapse formation, SPARC antagonizes the synaptogenic actions of hevin and limits excitatory synapse formation (Kucukdereli et al., 2011). In contrast to TSPs and hevin which promote the development of silent excitatory synapses, astrocyte-secreted glypicans 4 and 6 induce the formation of functional excitatory synapses through regulating α-amino-3-hydroxy-5-methyl-4-isoxazolepropionic acid receptor (AMPAR) clustering and localization (Allen et al., 2012). Interestingly, astrocyte secreted TGFβ promotes the development of both excitatory and inhibitory synapses through distinct mechanisms. While excitatory synaptogenesis mediated by TGFβ requires D-serine, also secreted by astrocytes, inhibitory synaptogenesis involves CAMKII signaling (Diniz et al., 2012; Diniz et al., 2014).

A number of cell adhesion molecules (CAMs) in astrocytes regulate synaptogenesis and synapse maturation in a contact dependent manner (Tan and Eroglu, 2021). Astrocytic neuroligins (NL)1-3 influence astrocyte synaptic coverage, through regulating astrocyte morphogenesis and process elaboration into the neuropil. In addition, NLs have been demonstrated to control both excitatory synaptogenesis and inhibitory synapse function. Deletion of NL2 in astrocytes reduced the number of structural and functional excitatory synapses near NL2 KO astrocytes. Although the number of

structural inhibitory synapses was not affected, miniature inhibitory post-synaptic current (mIPSC) frequency was increased in NL2 KOs, suggesting an increased number of functional inhibitory synapses (Stogsdill et al., 2017). Neurexin (Nrxn)1, a NL binding partner is also expressed in astrocytes and was demonstrated to regulate AMPAR mediated excitatory post-synaptic currents (EPSCs) and LTP. Deletion of Nrxn1 in astrocytes reduced the strength of AMPAR mediated synaptic transmission and impaired excitatory long term potentiation (LTP) (Trotter et al., 2021). Another CAMs expressed in astrocytes, γ-protocadherin appears to be critical for proper development of excitatory and inhibitory synapses. Deletion of γ-protocadherin from astrocytes delayed the development of both excitatory and inhibitory synapses. At embryonic day (E)15-E17, the number of synapses were reduced in the spinal cord (SC) of mice lacking γ-protocadherin in astrocytes, however the number of synapses normalized to control levels by P0, suggesting that the timing of synapse development was delayed (Garrett and Weiner, 2009). Recently, neuronal cell adhesion molecule (NrCAM) of the L1 family in astrocytes was identified as an important regulator of inhibitory synapse organization and function. Deletion of NrCAM in astrocytes did not affect excitatory synapse number, but significantly decreased the number of structural inhibitory synapses, as well as the amplitude and the frequency of mIPSCs in the mouse cortex. Investigation of the mIPSC kinetics revealed that fast (somatic) mIPSC rise times were increased, suggesting that astrocytic NrCAM specifically affects somatic innervation (Takano et al., 2020).

*1.1.2 Astrocytes in Synapse Elimination*

Evidence of glial phagocytosis of synapses was first observed using electron microscopy, where inclusions containing membrane bound vesicles resembling synaptic vesicles were observed in the cytoplasm of glial processes (Ronnevi, 1977), which were later identified as astrocytes (Ronnevi, 1978). Later, transcriptional analysis of astrocytes revealed an enrichment of genes associated with phagocytic pathways in astrocytes, including draper/Megf10 and Mertk/integrin $\alpha_v\beta_5$ pathways (Cahoy et al., 2008). Both pathways converge on and activate Rac1, which regulates the phagocytic capacity of astrocytes. The first enriched pathway contains Megf10 (ced-1), Abca1 (ced-7), and Gulp1 (ced-6), while the second pathway included Crk (ced-2), Dock1 (ced-5), and Elmo (ced-12) (Cahoy et al., 2008). In C. Elegans, Megf/Gulp/Abca1 signaling induces actin cytoskeleton reorganization and subsequent engulfment of apoptotic cells in a manner requiring Rac1 activation (Kinchen et al., 2005). The guanine nucleotide exchange factor (GEF) complex Crk/Mbc/Elmo and the GTPase Rac1 were also confirmed as pathways mediating glial activation and phagocytosis in an olfactory root nerve (ORN) injury model (Ziegenfuss et al., 2012). After ORN injury, Megf (an ortholog of Drosophilia Draper) triggered glial activation during the early phases of the injury response, whereas the Crk/Mbc/Elmo complex was required in the later phases of injury response and mediated phagocytosis of axonal debris (Ziegenfuss et al., 2012). BAI1, a phosphatidylserine receptor, was also identified as a receptor that promotes engulfment of apoptotic cells through intracellular interactions with the ELMO/Dock180/Rac complex (Park et al., 2007). Finally, both Megf and Mertk signaling in astrocytes were shown to

mediate developmental synapse elimination in the dorsal lateral geniculate nucleus (dLGN) of mice. Deletion of both Megf and Mertk in astrocytes reduced their engulfment ability by 85%, underscoring the importance of these signaling pathways in astrocyte phagocytosis during development (Chung et al., 2013).

Astrocytes also regulate synapse removal indirectly by several mechanisms, one being through the complement cascade. For example, culturing retinal ganglionic cells (RGCs) in the presence of immature astrocytes upregulated C1q mRNA levels in RGCs by 10-30-fold compared to cultures without astrocytes. Loss of C1q was shown to impair synaptic refinement in the dLGN, suggesting that the classical complement cascade mediates synapse elimination, and that initiation of the cascade is regulated by immature astrocytes through controlling C1q expression in neuronal synapses (Stevens et al., 2007). Astrocytes also regulate synaptic refinement through their interactions with microglia. During development, astrocyte secreted IL-33 instructs microglial synapse engulfment, and loss IL-33 impairs this process, leading to excess numbers of excitatory synapses (Vainchtein et al., 2018). Finally, APOE alleles in astrocytes seem to regulate astrocytic phagocytic capacity. Whereas APOE2 enhances astroglial phagocytosis, APOE4 impairs it (Chung et al., 2016).

### *1.1.3 Astrocytes Buffer Ions in the Extracellular Space*

One essential function of astrocytes is their ability to buffer ions and neurotransmitters in the extracellular space (Verkhratsky and Nedergaard, 2018). Neuronal hyperpolarization following action potential is driven by outward currents of $K^+$

through voltage-gated $K^+$ channels, which results in an increase in extracellular $K^+$ concentration (Hammond, 2014). To counteract the elevations in extracellular $K^+$, astrocytes uptake $K^+$ through $Na^+/K^+$-ATPase pump (D'Ambrosio et al., 2002; Larsen et al., 2014), $K_{ir}4.1$ channel (Chever et al., 2010), and NKCC1 channel (Larsen et al., 2014), thereby maintaining the extracellular $K^+$ concentration and preventing elevations in extracellular $K^+$ concentrations. Astrocytes also maintain extracellular chloride levels through effluxion of $Cl^-$ via GABA receptors and to some extent GAT transporters (Kettenmann et al., 1987; Egawa et al., 2013). The ability of astrocytes to release $Cl^-$ helps to maintain sufficient levels of extracellular $Cl^-$ during sustained GABAergic transmission as blockade of this process impairs GABAergic neurotransmission due to alterations in the $Cl^-$ driving force in neurons (Egawa et al., 2013). In addition, prolonged synaptic transmission depletes the extracellular space of $Ca^{2+}$, affecting presynaptic release probability (Rusakov and Fine, 2003). To combat this, it has been demonstrated in culture that astrocytes are able to release $Ca^{2+}$ from their intracellular stores in response to low levels of extracellular $Ca^{2+}$ (Zanotti and Charles, 1997). Thus, astrocytes control the extracellular concentrations of several ions critical for neuronal transmission.

### *1.1.4 Astrocytes Maintain Neurotransmitter Homeostasis*

Astrocytes play essential roles in both excitatory and inhibitory neurotransmitter homeostasis. For example, astrocytes are the only cells in the CNS which express pyruvate carboxylase, an enzyme required for synthesis of glutamate from glucose, therefore de novo synthesis of glutamate is limited to astrocytes (Shank et al., 1985).

Additionally, astrocytes are the only cell in the CNS that express glutamine synthetase (GS), an enzyme which converts glutamate to glutamine, a step which is critical for neurotransmitter recycling. After glutamate is converted to glutamine by astrocytes, glutamine is shuttled back to neurons to be recycled into glutamate or gamma-aminobutyric acid (GABA) (Schousboe et al., 2013). Astrocytes uptake glutamate via glutamate transporters GLAST and GLT-1 (Rothstein et al., 1996), which serves to facilitate astrocyte glutamate metabolism and also aids in terminating excitatory neurotransmission (Schousboe et al., 2013; Verkhratsky and Nedergaard, 2018). Astrocytes also express GABA receptors and GABA transporters, particularly GAT-3 and GAT-1, allowing astrocytes to sense GABAergic neurotransmission and uptake extracellular GABA, which facilitates the termination of inhibitory neurotransmission (Mederos and Perea, 2019). In addition, astrocytes synthesize GABA from putrescine, through the diamine oxidase (DAO) and aldehyde dehydrogenase 1a1 (Aldh1a1) pathway, and release this synthesized GABA through via the Best1 channel, which has been shown to play a role in tonic inhibition (Kwak et al., 2020). Therefore, astrocytes regulate glutamate and GABA neurotransmitter synthesis, metabolism, uptake, and neurotransmission in multiple ways.

### *1.1.5 Astrocytic Calcium Signaling and Gliotransmission*

Astrocyte calcium signaling has been suggested to regulate several important functions in astrocytes, including release of synaptogenic and trophic factors, regulating neurotransmitter uptake, neuromodulation, and gliotransmitter release (Khakh and

Sofroniew, 2015; Goenaga et al., 2023). Calcium signaling in astrocytes can be initiated by neuronal activity (Goenaga et al., 2023). One of the predominant ways that astrocytes convert information about neuronal activity into calcium signals is through the sodium-calcium exchanger (NCX), which imports $Ca^{2+}$ and exports $Na^{+}$ when working in the reverse mode. Uptake of glutamate, GABA, or $Na^{+}$ after neuronal activity causes astrocytes to become loaded with $Na^{+}$, which activates the NCX channel to work in reverse mode, increasing the uptake of $Ca^{2+}$ in exchange for extruding $Na^{+}$, thereby converting the information about neuronal activity into a calcium signal in the astrocyte (Rojas et al., 2007; Boddum et al., 2016; Rose et al., 2020). Additionally, astrocytes express a number of G-protein-coupled receptors (GPCRs) including metabotropic glutamate receptors (mGLUR), cannabinoid receptor 1 (CB1R), purinergic receptor 2 (P2RY), GABA receptor type B ($GABA_BR$), Dopamine receptor 1 (D1R), adensoine receptor (AR), and μ-type opioid receptor (MOR), which mainly drive increases in astrocytic $Ca^{2+}$ levels upon activation through DAG/IP3 activation and liberation of internal calcium stores (Kofuji and Araque, 2021). Accordingly, astrocytes possess several mechanisms for detecting neuronal activity and initiating $Ca^{2+}$ signaling in response to this activity.

Calcium signaling in astrocytes can initiate the release of gliotransmitters such as GABA, glutamate, ATP, D-serine, and TNFα which can modulate synaptic transmission and plasticity (Stellwagen and Malenka, 2006; Araque et al., 2014). For example, CB1R in astrocytes was shown to be required for LTP and working memory. The mechanism being that activation of CB1Rs in astrocytes increased astrocyte $Ca^{2+}$ levels, leading to D-

serine release, which acted on N-methyl-D-aspartate receptors (NMDARs) to promote LTP and subsequent recognition memory acquisition (Robin et al., 2018). Another group showed that activation of GABA receptors on astrocytes in the hippocampus led to both glutamate and ATP release by astrocytes. The result was a biphasic modulation of synaptic transmission where glutamate potentiated the strength of EPSCs recorded in excitatory CA1 pyramidal neurons and ATP subsequently induced synaptic depression (Covelo and Araque, 2018). Others showed that uptake of GABA through GAT-3 in astrocytes increased astrocytic intracellular $Ca^{2+}$ levels via the NCX transporter, leading to ATP/adenosine release, which suppressed excitatory neurotransmission in the hippocampus by activating presynaptic adenosine receptors (Boddum et al., 2016). These studies support that astrocytes can sense neuronal activity and respond in ways that modulate synaptic strength and plasticity through a variety of mechanisms.

### *1.1.6 Astrocytes in Neurodevelopmenta Disorders (NDDS)*

It is clear that astrocytes regulate many aspects of synapse development and physiology, therefore it is unsurprising that astrocyte dysfunctions have been linked to neurodevelopmental disorders (Sloan and Barres, 2014; Allen and Eroglu, 2017). An analysis of the SFARI database revealed that several astrocyte-enriched genes implicated in synaptogenesis including Gpc4, Gpc6, hevin, Tsp1, and FABP7, were associated with ASD cases (Allen and Eroglu, 2017). Alterations in the protein expression of the astrocyte markers aquaporin-4 (AQP4) and connexin 43 (CX43) were also identified in the cortices of subjects with ASD (Fatemi et al., 2008). Experimental models support the

idea that astrocytes are involved in the pathogenic mechanisms driving NDDs. For example, deletion of the MeCP2 gene, which causes Rett syndrome (RTT), in astrocytes resulted in abnormal development of neuronal dendrites in culture (Ballas et al., 2009). Additionally, re-expression of MeCP2 in astrocytes alone was able to restore dendritic morphology and reversed some of the behavioral phenotypes observed in a mouse model of RTT (Lioy et al., 2011). Astrocytes are also implicated in the pathogenesis of Fragile-X syndrome (FXS). Control hippocampal neurons cultured with astrocytes lacking FMR1, the gene responsible for FXS, exhibited delayed dendritic spine maturation and excessive excitatory synapses in early development (Jacobs et al., 2010). In vivo, deletion of FMR1 from astrocytes led to EEG signatures in mice similar to those observed in humans with FXS, deficits in sociability, dysregulation of GABA levels in astrocytes, and reduced levels of synaptic but not extra-synaptic GABA receptors (Rais et al., 2022). We have also shown that developmental deletion of ephrin-B1, a ligand for the ASD risk gene EphB2 receptor, in astrocytes impairs social novelty and social preference (Nguyen et al., 2020b). Therefore, dysfunctional astrocytes have the potential to contribute to the pathogenesis of NDDs.

## 1.2 Ephs/Ephrins

### *1.2.1 Eph/Ephrin Signaling*

Ephrins are ligands for Erythropoietin-producing hepatocellular carcinoma (Eph) receptor tyrosine kinases, which are the largest family of receptor tyrosine kinases

(RTKs) (Sloniowski and Ethell, 2012). Eph receptors are subdivided into the EphA and EphB class of receptors, based on their preference for binding to ephrin-A ligands, which lack an intracellular signaling domain, or ephrin-B ligands, which contain intracellular domains that are capable of signaling. (Pasquale, 2005; Sloniowski and Ethell, 2012). Ligand clustering and subsequent binding to the receptor results in the formation of ligand-receptor heterotetrameric complex (Davis et al., 1994; Himanen et al., 2001; Sloniowski and Ethell, 2012). Although the heterotetrameric complex is a functional signaling unit, the tetramers can further cluster, increasing the signaling capacity of the receptor (Wimmer-Kleikamp et al., 2004). Forward signaling in the Eph expressing cell is initiated upon activation of kinase activity in the receptor, resulting in autophosphorylation of the juxtamembrane tyrosine residues (Zisch et al., 1998; Kania and Klein, 2016). Phosphorylation of the juxtamembrane domain allows for interactions with SH2 domain containing proteins such as Src, Abl, Grb10, and Grb2 (Stein et al., 1996; Zisch et al., 1998; Noren et al., 2006; Henderson and Dalva, 2018), while the PDZ domain enables signaling through PDZ domain containing proteins such as GRIP and PICK1 (Torres et al., 1998; Hoogenraad et al., 2005). Reverse signaling in ephrin-B expressing cells is activated by Src kinase mediated phosphorylation (Palmer et al., 2002). Ephrin-Bs signal via their PDZ domain and interact with PDZ domain containing proteins such as GRIP1, GRIP2, and Syntenin (Brückner et al., 1999; McClelland et al., 2009). Ephs and ephrins are involved in a diverse array of neuronal developmental processes including cell migration, axon guidance, excitatory synaptogenesis, and synaptic plasticity (Dalva et al., 2000; Ethell et al., 2001; Henkemeyer et al., 2003;

Kayser et al., 2006; Sloniowski and Ethell, 2012). Ephrin-B/EphB signaling is particularly well studied in excitatory synapses (Lim et al., 2008; Pasquale, 2008; Klein, 2012; Sheffler-Collins and Dalva, 2012), where signaling regulates dendritic spine formation and maturation (Ethell et al., 2001; Moeller et al., 2006), AMPAR phosphorylation and trafficking to the synapse (Kayser et al., 2006; Hussain et al., 2015), NMDAR localization and function (Takasu et al., 2002; Nolt et al., 2011), and synaptic plasticity (Henderson et al., 2001b; Contractor et al., 2002).

### *1.2.2 EphB Receptor Signaling in Dendritic Spine Maturation and Excitatory Synapse Formation*

Multiple EphB receptors have been shown to regulate dendritic spine maturation. The first evidence that EphB receptors were involved in spine maturation came from a study from Ethell et al. 2001 showing that expression of a kinase inactive dominant negative EphB2 in cultured hippocampal neurons blocked normal spine formation (Ethell et al., 2001). Loss of kinase activity in EphB2 impaired syndecan-2 activation, which was previously shown to induce maturation of dendritic spines (Ethell and Yamaguchi, 1999; Ethell et al., 2001). The requirement of EphB signaling in vivo was confirmed as triple EphB1/2/3 knockout impaired dendritic spine formation in hippocampal CA3 excitatory pyramidal cells. Dendrites of triple KO mice lacked the “mushroom head” morphology characteristic of mature spines and showed a reduction in both the cross-sectional area of the post-synaptic density of asymmetrical (excitatory) synapses as well as the number of asymmetrical synapses, consistent with impairments in excitatory synapse formation and

maturation (Henkemeyer et al., 2003). EphB receptors regulate the maintenance of mature spine morphology through stabilizing the actin cytoskeleton. EphB2-FAK signaling was demonstrated to inhibit the activity of cofilin, an actin severing protein, which prevented spine remodeling, thereby maintaining mature dendritic spines. Furthermore, the RhoA-ROCK-LIMK1 pathway was implicated in the activation of cofilin (Shi et al., 2009). Interestingly, kinetics of EphB2 signaling seem to dictate stable contact formation. In an elegant study, Mao et al., 2018 (Mao et al., 2018) demonstrated that the magnitude of EphB signaling kinetics was inversely correlated with the likelihood of stable contact formation. Filopodia that exhibited rapid, focal increases in EphB2 activity were more likely to retract, while slower rises in EphB2 kinase activity was predictive of contact formation and subsequent development of an excitatory synapse, supporting a pivotal role for EphB2 signaling kinetics in initiating excitatory synaptic contact formation (Mao et al., 2018). Together, these studies illustrate that EphB receptors are critical regulators of spine dynamics and are required for initial contact formation and stabilization of excitatory synapses.

### *1.2.3 Ephrin/EphBs in Synapse Development and Plasticity*

Following initial contact formation, trans-synaptic ephrin-B/EphB signaling is essential for excitatory synapse development (Sloniowski and Ethell, 2012; Washburn et al., 2023). Presynaptic ephrin-B reverse signaling, particularly ephrin-B1, is required for presynaptic development. Trans-synaptic interactions between post-synaptic EphB2 and pre-synaptic ephrin-B1/2 activates ephrin-B reverse signaling, which induces presynaptic

development through PDZ-domain dependent interactions with syntenin-1. In culture, knockdown of ephrin-B1 or ephrin-B2 prevented presynaptic vesicle clustering induced by EphB2 (McClelland et al., 2009). In vitro, it was shown that trans-synaptic ephrin-B3/EphB2 interactions regulate excitatory synapse density through an interesting mechanism in which levels of post-synaptic ephrin-B3 mediate competition for presynaptic EphBs, allowing neurons with higher levels of ephrin-B3 to outcompete lower ephrin-B3 expressing neurons to ultimately form more synapses (McClelland et al., 2010). An elegant in vivo study confirmed these observations in vivo using "Mosaic Analysis with Double Markers" (MADM) mice in which mice had mosaic expression of ephrin-B3 (either EfnB3 +/+, EfnB3 -/-, or EfnB3 +/- neurons in the same animal!) that could be identified with expression of genetically encoded fluorescence tags. Subsets of EfnB3+/+ neurons in mosaic mice had a significantly higher density of dendritic spines compared to WT neurons in mice that did not have mosaic expression of EfnB3, as well as neurons with one or no copies of EfnB3 from the same mouse, indicating that levels of ephrin-B3 do indeed allow neurons with higher levels of ephrin-B3 to outcompete lower ephrin-B3 expressing neurons in vivo (Henderson et al., 2019). Trans-synaptic ephrin/EphB signaling also regulates localization and function of glutamate receptors. For example, EphB2 receptor regulates NMDAR trafficking and synaptic localization in mature neurons and EphB2 signaling increases calcium influx though NMDARs (Nolt et al., 2011). In cortical cultures, activation of post-synaptic EphB receptor signaling via treatment with ephrin-B2 was shown to potentiate NMDAR dependent calcium influx by activating Src, leading to phosphorylation of NMDAR (Takasu et al., 2002). EphB2 also

interacts with AMPA receptors through the PDZ binding domain, regulating the density and surface localization of AMPA receptors at synaptic sites (Kayser et al., 2006). Eph/ephrin trans-synaptic signaling also regulates the expression of LTP (Contractor et al., 2002). Mice lacking EphB2 showed a significant reduction in LTP and impaired NMDAR mediated responses (Henderson et al., 2001a). Furthermore, ephrin-B3 reverse signaling is required for induction of LTP at mossy fiber-CA3 synapses (Armstrong et al., 2006).

### *1.2.4 Astrocytic Ephrins*

Ephrin-A3 is expressed in astrocytic processes and its interaction with neuronal EphA4 has been shown to regulate both neuronal and astrocyte functions (Murai and Pasquale, 2011). Ephrin-A3/EphA4 signaling regulates the morphology of dendritic spines. Activation of EphA4 in hippocampal slices with ephrin-A3-Fc induced dendritic spine retraction. In addition, loss of EphA4 in vivo altered spine morphology and organization in CA1 pyramidal cells, with EphA4 knockout mice exhibiting an increased number and length of spines compared to controls. (Murai et al., 2003). EphA4 was shown to mediate these effects through inhibiting β-integrin, which normally functions to stabilize spines (Bourgin et al., 2007). Cdk-5 and ephexin-1 have also been implicated in the mechanism of ephrin-A3/EphA4 mediated spine retraction (Fu et al., 2007). Deletion of ephrin-A3, which is primarily expressed by astrocytes, altered dendritic spine morphogenesis, increased the expression of the glutamate transporters GLT-1 and GLAST on hippocampal astrocytes, and enhance glutamate uptake through astrocytic

glutamate transporters. Functionally, this resulted in impairments in hippocampal dependent learning tasks, including acquisition of contextual fear memory during fear conditioning as well as contextual memory in object placement test (Carmona et al., 2009). The learning and memory deficits are likely a result of impaired LTP, as astrocytic ephrin-A3/post-synaptic EphA4 signaling was found to be required for theta burst stimulation (TBS) induced LTP at hippocampal CA1-CA3 synapses (Filosa et al., 2009). Astrocytes also express EphBs 1-4 and ephrin-Bs 1-3. Activation of EphB3 or EphA4 signaling in cultured astrocytes was shown to stimulate D-serine synthesis and release (Zhuang et al., 2010). D-serine functions as a co-agonist at the glycine binding site of NMDARs, enhancing NMDAR mediated excitatory currents, and release of D-serine from astrocytes has been demonstrated to facilitate the induction of LTP via its actions at NMDARs (Stevens et al., 2003; Yang et al., 2003; Henneberger et al., 2010).

### *1.2.5 Astrocytic Ephrin-B1*

Astrocytic ephrin-B1 regulates synaptogenesis in both adult and developing hippocampi. Deletion of astrocytic ephrin-B1 in adult mice increased the number of excitatory synapses and immature dendritic spines with small spine heads on CA1 pyramidal neurons. The AMPAR/PSD95 synaptic protein ratio was also decreased in mice lacking astrocytic ephrin-B1, further supporting that the excessive spines were immature and that the increase in excitatory synapse numbers was due to an increase in silent, immature synapses. The increase in immature excitatory synapses led to enhanced long term contextual memory. In culture, it was shown that activation of ephrin-B1

reverse signaling in astrocytes enhanced the engulfment of synaptosomes containing EphB receptors, but not synaptosomes lacking EphB receptors. Therefore, the excess spinogenesis and excitatory synaptogenesis in adult mice lacking astrocytic ephrin-B1 is likely a consequence of impaired synapse engulfment (Koeppen et al., 2018). A follow up study further investigated the mechanism behind the enhancement in learning and memory in adult mice lacking astrocytic ephrin-B1 (Nguyen et al., 2020a). It was discovered that deletion of astrocytic ephrin-B1 in adult mice enhanced the formation of new dendritic spines, while overexpression impaired the formation of new spines during learning. These differences only existed in neurons that were activated during memory recall. These findings suggest that in adults, astrocytic ephrin-B1 limits learning induced dendritic spine and excitatory synapse formation by eliminating immature spines in an EphB dependent manner, thereby controlling the substrate for memory formation. Removal of this negative regulator enhanced excitatory synaptogenesis and memory recall, while too much negative regulation prevented synaptogenesis and memory recall. Importantly, while both of these studies showed that astrocytic ephrin-B1 regulates excitatory synaptogenesis in adult mice, neither of these studies showed any differences in inhibitory glutamic acid decarboxylase (GAD)65 positive puncta (Koeppen et al., 2018; Nguyen et al., 2020a).

Interestingly, astrocytic ephrin-B1 was found to regulate both excitatory and inhibitory synaptogenesis during development (Nguyen et al., 2020b). Developmental deletion of astrocytic ephrin-B1 enhanced the strength of postsynaptic excitatory responses in CA1 pyramidal cells and increased the number of excitatory synapses and

the number of small to medium sized dendritic spines. Conversely, overexpression (OE) decreased the strength of postsynaptic excitatory responses, suggesting that astrocytic ephrin-B1 negatively regulates excitatory synaptogenesis. In contrast, developmental deletion of astrocytic ephrin-B1 reduced the number of inhibitory synapses and the strength of postsynaptic inhibitory responses in CA1 pyramidal cells, while OE enhanced postsynaptic inhibitory responses, indicating that astrocytic ephrin-B1 positively regulates inhibitory synaptogenesis during development. In addition, developmental deletion of astrocytic ephrin-B1 reduced the number of cells with detectable parvalbumin (PV) levels in the CA1 hippocampus and the number of VGlut1 inputs on PV-expressing interneurons. These results suggest that developmental deletion of astrocytic ephrin-B1 enhanced excitatory neurotransmission but impaired inhibitory neurotransmission, which could lead to excitatory-inhibitory (E/I) imbalance (Nguyen et al., 2020b).

### 1.3 Excitatory-Inhibitory Imbalance and Impaired Inhibition in NDDs

Impaired inhibition and excitatory-inhibitory imbalance are suggested to underlie the development of hyperactive neuronal networks in NDDs such as ASD and epilepsy (Rubenstein and Merzenich, 2003; Ali Rodriguez et al., 2018; Sohal and Rubenstein, 2019; Contractor et al., 2021; Tang et al., 2021). In support of this hypothesis, several genes associated with inhibitory neurotransmission, inhibitory interneurons, and inhibitory synapses have been identified as risk genes for NDDs including GABA receptors (Chen et al., 2014), gephyrin (Prasad et al., 2012), neurexins (Gauthier et al.,

2011; Vaags et al., 2012), and GAT-1 (Johannesen et al., 2018). Additionally, mouse models of NDDs show evidence of E/I imbalance. For example, cortical layer 2/3 neurons in the MeCP2 model of Rett syndrome have been shown to have reduced conductance of both excitatory and inhibitory currents, as well as a higher E/I ratio (Banerjee et al., 2016). Inhibitory neurotransmission is also altered in the Ts65Dn mouse model of Down syndrome (DS). In CA1 excitatory neurons the $Cl^-$ reversal potential was demonstrated to above the resting membrane potential (at around -58mV where Vm was typically around -64mV), rendering $GABA_AR$ currents excitatory. The altered $Cl^-$ reversal was due to increased expression of NKCC1 chloride importer, which lead to high levels of intracellular chloride. The increased expression of NKCC1 was also observed in human subjects with DS. Intriguingly, application of the NKCC1 inhibitor bumetanide reversed the altered inhibitory neurotransmission, impairments in LTP, and restored the cognitive impairments observed in the Ts65Dn model (Deidda et al., 2015). Lastly, EEG phenotypes in a mouse model of Fragile-X syndrome (FXS) are also suggestive of neuronal hyperexcitability. For example, FXS mice exhibit increased resting state cortical EEG gamma power and increased amplitude of sound evoked event related potentials (ERPs) (Lovelace et al., 2018; Kulinich et al., 2020).

## 1.4 Parvalbumin Interneurons

### *1.4.1 Parvalbumin Interneuron Connectivity and Function*

Parvalbumin (PV) interneurons comprise about 24% of all of the interneurons of the CA1 hippocampus (Bezaire and Soltesz, 2013). PV interneurons are characterized by their expression of the calcium binding protein parvalbumin (Kawaguchi et al., 1987) and their fast-spiking action potential (AP) phenotype (Hu et al., 2014; Booker and Vida, 2018). PV basket interneuron (PVBCs) somata reside in the stratum pyramidale (SP) layer of the CA1 hippocampus and their axons extensively branch throughout the SP, innervating the somata and proximal dendrites of CA1 pyramidal cells (PCs), where each PVBC is estimated to innervate over 1,100 pyramidal cells (Halasy et al., 1996; Cobb et al., 1997)! This extensive coverage of CA1 pyramidal cells at sites close to AP generation suggest that PVBCs are likely to potently control AP generation in CA1 PCs. PVBCs provide both feedforward and feedback inhibition to CA1 pyramidal cells (Hu et al., 2014). Feedforward inhibition does much more than providing simple inhibition over neuronal activity and firing, it also expands the complexity of possible neuronal operations. For example, engaging BCs in the CA1 by Schaffer collateral stimulation reduced the integration window for EPSP summation and AP initiation, increasing the temporal fidelity of CA1 pyramidal cell firing (Pouille and Scanziani, 2001). Additionally, feedforward inhibition widens the dynamic range of pyramidal cell activation, expanding the range of afferent input strengths that will trigger action potential generation in PCs, and allowing the hippocampal PCs to respond to weaker

stimuli without becoming saturated with activity during stronger stimuli. This is achieved through modulation of the excitatory conductance required to reach threshold. As afferent input strength increases, the magnitude of feedforward inhibition also increases, resulting in the requirement for greater conductance of excitatory currents in order for PCs to reach AP threshold (Pouille et al., 2009). These findings were substantiated by other work showing that PV interneurons influence the gain of incoming sensory stimuli, regulating the firing rate of cortical layer 2/3 pyramidal cells in response to visual stimuli (Atallah et al., 2012). In larger brain networks, PVBCs are critical for generating gamma oscillations (20-80Hz). Indeed, optogentically driving PV interneurons at 40Hz frequency increases the power of gamma oscillations in vivo (Cardin et al., 2009), while inhibiting PV interneurons in vivo suppresses the power of gamma oscillations (Sohal et al., 2009). Additionally, gamma oscillations were demonstrated to enhance cortical signal transmission by reducing noise in cortical circuits (Sohal et al., 2009).

### *1.4.2 PV interneurons in NDDs*

Dysfunctions in PV interneurons, including reduced density of PV interneurons, reduced PV expression, impaired PNN formation, and reduced PV interneuron activity have been observed in ASD, suggesting that PV interneurons may play a critical role in regulating E/I balance and the pathogenesis of NDDs (Lawrence et al., 2010; Hashemi et al., 2016; Filice et al., 2020; Contractor et al., 2021). Strikingly, parvalbumin is one of the most downregulated genes in the cortex of postmortem individuals with ASD (Gandal et al., 2018; Haney et al., 2020). In addition, examination of neocortical tissue revealed

that individuals with ASD showed reduced numbers of PV interneurons, supporting the hypothesis that PV dysfunction might drive pathological phenotypes in ASD (Hashemi et al., 2017). Several mouse models show alterations in PV cells. For example, both Shank1 and Shank3b mouse models of ASD showed reductions in PV protein and mRNA levels (Filice et al., 2016). Additionally, in the Cntnap2 mouse model, the number of PV interneurons in the somatosensory cortex was reduced and the intrinsic electrical properties were also altered (Peñagarikano et al., 2011; Vogt et al., 2017). The valproic acid mouse model also showed reductions in PV mRNA and protein levels in the striatum (Lauber et al., 2016). However, the MeCP2 mouse model of Rett syndrome seemed to accelerate PV maturation (Patrizi et al., 2019). Alterations in gamma oscillations and gamma power in EEG studies also provide evidence of impaired PV activity. Altered gamma oscillations were observed in humans with ASD (Gandal et al., 2010) and FXS (Ethridge et al., 2017). Abnormalities in gamma oscillations were similarly altered in animal models of ASD such as FXS (Lovelace et al., 2018) and the 22q11.2 deletion model (LgDel mouse model) (Mukherjee et al., 2019). Furthermore, hypoactivity of PV interneurons has been observed in several genetic mouse models of ASD such as Fmr1, Shank3, Mecp2, and Cntnap2 (Contractor et al., 2021). The significance of these changes in PV interneurons are demonstrated by a study in which PV was deleted in mice, resulting in behavioral phenotypes characteristic of ASD including deficits in social behaviors and impaired communication (USVs) (Wöhr et al., 2015).

## 1.5 Astrocyte-Oligodendrocyte Interactions

Oligodendrocytes are the glial cells in the CNS responsible for myelin sheath generation around axons of CNS neurons (De Robertis et al., 1958; Baumann and Pham-Dinh, 2001). Astrocytes influence oligodendrocyte development and function through releasing astrocyte-secreted factors such as platelet derived growth factor (PDGF) and leukemia inhibitory factor-like (LIF) protein, both of which are required for proper oligodendrocyte development, survival (Raff et al., 1988; Gard et al., 1995; Clemente et al., 2013), differentiation, and myelination (Richardson et al., 1988; Ishibashi et al., 2006). Additionally, astrocytes express the connexin proteins Cx30 and Cx43 and oligodendrocytes express Cx47 and Cx32. Importantly, astrocytes and oligodendrocytes are functionally coupled through gap junctions composed of Cx47/Cx43 or Cx32/Cx30 pairs (Altevogt and Paul, 2004; Kleopa et al., 2004; Kamasawa et al., 2005; Stadelmann et al., 2019). These gap junctional connections represent another mechanism by which astrocytes regulate oligodendrocytes, as they allow for direct transfer of metabolites, as well as electrical coupling between the cells (Kleopa et al., 2004; Kamasawa et al., 2005; Stadelmann et al., 2019). For example, lipid synthesis in astrocytes is required for proper myelination (Camargo et al., 2017) and cholesterol transfer from astrocytes to oligodendrocytes regulates oligodendrocyte survival and remyelination (Molina-Gonzalez et al., 2023). The importance of these functional connections between astrocytes and oligodendrocytes is underscored by the fact that double deletion of

Cx47/Cx30 impairs myelin formation and results in the development of thinner myelin sheaths (Menichella et al., 2003; Tress et al., 2012).

### 1.6 Oligodendrocyte Ephs/Ephrins

Oligodendrocyte precursor cells (OPCs) express several Ephs and ephrins, including EphA2, -A4, -B1, and -B2, and ephrin-A1, -A5, -B1, -B2, and -B3, and EphA4 (Linneberg et al., 2015). Some evidence suggests that Eph/ephrin signaling in oligodendrocytes regulates myelin formation. For example, it was demonstrated that EphB forward signaling in oligodendrocytes impaired myelination, while ephrin-B reverse signaling in oligodendrocytes enhanced myelination (Linneberg et al., 2015). Oligodendrocyte development may also be regulated by Eph/ephrin signaling as ephrin-B and ephrin-A signaling in OPCs was found to control OPC adhesion and migration (Chatzopoulou et al., 2004). Additionally, treatment of OPCs with ephrin-B1 and -B3 inhibited OPC differentiation in culture by activating EphA4 signaling in OPCs, resulting in inhibition of focal adhesion (FAK), a positive regulator of OPC development and myelination (Forrest et al., 2009; Syed et al., 2016). Eph/ephrin signaling in oligodendrocytes may also be important for formation of neural circuits during development or during regenerative processes as myelinating oligodendrocytes in particular express ephrin-B3, which acts as an inhibitor of cortical neurite outgrowth by interacting with Eph receptors in cortical neurons (Benson et al., 2005).

REFERENCES FOR CHAPTER ONE

Ali Rodriguez R, Joya C, Hines RM (2018) Common Ribs of Inhibitory Synaptic Dysfunction in the Umbrella of Neurodevelopmental Disorders. Frontiers in Molecular Neuroscience 11.

Allen NJ, Eroglu C (2017) Cell Biology of Astrocyte-Synapse Interactions. Neuron 96:697-708.

Allen NJ, Bennett ML, Foo LC, Wang GX, Chakraborty C, Smith SJ, Barres BA (2012) Astrocyte glypicans 4 and 6 promote formation of excitatory synapses via GluA1 AMPA receptors. Nature 486:410-414.

Altevogt BM, Paul DL (2004) Four Classes of Intercellular Channels between Glial Cells in the CNS. The Journal of Neuroscience 24:4313-4323.

Araque A, Carmignoto G, Haydon Philip G, Oliet Stéphane HR, Robitaille R, Volterra A (2014) Gliotransmitters Travel in Time and Space. Neuron 81:728-739.

Armstrong JN, Saganich MJ, Xu N-J, Henkemeyer M, Heinemann SF, Contractor A (2006) B-Ephrin Reverse Signaling Is Required for NMDA-Independent Long-Term Potentiation of Mossy Fibers in the Hippocampus. The Journal of Neuroscience 26:3474-3481.

Atallah BV, Bruns W, Carandini M, Scanziani M (2012) Parvalbumin-expressing interneurons linearly transform cortical responses to visual stimuli. Neuron 73:159-170.

Ballas N, Lioy DT, Grunseich C, Mandel G (2009) Non–cell autonomous influence of MeCP2-deficient glia on neuronal dendritic morphology. Nature Neuroscience 12:311-317.

Banerjee A, Rikhye RV, Breton-Provencher V, Tang X, Li C, Li K, Runyan CA, Fu Z, Jaenisch R, Sur M (2016) Jointly reduced inhibition and excitation underlies circuit-wide changes in cortical processing in Rett syndrome. Proceedings of the National Academy of Sciences 113:E7287-E7296.

Barres BA (2008) The Mystery and Magic of Glia: A Perspective on Their Roles in Health and Disease. Neuron 60:430-440.

Baumann N, Pham-Dinh D (2001) Biology of Oligodendrocyte and Myelin in the Mammalian Central Nervous System. Physiological Reviews 81:871-927.

Ben-Ari Y (2001) Developing networks play a similar melody. Trends in Neurosciences 24:353-360.

Benson MD, Romero MI, Lush ME, Lu QR, Henkemeyer M, Parada LF (2005) Ephrin-B3 is a myelin-based inhibitor of neurite outgrowth. Proceedings of the National Academy of Sciences 102:10694-10699.

Bezaire MJ, Soltesz I (2013) Quantitative assessment of CA1 local circuits: Knowledge base for interneuron-pyramidal cell connectivity. Hippocampus 23:751-785.

Boddum K, Jensen TP, Magloire V, Kristiansen U, Rusakov DA, Pavlov I, Walker MC (2016) Astrocytic GABA transporter activity modulates excitatory neurotransmission. Nature Communications 7:13572.

Booker SA, Vida I (2018) Morphological diversity and connectivity of hippocampal interneurons. Cell Tissue Res 373:619-641.

Bourgin C, Murai KK, Richter M, Pasquale EB (2007) The EphA4 receptor regulates dendritic spine remodeling by affecting β1-integrin signaling pathways. Journal of Cell Biology 178:1295-1307.

Brückner K, Labrador JP, Scheiffele P, Herb A, Seeburg PH, Klein R (1999) EphrinB ligands recruit GRIP family PDZ adaptor proteins into raft membrane microdomains. Neuron 22:511-524.

Cahoy JD, Emery B, Kaushal A, Foo LC, Zamanian JL, Christopherson KS, Xing Y, Lubischer JL, Krieg PA, Krupenko SA, Thompson WJ, Barres BA (2008) A Transcriptome Database for Astrocytes, Neurons, and Oligodendrocytes: A New Resource for Understanding Brain Development and Function. The Journal of Neuroscience 28:264-278.

Camargo N, Goudriaan A, van Deijk A-LF, Otte WM, Brouwers JF, Lodder H, Gutmann DH, Nave K-A, Dijkhuizen RM, Mansvelder HD, Chrast R, Smit AB, Verheijen MHG (2017) Oligodendroglial myelination requires astrocyte-derived lipids. PLOS Biology 15:e1002605.

Cardin JA, Carlén M, Meletis K, Knoblich U, Zhang F, Deisseroth K, Tsai L-H, Moore CI (2009) Driving fast-spiking cells induces gamma rhythm and controls sensory responses. Nature 459:663-667.

Carmona MA, Murai KK, Wang L, Roberts AJ, Pasquale EB (2009) Glial ephrin-A3 regulates hippocampal dendritic spine morphology and glutamate transport. Proceedings of the National Academy of Sciences 106:12524-12529.

Chatzopoulou E, Ikenaka K, Kagawa T, Lebras B, Lemkine G, Prestoz L, Spassky N, Thomas J-L, Zalc B (2004) Control of axonophilic migration of oligodendrocyte precursor cells by Eph–ephrin interaction. Neuron Glia Biology 1:73-83.

Chen C-H, Huang C-C, Cheng M-C, Chiu Y-N, Tsai W-C, Wu Y-Y, Liu S-K, Gau SS-F (2014) Genetic analysis of GABRB3 as a candidate gene of autism spectrum disorders. Molecular autism 5:1-13.

Chever O, Djukic B, McCarthy KD, Amzica F (2010) Implication of K<sub>ir</sub>4.1 Channel in Excess Potassium Clearance: An In Vivo Study on Anesthetized Glial-Conditional K<sub>ir</sub>4.1 Knock-Out Mice. The Journal of Neuroscience 30:15769-15777.

Christopherson KS, Ullian EM, Stokes CCA, Mullowney CE, Hell JW, Agah A, Lawler J, Mosher DF, Bornstein P, Barres BA (2005) Thrombospondins Are Astrocyte-Secreted Proteins that Promote CNS Synaptogenesis. Cell 120:421-433.

Chung W-S, Verghese PB, Chakraborty C, Joung J, Hyman BT, Ulrich JD, Holtzman DM, Barres BA (2016) Novel allele-dependent role for APOE in controlling the rate of synapse pruning by astrocytes. Proceedings of the National Academy of Sciences 113:10186-10191.

Chung W-S, Clarke LE, Wang GX, Stafford BK, Sher A, Chakraborty C, Joung J, Foo LC, Thompson A, Chen C, Smith SJ, Barres BA (2013) Astrocytes mediate synapse elimination through MEGF10 and MERTK pathways. Nature 504:394-400.

Clemente D, Ortega MC, Melero-Jerez C, De Castro F (2013) The effect of glia-glia interactions on oligodendrocyte precursor cell biology during development and in demyelinating diseases. Frontiers in Cellular Neuroscience 7.

Cobb SR, Halasy K, Vida I, Nyı´ri G, Tamás G, Buhl EH, Somogyi P (1997) Synaptic effects of identified interneurons innervating both interneurons and pyramidal cells in the rat hippocampus. Neuroscience 79:629-648.

Contractor A, Ethell IM, Portera-Cailliau C (2021) Cortical interneurons in autism. Nature Neuroscience 24:1648-1659.

Contractor A, Rogers C, Maron C, Henkemeyer M, Swanson GT, Heinemann SF (2002) Trans-Synaptic Eph Receptor-Ephrin Signaling in Hippocampal Mossy Fiber LTP. Science 296:1864-1869.

Covelo A, Araque A (2018) Neuronal activity determines distinct gliotransmitter release from a single astrocyte. eLife 7:e32237.

D'Ambrosio R, Gordon DS, Winn HR (2002) Differential Role of KIR Channel and Na+/K+-Pump in the Regulation of Extracellular K+ in Rat Hippocampus. Journal of Neurophysiology 87:87-102.

Dalva MB, Takasu MA, Lin MZ, Shamah SM, Hu L, Gale NW, Greenberg ME (2000) EphB Receptors Interact with NMDA Receptors and Regulate Excitatory Synapse Formation. Cell 103:945-956.

Davis S, Gale NW, Aldrich TH, Maisonpierre PC, Lhotak V, Pawson T, Goldfarb M, Yancopoulos GD (1994) Ligands for EPH-related receptor tyrosine kinases that require membrane attachment or clustering for activity. Science 266:816-819.

de Lecea L, del Río JA, Soriano E (1995) Developmental expression of parvalbumin mRNA in the cerebral cortex and hippocampus of the rat. Brain Res Mol Brain Res 32:1-13.

De Robertis E, Gerschenfeld HM, Wald F (1958) Cellular mechanism of myelination in the central nervous system. J Biophys Biochem Cytol 4:651-656.

DeFreitas MF, Yoshida CK, Frazier WA, Mendrick DL, Kypta RM, Reichard LF (1995) Identification of integrin $\alpha 3\beta 1$ as a neuronal thrombospondin receptor mediating neurite outgrowth. Neuron 15:333-343.

Deidda G, Parrini M, Naskar S, Bozarth IF, Contestabile A, Cancedda L (2015) Reversing excitatory GABAAR signaling restores synaptic plasticity and memory in a mouse model of Down syndrome. Nature Medicine 21:318-326.

Diniz LP, Tortelli V, Garcia MN, Araújo APB, Melo HM, Seixas da Silva GS, De Felice FG, Alves-Leon SV, de Souza JM, Romao LF (2014) Astrocyte transforming growth factor beta 1 promotes inhibitory synapse formation via CaM kinase II signaling. Glia 62:1917-1931.

Diniz LP, Almeida JC, Tortelli V, Vargas Lopes C, Setti-Perdigão P, Stipursky J, Kahn SA, Romão LF, de Miranda J, Alves-Leon SV, de Souza JM, Castro NG, Panizzutti R, Gomes FCA (2012) Astrocyte-induced Synaptogenesis Is Mediated by Transforming Growth Factor β Signaling through Modulation of d-Serine Levels in Cerebral Cortex Neurons *. Journal of Biological Chemistry 287:41432-41445.

Egawa K, Yamada J, Furukawa T, Yanagawa Y, Fukuda A (2013) $Cl^-$ homeodynamics in gap junction-coupled astrocytic networks on activation of GABAergic synapses. J Physiol 591:3901-3917.

Eroglu C, Allen NJ, Susman MW, O'Rourke NA, Park CY, Ozkan E, Chakraborty C, Mulinyawe SB, Annis DS, Huberman AD, Green EM, Lawler J, Dolmetsch R, Garcia KC, Smith SJ, Luo ZD, Rosenthal A, Mosher DF, Barres BA (2009) Gabapentin receptor alpha2delta-1 is a neuronal thrombospondin receptor responsible for excitatory CNS synaptogenesis. Cell 139:380-392.

Ethell IM, Yamaguchi Y (1999) Cell Surface Heparan Sulfate Proteoglycan Syndecan-2 Induces the Maturation of Dendritic Spines in Rat Hippocampal Neurons. Journal of Cell Biology 144:575-586.

Ethell IM, Irie F, Kalo MS, Couchman JR, Pasquale EB, Yamaguchi Y (2001) EphB/Syndecan-2 Signaling in Dendritic Spine Morphogenesis. Neuron 31:1001-1013.

Ethridge LE, White SP, Mosconi MW, Wang J, Pedapati EV, Erickson CA, Byerly MJ, Sweeney JA (2017) Neural synchronization deficits linked to cortical hyper-excitability and auditory hypersensitivity in fragile X syndrome. Molecular autism 8:1-11.

Fatemi SH, Folsom TD, Reutiman TJ, Lee S (2008) Expression of astrocytic markers aquaporin 4 and connexin 43 is altered in brains of subjects with autism. Synapse 62:501-507.

Filice F, Vörckel KJ, Sungur AÖ, Wöhr M, Schwaller B (2016) Reduction in parvalbumin expression not loss of the parvalbumin-expressing GABA interneuron subpopulation in genetic parvalbumin and shank mouse models of autism. Molecular Brain 9:10.

Filice F, Janickova L, Henzi T, Bilella A, Schwaller B (2020) The Parvalbumin Hypothesis of Autism Spectrum Disorder. Frontiers in Cellular Neuroscience 14.

Filosa A, Paixão S, Honsek SD, Carmona MA, Becker L, Feddersen B, Gaitanos L, Rudhard Y, Schoepfer R, Klopstock T, Kullander K, Rose CR, Pasquale EB, Klein R (2009) Neuron-glia communication via EphA4/ephrin-A3 modulates LTP through glial glutamate transport. Nature Neuroscience 12:1285-1292.

Forrest AD, Beggs HE, Reichardt LF, Dupree JL, Colello RJ, Fuss B (2009) Focal adhesion kinase (FAK): A regulator of CNS myelination. Journal of Neuroscience Research 87:3456-3464.

Fu W-Y, Chen Y, Sahin M, Zhao X-S, Shi L, Bikoff JB, Lai K-O, Yung W-H, Fu AKY, Greenberg ME, Ip NY (2007) Cdk5 regulates EphA4-mediated dendritic spine retraction through an ephexin1-dependent mechanism. Nature Neuroscience 10:67-76.

Gandal MJ, Edgar JC, Ehrlichman RS, Mehta M, Roberts TPL, Siegel SJ (2010) Validating γ Oscillations and Delayed Auditory Responses as Translational Biomarkers of Autism. Biological Psychiatry 68:1100-1106.

Gandal MJ, Haney JR, Parikshak NN, Leppa V, Ramaswami G, Hartl C, Schork AJ, Appadurai V, Buil A, Werge TM (2018) Shared molecular neuropathology across major psychiatric disorders parallels polygenic overlap. Science 359:693-697.

Gard AL, Burrell MR, Pfeiffer SE, Rudge JS, Williams WC, II (1995) Astroglial control of oligodendrocyte survival mediated by PDGF and Leukemia Inhibitory Factor-like protein. Development 121:2187-2197.

Garrett AM, Weiner JA (2009) Control of CNS Synapse Development by γ-Protocadherin-Mediated Astrocyte–Neuron Contact. The Journal of Neuroscience 29:11723-11731.

Gauthier J, Siddiqui TJ, Huashan P, Yokomaku D, Hamdan FF, Champagne N, Lapointe M, Spiegelman D, Noreau A, Lafrenière RG (2011) Truncating mutations in NRXN2 and NRXN1 in autism spectrum disorders and schizophrenia. Human genetics 130:563-573.

Goenaga J, Araque A, Kofuji P, Herrera Moro Chao D (2023) Calcium signaling in astrocytes and gliotransmitter release. Frontiers in Synaptic Neuroscience 15.

Gradisnik L, Velnar T (2023) Astrocytes in the central nervous system and their functions in health and disease: A review. World J Clin Cases 11:3385-3394.

Halasy K, Buhl EH, Lörinczi Z, Tamás G, Somogyi P (1996) Synaptic target selectivity and input of GABAergic basket and bistratified interneurons in the CA1 area of the rat hippocampus. Hippocampus 6:306-329.

Hammond C (2014) Cellular and molecular neurophysiology: Academic Press.

Haney JR et al. (2020) Broad transcriptomic dysregulation across the cerebral cortex in ASD. bioRxiv:2020.2012.2017.423129.

Hashemi E, Ariza J, Rogers H, Noctor SC, Martínez-Cerdeño V (2016) The Number of Parvalbumin-Expressing Interneurons Is Decreased in the Prefrontal Cortex in Autism. Cerebral Cortex 27:1931-1943.

Hashemi E, Ariza J, Rogers H, Noctor SC, Martínez-Cerdeño V (2017) The number of parvalbumin-expressing interneurons is decreased in the prefrontal cortex in autism. Cerebral cortex 27:1931-1943.

Henderson JT, Georgiou J, Jia Z, Robertson J, Elowe S, Roder JC, Pawson T (2001a) The receptor tyrosine kinase EphB2 regulates NMDA-dependent synaptic function. Neuron 32:1041-1056.

Henderson JT, Georgiou J, Jia Z, Robertson J, Elowe S, Roder JC, Pawson T (2001b) The receptor tyrosine kinase EphB2 regulates NMDA-dependent synaptic function. Neuron 32:1041-1056.

Henderson NT, Dalva MB (2018) EphBs and ephrin-Bs: Trans-synaptic organizers of synapse development and function. Mol Cell Neurosci 91:108-121.

Henderson NT, Le Marchand SJ, Hruska M, Hippenmeyer S, Luo L, Dalva MB (2019) Ephrin-B3 controls excitatory synapse density through cell-cell competition for EphBs. eLife 8:e41563.

Henkemeyer M, Itkis OS, Ngo M, Hickmott PW, Ethell IM (2003) Multiple EphB receptor tyrosine kinases shape dendritic spines in the hippocampus. Journal of Cell Biology 163:1313-1326.

Henneberger C, Papouin T, Oliet SH, Rusakov DA (2010) Long-term potentiation depends on release of D-serine from astrocytes. Nature 463:232-236.

Himanen J-P, Rajashankar KR, Lackmann M, Cowan CA, Henkemeyer M, Nikolov DB (2001) Crystal structure of an Eph receptor–ephrin complex. Nature 414:933-938.

Hoogenraad CC, Milstein AD, Ethell IM, Henkemeyer M, Sheng M (2005) GRIP1 controls dendrite morphogenesis by regulating EphB receptor trafficking. Nature neuroscience 8:906-915.

Hu H, Gan J, Jonas P (2014) Fast-spiking, parvalbumin<sup>+</sup> GABAergic interneurons: From cellular design to microcircuit function. Science 345:1255263.

Hussain NK, Thomas GM, Luo J, Huganir RL (2015) Regulation of AMPA receptor subunit GluA1 surface expression by PAK3 phosphorylation. Proceedings of the National Academy of Sciences 112:E5883-E5890.

Ishibashi T, Dakin KA, Stevens B, Lee PR, Kozlov SV, Stewart CL, Fields RD (2006) Astrocytes promote myelination in response to electrical impulses. Neuron 49:823-832.

Jacobs S, Nathwani M, Doering LC (2010) Fragile X astrocytes induce developmental delays in dendrite maturation and synaptic protein expression. BMC Neuroscience 11:132.

Johannesen KM, Gardella E, Linnankivi T, Courage C, de Saint Martin A, Lehesjoki AE, Mignot C, Afenjar A, Lesca G, Abi-Warde MT (2018) Defining the phenotypic spectrum of SLC6A1 mutations. Epilepsia 59:389-402.

Kamasawa N, Sik A, Morita M, Yasumura T, Davidson KGV, Nagy JI, Rash JE (2005) Connexin-47 and connexin-32 in gap junctions of oligodendrocyte somata, myelin sheaths, paranodal loops and Schmidt-Lanterman incisures: Implications for ionic homeostasis and potassium siphoning. Neuroscience 136:65-86.

Kania A, Klein R (2016) Mechanisms of ephrin-Eph signalling in development, physiology and disease. Nat Rev Mol Cell Biol 17:240-256.

Kawaguchi Y, Katsumaru H, Kosaka T, Heizmann CW, Hama K (1987) Fast spiking cells in rat hippocampus (CA1 region) contain the calcium-binding protein parvalbumin. Brain Research 416:369-374.

Kayser MS, McClelland AC, Hughes EG, Dalva MB (2006) Intracellular and Trans-Synaptic Regulation of Glutamatergic Synaptogenesis by EphB Receptors. The Journal of Neuroscience 26:12152-12164.

Kettenmann H, Backus KH, Schachner M (1987) γ-Aminobutyric acid opens Cl-channels in cultured astrocytes. Brain Research 404:1-9.

Khakh BS, Sofroniew MV (2015) Diversity of astrocyte functions and phenotypes in neural circuits. Nature Neuroscience 18:942-952.

Khakh BS, Deneen B (2019) The Emerging Nature of Astrocyte Diversity. Annu Rev Neurosci 42:187-207.

Kinchen JM, Cabello J, Klingele D, Wong K, Feichtinger R, Schnabel H, Schnabel R, Hengartner MO (2005) Two pathways converge at CED-10 to mediate actin rearrangement and corpse removal in C. elegans. Nature 434:93-99.

Klein R (2012) Eph/ephrin signalling during development. Development 139:4105-4109.

Kleopa KA, Orthmann JL, Enriquez A, Paul DL, Scherer SS (2004) Unique distributions of the gap junction proteins connexin29, connexin32, and connexin47 in oligodendrocytes. Glia 47:346-357.

Koeppen J, Nguyen AQ, Nikolakopoulou AM, Garcia M, Hanna S, Woodruff S, Figueroa Z, Obenaus A, Ethell IM (2018) Functional Consequences of Synapse Remodeling Following Astrocyte-Specific Regulation of Ephrin-B1 in the Adult Hippocampus. The Journal of Neuroscience 38:5710-5726.

Kofuji P, Araque A (2021) G-Protein-Coupled Receptors in Astrocyte–Neuron Communication. Neuroscience 456:71-84.

Kucukdereli H, Allen NJ, Lee AT, Feng A, Ozlu MI, Conatser LM, Chakraborty C, Workman G, Weaver M, Sage EH, Barres BA, Eroglu C (2011) Control of excitatory CNS synaptogenesis by astrocyte-secreted proteins Hevin and SPARC. Proceedings of the National Academy of Sciences 108:E440-E449.

Kulinich AO, Reinhard SM, Rais M, Lovelace JW, Scott V, Binder DK, Razak KA, Ethell IM (2020) Beneficial effects of sound exposure on auditory cortex development in a mouse model of Fragile X Syndrome. Neurobiology of Disease 134:104622.

Kwak H et al. (2020) Astrocytes Control Sensory Acuity via Tonic Inhibition in the Thalamus. Neuron 108:691-706.e610.

Larsen BR, Assentoft M, Cotrina ML, Hua SZ, Nedergaard M, Kaila K, Voipio J, MacAulay N (2014) Contributions of the Na+/K+-ATPase, NKCC1, and Kir4.1 to hippocampal K+ clearance and volume responses. Glia 62:608-622.

Lauber E, Filice F, Schwaller B (2016) Prenatal Valproate Exposure Differentially Affects Parvalbumin-Expressing Neurons and Related Circuits in the Cortex and Striatum of Mice. Frontiers in Molecular Neuroscience 9.

Lawrence YA, Kemper TL, Bauman ML, Blatt GJ (2010) Parvalbumin-, calbindin-, and calretinin-immunoreactive hippocampal interneuron density in autism. Acta Neurol Scand 121:99-108.

Liddelow SA, Barres BA (2017) Reactive Astrocytes: Production, Function, and Therapeutic Potential. Immunity 46:957-967.

Lim BK, Matsuda N, Poo M-m (2008) Ephrin-B reverse signaling promotes structural and functional synaptic maturation in vivo. Nature Neuroscience 11:160-169.

Linneberg C, Harboe M, Laursen LS (2015) Axo-Glia Interaction Preceding CNS Myelination Is Regulated by Bidirectional Eph-Ephrin Signaling. ASN Neuro 7:1759091415602859.

Lioy DT, Garg SK, Monaghan CE, Raber J, Foust KD, Kaspar BK, Hirrlinger PG, Kirchhoff F, Bissonnette JM, Ballas N, Mandel G (2011) A role for glia in the progression of Rett's syndrome. Nature 475:497-500.

Lovelace JW, Ethell IM, Binder DK, Razak KA (2018) Translation-relevant EEG phenotypes in a mouse model of Fragile X Syndrome. Neurobiology of Disease 115:39-48.

Mao YT, Zhu JX, Hanamura K, Iurilli G, Datta SR, Dalva MB (2018) Filopodia Conduct Target Selection in Cortical Neurons Using Differences in Signal Kinetics of a Single Kinase. Neuron 98:767-782.e768.

McClelland AC, Sheffler-Collins SI, Kayser MS, Dalva MB (2009) Ephrin-B1 and ephrin-B2 mediate EphB-dependent presynaptic development via syntenin-1. Proceedings of the National Academy of Sciences 106:20487-20492.

McClelland AC, Hruska M, Coenen AJ, Henkemeyer M, Dalva MB (2010) Trans-synaptic EphB2–ephrin–B3 interaction regulates excitatory synapse density by inhibition of postsynaptic MAPK signaling. Proceedings of the National Academy of Sciences 107:8830-8835.

Mederos S, Perea G (2019) GABAergic-astrocyte signaling: A refinement of inhibitory brain networks. Glia 67:1842-1851.

Menichella DM, Goodenough DA, Sirkowski E, Scherer SS, Paul DL (2003) Connexins Are Critical for Normal Myelination in the CNS. The Journal of Neuroscience 23:5963-5973.

Moeller ML, Shi Y, Reichardt LF, Ethell IM (2006) EphB receptors regulate dendritic spine morphogenesis through the recruitment/phosphorylation of focal adhesion kinase and RhoA activation. Journal of Biological Chemistry 281:1587-1598.

Molina-Gonzalez I et al. (2023) Astrocyte-oligodendrocyte interaction regulates central nervous system regeneration. Nature Communications 14:3372.

Mukherjee A, Carvalho F, Eliez S, Caroni P (2019) Long-lasting rescue of network and cognitive dysfunction in a genetic schizophrenia model. Cell 178:1387-1402. e1314.

Murai KK, Pasquale EB (2011) Eph receptors and ephrins in neuron–astrocyte communication at synapses. Glia 59:1567-1578.

Murai KK, Nguyen LN, Irie F, Yamaguchi Y, Pasquale EB (2003) Control of hippocampal dendritic spine morphology through ephrin-A3/EphA4 signaling. Nature Neuroscience 6:153-160.

Nguyen AQ, Koeppen J, Woodruff S, Mina K, Figueroa Z, Ethell IM (2020a) Astrocytic Ephrin-B1 Controls Synapse Formation in the Hippocampus During Learning and Memory. Frontiers in Synaptic Neuroscience 12.

Nguyen AQ, Sutley S, Koeppen J, Mina K, Woodruff S, Hanna S, Vengala A, Hickmott PW, Obenaus A, Ethell IM (2020b) Astrocytic Ephrin-B1 Controls Excitatory-Inhibitory Balance in Developing Hippocampus. The Journal of Neuroscience 40:6854-6871.

Nolt MJ, Lin Y, Hruska M, Murphy J, Sheffler-Colins SI, Kayser MS, Passer J, Bennett MVL, Zukin RS, Dalva MB (2011) EphB Controls NMDA Receptor Function and Synaptic Targeting in a Subunit-Specific Manner. The Journal of Neuroscience 31:5353-5364.

Noren NK, Foos G, Hauser CA, Pasquale EB (2006) The EphB4 receptor suppresses breast cancer cell tumorigenicity through an Abl–Crk pathway. Nature cell biology 8:815-825.

Palmer A, Zimmer M, Erdmann KS, Eulenburg V, Porthin A, Heumann R, Deutsch U, Klein R (2002) EphrinB phosphorylation and reverse signaling: regulation by Src kinases and PTP-BL phosphatase. Mol Cell 9:725-737.

Park D, Tosello-Trampont A-C, Elliott MR, Lu M, Haney LB, Ma Z, Klibanov AL, Mandell JW, Ravichandran KS (2007) BAI1 is an engulfment receptor for apoptotic cells upstream of the ELMO/Dock180/Rac module. Nature 450:430-434.

Pasquale EB (2005) Eph receptor signalling casts a wide net on cell behaviour. Nature Reviews Molecular Cell Biology 6:462-475.

Pasquale EB (2008) Eph-ephrin bidirectional signaling in physiology and disease. Cell 133:38-52.

Patrizi A, Awad PN, Chattopadhyaya B, Li C, Di Cristo G, Fagiolini M (2019) Accelerated Hyper-Maturation of Parvalbumin Circuits in the Absence of MeCP2. Cerebral Cortex 30:256-268.

Pelkey KA, Chittajallu R, Craig MT, Tricoire L, Wester JC, McBain CJ (2017) Hippocampal GABAergic Inhibitory Interneurons. Physiol Rev 97:1619-1747

Peñagarikano O, Abrahams Brett S, Herman Edward I, Winden Kellen D, Gdalyahu A, Dong H, Sonnenblick Lisa I, Gruver R, Almajano J, Bragin A, Golshani P, Trachtenberg Joshua T, Peles E, Geschwind Daniel H (2011) Absence of CNTNAP2 Leads to Epilepsy, Neuronal Migration Abnormalities, and Core Autism-Related Deficits. Cell 147:235-246.

Pouille F, Scanziani M (2001) Enforcement of Temporal Fidelity in Pyramidal Cells by Somatic Feed-Forward Inhibition. Science 293:1159-1163.

Pouille F, Marin-Burgin A, Adesnik H, Atallah BV, Scanziani M (2009) Input normalization by global feedforward inhibition expands cortical dynamic range. Nature Neuroscience 12:1577-1585.

Prasad A, Merico D, Thiruvahindrapuram B, Wei J, Lionel AC, Sato D, Rickaby J, Lu C, Szatmari P, Roberts W (2012) A discovery resource of rare copy number variations in individuals with autism spectrum disorder. G3: Genes| Genomes| Genetics 2:1665-1685.

Raff MC, Lillien LE, Richardson WD, Burne JF, Noble MD (1988) Platelet-derived growth factor from astrocytes drives the clock that times oligodendrocyte development in culture. Nature 333:562-565.

Rais M, Kulinich AO, Wagner V, Woodard W, Shuai XS, Sutley SN, Kokash J, Piepponen TP, Castren M, Razak KA, Ethell IM (2022) Astrocytes regulate inhibition in Fragile X Syndrome. bioRxiv:2022.2002.2008.479618.

Richardson WD, Pringle N, Mosley MJ, Westermark B, Dubois-Dalcg M (1988) A role for platelet-derived growth factor in normal gliogenesis in the central nervous system. Cell 53:309-319.

Robin LM, da Cruz JFO, Langlais VC, Martin-Fernandez M, Metna-Laurent M, Busquets-Garcia A, Bellocchio L, Soria-Gomez E, Papouin T, Varilh M (2018) Astroglial CB1 receptors determine synaptic D-serine availability to enable recognition memory. Neuron 98:935-944. e935.

Rojas H, Colina C, Ramos M, Benaim G, Jaffe EH, Caputo C, DiPolo R (2007) Na+ entry via glutamate transporter activates the reverse Na+/Ca2+ exchange and triggers -induced Ca2+ release in rat cerebellar Type-1 astrocytes. Journal of Neurochemistry 100:1188-1202.

Ronnevi L-O (1977) Spontaneous phagocytosis of boutons on spinal motoneurons during early postnatal development. An electron microscopical study in the cat. Journal of Neurocytology 6:487-504.

Ronnevi L-O (1978) Origin of the glial processes responsible for the spontaneous postnatal phagocytosis of boutons on cat spinal motoneurons. Cell and tissue research 189:203-217.

Rose CR, Ziemens D, Verkhratsky A (2020) On the special role of NCX in astrocytes: Translating Na+-transients into intracellular Ca2+ signals. Cell Calcium 86:102154.

Rothstein JD, Dykes-Hoberg M, Pardo CA, Bristol LA, Jin L, Kuncl RW, Kanai Y, Hediger MA, Wang Y, Schielke JP, Welty DF (1996) Knockout of glutamate transporters reveals a major role for astroglial transport in excitotoxicity and clearance of glutamate. Neuron 16:675-686.

Rubenstein JL, Merzenich MM (2003) Model of autism: increased ratio of excitation/inhibition in key neural systems. Genes Brain Behav 2:255-267.

Rusakov DA, Fine A (2003) Extracellular Ca2+ Depletion Contributes to Fast Activity-Dependent Modulation of Synaptic Transmission in the Brain. Neuron 37:287-297.

Schousboe A, Bak L, Waagepetersen H (2013) Astrocytic Control of Biosynthesis and Turnover of the Neurotransmitters Glutamate and GABA. Frontiers in Endocrinology 4.

Seto-Ohshima A, Aoki E, Semba R, Emson PC, Heizmann CW (1990) Appearance of parvalbumin-specific immunoreactivity in the cerebral cortex and hippocampus of the developing rat and gerbil brain. 94

Shank RP, Bennett GS, Freytag SO, Campbell GL (1985) Pyruvate car□ylase: an astrocyte-specific enzyme implicated in the replenishment of amino acid neurotransmitter pools. Brain Research 329:364-367.

Sheffler-Collins SI, Dalva MB (2012) EphBs: an integral link between synaptic function and synaptopathies. Trends Neurosci 35:293-304.

Shi Y, Pontrello CG, DeFea KA, Reichardt LF, Ethell IM (2009) Focal Adhesion Kinase Acts Downstream of EphB Receptors to Maintain Mature Dendritic Spines by Regulating Cofilin Activity. The Journal of Neuroscience 29:8129-8142.

Sloan SA, Barres BA (2014) Mechanisms of astrocyte development and their contributions to neurodevelopmental disorders. Current Opinion in Neurobiology 27:75-81.

Sloniowski S, Ethell IM (2012) Looking forward to EphB signaling in synapses. Semin Cell Dev Biol 23:75-82.

Sofroniew MV (2020) Astrocyte Reactivity: Subtypes, States, and Functions in CNS Innate Immunity. Trends Immunol 41:758-770.

Sohal VS, Rubenstein JLR (2019) Excitation-inhibition balance as a framework for investigating mechanisms in neuropsychiatric disorders. Molecular Psychiatry 24:1248-1257.

Sohal VS, Zhang F, Yizhar O, Deisseroth K (2009) Parvalbumin neurons and gamma rhythms enhance cortical circuit performance. Nature 459:698-702.

Stadelmann C, Timmler S, Barrantes-Freer A, Simons M (2019) Myelin in the Central Nervous System: Structure, Function, and Pathology. Physiological Reviews 99:1381-1431.

Stein E, Cerretti DP, Daniel TO (1996) Ligand activation of ELK receptor tyrosine kinase promotes its association with Grb10 and Grb2 in vascular endothelial cells. Journal of Biological Chemistry 271:23588-23593.

Stellwagen D, Malenka RC (2006) Synaptic scaling mediated by glial TNF-α. Nature 440:1054-1059.

Stevens B, Allen NJ, Vazquez LE, Howell GR, Christopherson KS, Nouri N, Micheva KD, Mehalow AK, Huberman AD, Stafford B, Sher A, Litke Alan M, Lambris JD, Smith SJ, John SWM, Barres BA (2007) The Classical Complement Cascade Mediates CNS Synapse Elimination. Cell 131:1164-1178.

Stevens ER, Esguerra M, Kim PM, Newman EA, Snyder SH, Zahs KR, Miller RF (2003) D-serine and serine racemase are present in the vertebrate retina and contribute to the physiological activation of NMDA receptors. Proceedings of the National Academy of Sciences 100:6789-6794.

Stogsdill JA, Ramirez J, Liu D, Kim YH, Baldwin KT, Enustun E, Ejikeme T, Ji R-R, Eroglu C (2017) Astrocytic neuroligins control astrocyte morphogenesis and synaptogenesis. Nature 551:192-197.

Syed YA, Zhao C, Mahad D, Möbius W, Altmann F, Foss F, Sentürk A, Acker-Palmer A, Lubec G, Lilley K, Franklin RJM, Nave K-A, Kotter MRN (2016) Antibody-mediated neutralization of myelin-associated EphrinB3 accelerates CNS remyelination. Acta Neuropathologica 131:281-298.

Takano T, Wallace JT, Baldwin KT, Purkey AM, Uezu A, Courtland JL, Soderblom EJ, Shimogori T, Maness PF, Eroglu C, Soderling SH (2020) Chemico-genetic discovery of astrocytic control of inhibition in vivo. Nature 588:296-302.

Takasu MA, Dalva MB, Zigmond RE, Greenberg ME (2002) Modulation of NMDA receptor-dependent calcium influx and gene expression through EphB receptors. Science 295:491-495.

Tan CX, Eroglu C (2021) Cell adhesion molecules regulating astrocyte–neuron interactions. Current Opinion in Neurobiology 69:170-177.

Tang X, Jaenisch R, Sur M (2021) The role of GABAergic signalling in neurodevelopmental disorders. Nature Reviews Neuroscience 22:290-307.

Torres R, Firestein BL, Dong H, Staudinger J, Olson EN, Huganir RL, Bredt DS, Gale NW, Yancopoulos GD (1998) PDZ proteins bind, cluster, and synaptically colocalize with Eph receptors and their ephrin ligands. Neuron 21:1453-1463.

Tress O, Maglione M, May D, Pivneva T, Richter N, Seyfarth J, Binder S, Zlomuzica A, Seifert G, Theis M, Dere E, Kettenmann H, Willecke K (2012) Panglial Gap Junctional Communication is Essential for Maintenance of Myelin in the CNS. The Journal of Neuroscience 32:7499-7518.

Tricoire L, Pelkey KA, Erkkila BE, Jeffries BW, Yuan X, McBain CJ (2011) A Blueprint for the Spatiotemporal Origins of Mouse Hippocampal Interneuron Diversity. Journal of Neuroscience 31:10948-10970.

Trotter JH, Dargaei Z, Sclip A, Essayan-Perez S, Liakath-Ali K, Raju K, Nabet A, Liu X, Wöhr M, Südhof TC (2021) Compartment-Specific Neurexin Nanodomains Orchestrate Tripartite Synapse Assembly. bioRxiv:2020.2008.2021.262097.

Vaags AK, Lionel AC, Sato D, Goodenberger M, Stein QP, Curran S, Ogilvie C, Ahn JW, Drmic I, Senman L (2012) Rare deletions at the neurexin 3 locus in autism spectrum disorder. The American Journal of Human Genetics 90:133-141.

Vainchtein ID, Chin G, Cho FS, Kelley KW, Miller JG, Chien EC, Liddelow SA, Nguyen PT, Nakao-Inoue H, Dorman LC, Akil O, Joshita S, Barres BA, Paz JT, Molofsky AB, Molofsky AV (2018) Astrocyte-derived interleukin-33 promotes microglial synapse engulfment and neural circuit development. Science 359:1269-1273.

Ventura R, Harris KM (1999) Three-dimensional relationships between hippocampal synapses and astrocytes. J Neurosci 19:6897-6906.

Verkhratsky A, Nedergaard M (2018) Physiology of Astroglia. Physiological Reviews 98:239-389.

Vogt D, Cho KKA, Shelton SM, Paul A, Huang ZJ, Sohal VS, Rubenstein JLR (2017) Mouse Cntnap2 and Human CNTNAP2 ASD Alleles Cell Autonomously Regulate PV+ Cortical Interneurons. Cerebral Cortex 28:3868-3879.

Volterra A, Meldolesi J (2005) Astrocytes, from brain glue to communication elements: the revolution continues. Nature Reviews Neuroscience 6:626-640.

Washburn HR, Chander P, Srikanth KD, Dalva MB (2023) Transsynaptic Signaling of Ephs in Synaptic Development, Plasticity, and Disease. Neuroscience 508:137-152.

Wimmer-Kleikamp SH, Janes PW, Squire A, Bastiaens PIH, Lackmann M (2004) Recruitment of Eph receptors into signaling clusters does not require ephrin contact. Journal of Cell Biology 164:661-666.

Wöhr M, Orduz D, Gregory P, Moreno H, Khan U, Vörckel KJ, Wolfer DP, Welzl H, Gall D, Schiffmann SN, Schwaller B (2015) Lack of parvalbumin in mice leads to behavioral deficits relevant to all human autism core symptoms and related neural morphofunctional abnormalities. Translational Psychiatry 5:e525-e525.

Xu J, Xiao N, Xia J (2010) Thrombospondin 1 accelerates synaptogenesis in hippocampal neurons through neuroligin 1. Nature neuroscience 13:22-24.

Yang Y, Ge W, Chen Y, Zhang Z, Shen W, Wu C, Poo M, Duan S (2003) Contribution of astrocytes to hippocampal long-term potentiation through release of D-serine. Proceedings of the National Academy of Sciences 100:15194-15199.

Zanotti S, Charles A (1997) Extracellular Calcium Sensing by Glial Cells: Low Extracellular Calcium Induces Intracellular Calcium Release and Intercellular Signaling. Journal of Neurochemistry 69:594-602.

Zhuang Z, Yang B, Theus MH, Sick JT, Bethea JR, Sick TJ, Liebl DJ (2010) EphrinBs Regulate d-Serine Synthesis and Release in Astrocytes. The Journal of Neuroscience 30:16015-16024.

Ziegenfuss JS, Doherty J, Freeman MR (2012) Distinct molecular pathways mediate glial activation and engulfment of axonal debris after axotomy. Nature Neuroscience 15:979-987.

Zisch AH, Kalo MS, Chong LD, Pasquale EB (1998) Complex formation between EphB2 and Src requires phosphorylation of tyrosine 611 in the EphB2 juxtamembrane region. Oncogene 16:2657-2670.

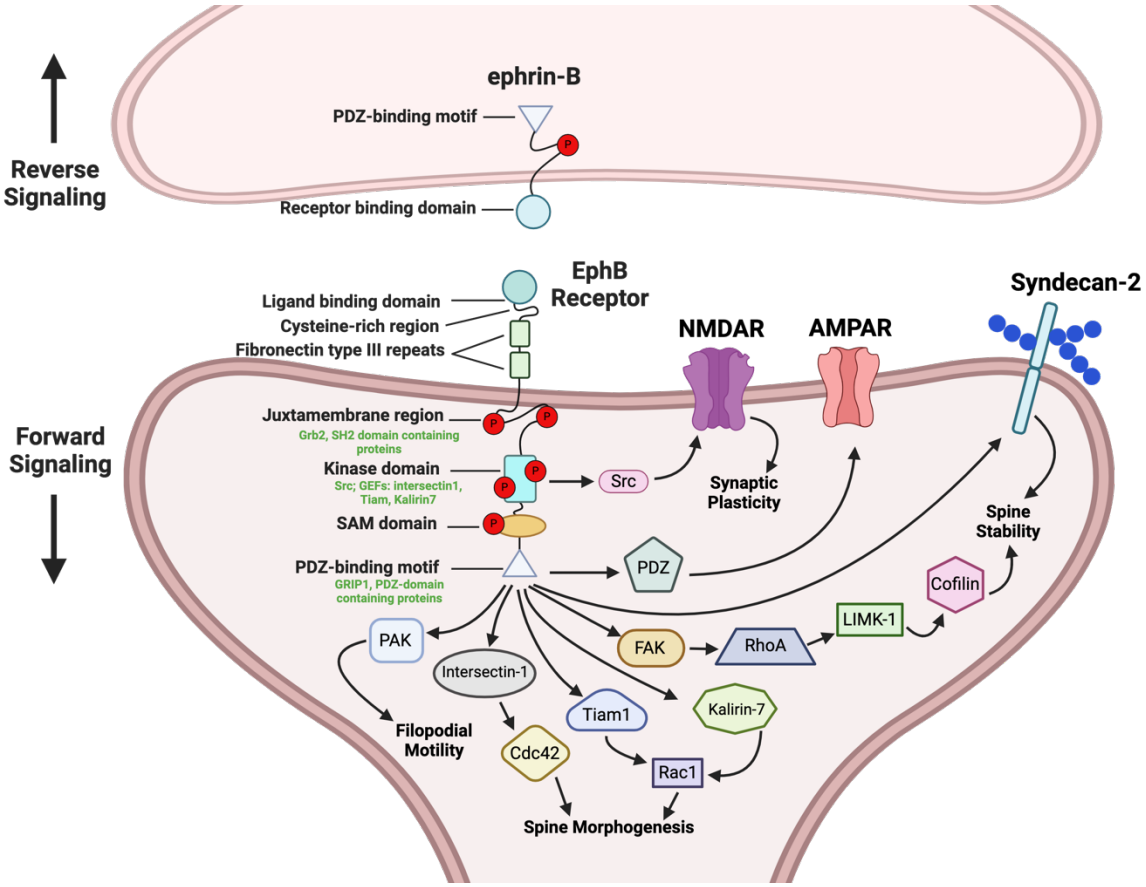


**Figure 1.1: Ephrin-B and EphB structure, interaction sites, and signaling pathways in postsynaptic sites.** The illustration shows the protein structure of ephrin-B/EphB receptor, sites of protein interactions, and phosphorylation sites. Interaction partners are shown in green at their respective interaction sites. Signaling pathways initiated by EphB forward signaling at post-synaptic sites are also depicted. The outcomes of EphB signaling in dendritic spines include filopodial motility, spine morphogenesis, spine stability, synaptic plasticity, and insertion and retention of AMPA/NMDA receptors in the postsynaptic membrane. Figure was adapted from (Sloniowski and Ethell, 2012).

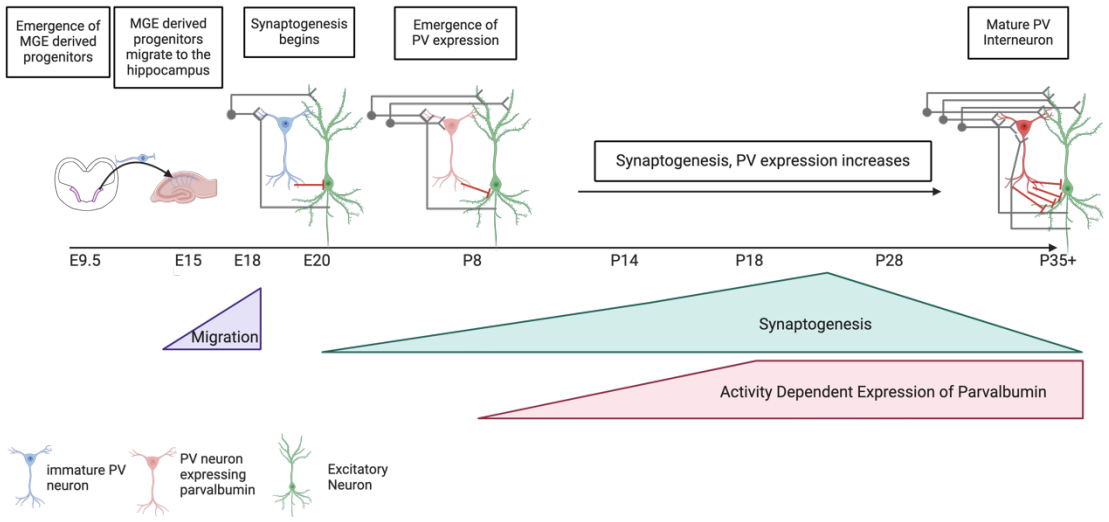


**Figure 1.2: Timeline of PV interneuron development.** PV interneuron progenitors arise around embryonic day (E) 9.5 and infiltrate the developing hippocampus by E18 (Tricoire et al., 2011; Pelkey et al., 2017). Immature PV interneurons begin to form synapses around the time of birth, then undergo a period of rapid synaptogenesis lasting until approximately the third postnatal week of development, followed by a period of synaptic refinement (Ben-Ari, 2001; Contractor et al., 2021). Activity dependent expression of parvalbumin begins after the first postnatal week and increases, reaching adult levels by the third postnatal week (Seto-Ohshima et al., 1990; de Lecea et al., 1995).

# CHAPTER TWO:

## Astrocytic Ephrin-B1 Regulates PV Inhibitory Synapse Development through EphB2 Signaling

A version of this chapter was submitted for publication in the Journal of Neuroscience (Sutley-Koury et al., J Neurosci 2024 under review)

## 2.1 Abstract

Impaired inhibitory synapse development is suggested to drive neuronal hyperactivity in autism spectrum disorders (ASD) and epilepsy. I propose a novel mechanism by which astrocytes control the development of parvalbumin (PV)-specific inhibitory synapses in the hippocampus, implicating ephrin-B/EphB signaling. Here, I utilize genetic approaches to assess functional and structural connectivity between PV and pyramidal cells (PC) through whole-cell patch-clamp electrophysiology, optogenetics, immunohistochemical analysis, and mouse behaviors. While inhibitory synapse development is adversely affected by PV-specific expression of EphB2, a strong candidate ASD risk gene, astrocytic ephrin-B1 facilitates PV->PC connectivity by interfering with EphB signaling in PV boutons. In contrast, the loss of astrocytic ephrin-B1 reduces PV->PC connectivity and inhibition, resulting in increased seizure susceptibility and an ASD-like phenotype. My findings underscore the crucial role of astrocytes in regulating inhibitory circuit development and discover a new role for EphB2 receptors in PV-specific inhibitory synapse development.

## 2.2 Introduction

Astrocytes critically regulate many aspects of synaptic physiology, including synaptogenesis, synapse elimination, synaptic transmission, and synapse plasticity through both contact dependent mechanisms and release of soluble factors (Allen and

Eroglu, 2017; Augusto-Oliveira et al., 2020). Although several mechanisms by which astrocytes regulate excitatory synapse development and function have been described, our knowledge of how astrocytes regulate inhibitory synapse development and function remain limited (Clarke and Barres, 2013; Allen and Eroglu, 2017; Augusto-Oliveira et al., 2020). Astrocytes are shown to promote the development of inhibitory synapses, increasing the number of presynaptically active GABAergic synapses and the frequency of mIPSCs in mixed cultures (Elmariah et al., 2005; Hughes et al., 2010). Additionally, the strength of $GABA_AR$ mediated currents is potentiated by astrocytes in cultured hippocampal neurons, showing enhanced GABA mediated currents only in neuronal somata contacting astrocytes (Liu et al., 1996). Here I report a novel mechanism by which astrocytes regulate inhibitory synapse development, specifically PV->PC connectivity, and propose a new role of ephrin-B/EphB receptor signaling as the underlying mechanism.

Ephrin-B/EphB signaling is well studied in excitatory synapses (Lim et al., 2008; Pasquale, 2008; Klein, 2012; Sheffler-Collins and Dalva, 2012), including their role in dendritic spine formation and maturation (Ethell et al., 2001; Moeller et al., 2006), AMPAR phosphorylation and trafficking to the synapse (Kayser et al., 2006; Hussain et al., 2015), NMDAR localization and function (Takasu et al., 2002; Nolt et al., 2011), as well as regulation of LTP (Henderson et al., 2001; Contractor et al., 2002). However, little is known about the mechanism of ephrin-B/EphB signaling in inhibitory synapse development. Although postsynaptic EphB receptors are known to facilitate excitatory synapse formation between axon terminals and dendrites (Henkemeyer et al., 2003; Lim

et al., 2008; Pasquale, 2008; Klein, 2012; Sheffler-Collins and Dalva, 2012; Yang et al., 2013), here I propose that presynaptic EphB2 may act as a repellent, preventing innervation between the inhibitory axon terminals of PV interneurons and pyramidal cells.

Impaired inhibition, including inhibitory synapse pathologies and PV interneuron hypofunction, as well as glial cell dysfunction, are common findings in many neurodevelopmental disorders (NDDs) (Petrelli et al., 2016; Ali Rodriguez et al., 2018; Filice et al., 2020; Contractor et al., 2021; Tan and Eroglu, 2021). Indeed, E/I imbalance is hypothesized to drive pathology in NDDs (Rubenstein and Merzenich, 2003). More specifically, impaired inhibition is thought to underlie the development of hyperactive neuronal networks in ASD and epilepsy (Sohal and Rubenstein, 2019; Tang et al., 2021). Dysfunctions in PV interneurons, including reduced density of PV interneurons, reduced PV expression, impaired PNN formation, and reduced PV cell activity have been observed in ASD, suggesting that PV interneurons may play a critical role in regulating E/I balance and the pathogenesis of NDDs (Lawrence et al., 2010; Hashemi et al., 2016; Contractor et al., 2021).

The goal of this study was to determine whether astrocytes regulate PV->PC connectivity through ephrin-B/EphB signaling. I targeted the postnatal day (P)14-P28 developmental period that is critical for PV interneuron development in the hippocampus (Contractor et al., 2021) and used loss- and gain-of-function approaches to regulate ephrin-B1 levels in astrocytes and EphB2 receptor expression in PV interneurons during this period. Functional and structural PV->PC connectivity was assessed through whole-

cell patch-clamp electrophysiology, optogenetics, immunohistochemical and biochemical analysis, seizure susceptibility assays and mouse behaviors. My findings elucidate a novel mechanism by which astrocytes regulate the establishment of PV->PC connections and control inhibitory circuit assembly in the developing hippocampus.

## 2.3 Methods

### *2.3.1 Ethics statement.*

All mouse studies were done according to National Institutes of Health and Institutional Animal Care and Use Committee at the University of California Riverside guidelines; animal welfare assurance #A3439-01 is on file with the Office of Laboratory Animal Welfare. Mice were maintained in an Association for Assessment and Accreditation of Laboratory Animal Care-accredited facility under 12 h light/dark cycle and fed standard mouse chow.

### *2.3.2 Mouse lines*

I used several mouse lines to analyze the effects of ephrin-B1 KO in astrocytes as follows: (1) ERT2-CreGFAP$^{+/+}$ephrin-B1flo$^{x/y}$ KO or ERT2-CreGFAP$^{-/-}$ephrin-B1flo$^{x/y}$ control mice were generated by breeding ephrin-B1$^{flox/flox}$ (129S-Efnb1 flox/+/J, RRID:IMSR_JAX:007664) mice with ERT2-CreGFAP$^{+/+}$ or ERT2-CreGFAP$^{-/-}$(B6.Cg-Tg(GFAP-cre/ERT2)505Fmv/J, RRID:IMSR_JAX: 012849) mice. (2) Thy1GFP-ERT2-CreGFAP$^{+/+}$ephrin-B1$^{flox/y}$ KO and Thy1GFP-ERT2-CreGFAP$^{-/-}$ephrin-B1$^{flox/y}$ control

male mice, in which GFP was expressed in excitatory cells of the hippocampus with active Thy1 promotors, were generated by crossing Thy1GFP mice (Tg(Thy1-EGFP)MJrs/J, RRID:IMSR_JAX:007788) with ERT2-CreGFAP$^{+/+}$ephrin-B1$^{flox/flox}$ KO or ERT2-CreGFAP$^{-/-}$ephrin-B1$^{flox/flox}$ control mice. (3) PV-tdTomato-CreGFAP$^{+/+}$ephrin-B1$^{flox/y}$ KO or PV-tdTomato ERT2-CreGFAP$^{-/-}$ephrin-B1$^{flox/y}$ control mice were generated by crossing C57BL/6-Tg(Pvalb-tdTomato)15Gfng/J mice (RRID:IMSR_JAX:027395) with ERT2-CreGFAP$^{+/+}$ephrin-B1$^{flox/flox}$ KO female or ERT2-CreGFAP$^{-/-}$ephrin-B1$_{flox/flox}$ female control mice. (4) Rosa-CAG-LSL-tdTomato reporter mice (CAG-tdTomato; RRID:IMSR_JAX:007909) were bred with ERT2-CreGFAP$^{+/+}$ or ERT2-CreGFAP$^{-/-}$ (B6.Cg-Tg(GFAP-cre/ERT2)505Fmv/J RRID:IMSR_JAX:012849) mice to generate tdTomatoERT2-CreGFAP mice first. Then, tdTomatoERT2-CreGFAP male mice were crossed with ephrin-B1$^{flox/flox}$ or with ephrin-B1$^{+/+}$ female mice to obtain either tdTomatoERT2-CreGFAPephrin-B1$^{flox/y}$ KO or tdTomatoERT2-CreGFAP control male mice, allowing for tdTomato expression in astrocytes and analysis of ephrin-B1 levels. All KO and control mice received tamoxifen at P14 intraperitoneally (0.5 mg in 5 mg/ml of 1:9 ethanol/sunflower seed oil solution) once a day for 5 consecutive days. Analysis was performed at P28 except for PTZ seizure tests at P48.

To achieve OE of ephrin-B1 in hippocampal astrocytes, adeno-associated viral particles (VPs) containing ephrin-B1 cDNA under GFAP promoter (AAV7.GfaABC1D.ephrin-B1.SV40) (referenced in the text as AAV-ephrin-B1) were stereotaxically injected into the hippocampus of P14 mice. Control AAV-tdTomato VP contained tdTomato cDNA under the same GFAP promoter

(AAV7.GfaABC1D.tdTomato.SV40). AAV-ephrin-B1 VP (final concentration 7.56 × 1012 VPs/ml) and control AAV-tdTomato VP (final concentration 4.46 × 1012 VPs/ml) were both obtained from UPenn Vector Core (http://www.med.upenn.edu/gtp/vectorcore) and processed as previously described58 with modifications. VPs were concentrated with Amicon ultra-0.5 centrifugal filters (UFC505024, Sigma Millipore) pretreated with 0.1% Pluronic F-68 nonionic surfactant (24040032, Thermo Fisher Scientific).

I used several mouse lines to analyze the effects of ephrin-B1 OE in astrocytes as follows: (5) ChR2-YFPflox/flox mice (Chr2-YFP:B6;129S-Gt(ROSA) 26Sortm32 (CAG-COP4pH134R/EYFP) Hze/J; RRID: IMSR_JAX#12569) were bred with mice expressing cre recombinase under the PV promotor (CrePV$^{+/+}$) (B6;129P2-Pvalbtm1(cre)Arbr/J; RRID: IMSR_JAX:017320) to obtain CrePV$^{+/-}$ChR2-YFP$^{+/-}$ mice expressing ChR2-YFP selectively in PV interneurons. This line was stereotaxically injected intrahippocampally with either AAV7.GfaABC1D.ephrin-B1.SV40 to overexpress astrocytic ephrin-B1 or AAV7.GfaABC1D.tdTomato.SV40 as a control and used for whole-cell recordings. (6) EphB2flox mice for conditional deletion of EphB2 using a Cre driver were generated by inserting the loxP site upstream of exon 2 and downstream of exon3 (Fig. S2.4). Deletion of this region should result in the loss of the ligand binding domain of EphB2 receptor. CrePV$^{+/+}$ mice (B6;129P2-Pvalbtm1(cre)Arbr/J; RRID: IMSR_JAX:017320) were bred with EphB2$^{flox/flox}$ mice to generate CrePV$^{+/-}$EphB2$^{flox/+}$ (heterozygous mice). Heterozygous mice were used for breeding to generate CrePV$^{+}$EphB2$^{flox/flox}$ (KO), CrePV$^{+}$EphB2$^{flox/+}$ (HET), or littermate controls which either did not express Cre or did not contain the floxed EphB2. Mice from

these groups were used for immunofluorescence staining analysis. Additionally, EphB2$^{flox/flox}$ (KO) mice were stereotaxically injected intrahippocampally with AAV7.GfaABC1D.ephrin-B1.SV40 to overexpress astrocytic ephrin-B1 and used for immunofluorescence staining analysis. (7) EphB2$^{flox/flox}$ line was also bred with ChR2-YFP$^{flox/flox}$ mice (Chr2-YFP:B6;129S-Gt(ROSA) 26Sortm32 (CAG-COP4pH134R/EYFP)Hze/J; RRID:IMSR_JAX#12569) to generate EphB2$^{flox/+}$ChR2-YFP$^{flox/flox}$ mice and were bred with CrePV$^{+/+}$EphB2$^{flox/+}$ mice to generate CrePV$^{+/-}$ EphB2$^{flox/flox}$ChR2-YFP$^{flox/+}$ (KO) or CrePV$^{+/-}$EphB2$^{+/+}$ChR2-YFP$^{flox/+}$ (control) mice. This line expressed ChR2-YFP but lacked EphB2 in PV interneurons and was used for whole-cell electrophysiology recordings. Additionally, CrePV$^{+/-}$EphB2$^{flox/flox}$ChR2-YFP$^{flox/+}$ (KO) mice were stereotaxically injected intrahippocampally with either AAV7.GfaABC1D.ephrin-B1.SV40 to overexpress astrocytic ephrin-B1 or AAV7.GfaABC1D.tdTomato.SV40 as a control and used for whole-cell recordings. Real-time PCR-based analysis of genomic DNA isolated from mouse tails was used to confirm genotypes for all mouse lines by Transnetyx.

*2.3.3 Surgery*

Mice were anesthetized with a ketamine/xylazine mixture (80 mg/kg ketamine and 10 mg/kg xylazine) given intraperitoneally. Paw pad pinch test, respiratory rhythm, righting reflex, and/or loss of corneal reflex were assessed to ensure the mice were adequately anesthetized. P14 B6/C57 mice (RRID:IMSR_JAX: 000664) received craniotomies (1 mm in diameter), and VPs were stereotaxic injected into the dorsal

hippocampus (1.8 mm posterior to bregma, 1.1 mm lateral to midline, and 1.3 mm from the pial surface; scaled to the appropriate coordinates based on bregma-lambda distance). Control mice were injected with 1 μl of 1.16 × 1013 VP/ml AAV-tdTomato, and OE animals were injected with 1 μl of 3.78 × 1013 VP/ml AAV-ephrin-B1. Prior to surgery, mice were injected subcutaneously with 3.25 mg/kg extended-release buprenorphine (Ethiqa XR) to manage pain. Additionally, mice received 5 mg/kg meloxicam every 12 h for pain management. Animals were allowed to recover for 14 d before analysis. P28 mice were used for immunohistochemistry, mRNA analysis, and whole-cell electrophysiology experiments. There was a significant increase in ephrin-B1 immunoreactivity in CA1 hippocampus on the injected ipsilateral side (OE) compared with noninjected contralateral control side (Fig. S2.1).

*2.3.4 Immunohistochemistry*

Immunohistochemistry was performed as described previously in Nguyen et. al. 2020 (Nguyen et al., 2020) with modifications. Animals were anesthetized with isoflurane and trancardially perfused with 0.1M PBS followed by fixation with 4% paraformaldehyde (PFA) in 0.1M PBS, pH 7.4. Brains were postfixed for 2 h or overnight at 4°C in either 2% or 4% PFA in 0.1M PBS. 100 μm coronal brain slices were obtained via vibratome sectioning. Samples were fixed for 30 min in 2% PFA, quenched with 50 mM NH4Cl, washed in 0.1% Tween in PBS (0.1% PBST), permeabilized in 0.1% Triton in PBS for 30 min, blocked for 2 h in 10% NDS, 1% BSA, and 0.1% Triton in PBS. Primary and secondary antibodies were diluted in the buffer containing 1%

normal donkey serum (NDS), 0.5% BSA, and 0.1% Triton in PBS. Primary antibodies were incubated overnight at 4°C. PV positive cells and boutons were immunolabled using mouse anti-PV antibody (1:500, Sigma-Aldrich, P3088, RRID:AB_477329). Inhibitory presynaptic sites were identified using rabbit anti-VGAT antibody (1:100, Synaptic systems, 131002, RRID:AB_887871). CB1R positive puncta were identified using rabbit anti-CB1R antibody (1 µg/mL, Immunogene, NM_007726.3). EphB receptors 1-4 were detected using rabbit anti-EphB(1-4) antibody (1:200, Abcam, ab64820, RRID:AB_2278009). Ephrin-B1 was detected using goat anti-ephrin-B1 antibody (1:50, R&D Systems, AF473, RRID:AB_2293419). Astrocytes were identified using rabbit anti-GFAP antibody (1:500, Cell Signaling Technology, 12389, RRID:AB_2631098). EphB2 was labeled using goat anti-EphB2 antibody (1:50, Invitrogen, PA5-47017, RRID:AB_2609043). Following incubation with primary antibodies, samples were washed in 0.5% PBST, then incubated in secondary antibodies diluted in the same buffer for 2 h at RT. The following secondary antibodies were used: Donkey anti-goat 488 IgG (1:500, Invitrogen, A-11055, RRID:AB_2534102), Donkey anti-rabbit 488 IgG (1:500, Invitrogen, A-21206, RRID:AB_2535792), Donkey anti-mouse 488 IgG (1:500, Invitrogen, A-21202, RRID:AB_141607), Donkey anti-mouse 594 IgG (1:500, Invitrogen, A-21203, RRID:AB_141633), Donkey anti-rabbit IgG 594 (1:500, Invitrogen, A-21207, RRID:AB_141637 ), Donkey anti-rabbit 647, IgG (1:500, Invitrogen, A-31573, RRID:AB_2536183) Donkey anti-goat 647, IgG (1:500, Invitrogen, A-21447, RRID:AB_2535864). Samples were washed in 0.5% PBST, followed by PBS,

then mounted on coverslips with Vectashield plus antifade mounting medium with Dapi (Vector Laboratories, H-2000).

*2.3.5 Confocal imaging and analysis.*

Confocal images of coronal brain slices containing the stratum oriens (SO), stratum pyramidal (SP), and stratum radiatum (SR) of the dorsal CA1 hippocampus were taken using Zeiss LSM 880 inverted laser scanning microscope and Zeiss LSM 880 upright laser scanning microscope. High resolution optical sections were acquired with a 20x air objective (0.8 NA), 1x zoom at 1 μm step intervals to measure PV, EphB, and Ephrin-B1 immunoreactivity. Confocal images of synaptic puncta and high magnification images of Ephrin-B1/EphB receptors, PV boutons, and GFP-labeled soma and dendrites were taken using an air 40× (1.2 NA) or oil 63x objectives, (1.4 NA), at 1x zoom, (1024x1024) or (2048x2048) pixel format, with 0.5 μm step size. Images were acquired and processed under identical conditions for analysis.

For analysis of PV/VGAT colocalization, images were analyzed using Neurolucida 360 (MBF Bioscience, RRID:SCR_016788) and Neurolucida Explorer software (MBF Bioscience, RRID:SCR_017348). Z-stacks were imported into Neurolucida, background subtracted, histogram equalized, and contrast was enhanced. Image stacks were trimmed in the Z plane to analyze stacks of an equal number of Z planes and contours were drawn around regions of interest (ROI) to be analyzed. 3D renderings were generated by rendering all VGAT puncta greater than 0.15 μm3 within the ROI, followed by rendering PV puncta that were at least 0.15 μm3-0.2 μm3 in size

and were at most 0.5-1 μm from a VGAT puncta. If the images contained background VGAT somatic staining, puncta rendered in the soma were removed prior to rendering PV boutons. Images were analyzed in Neurolucida explorer by selecting puncta within the ROI and measuring the total number of puncta as well as the number of colocalized puncta using the puncta feature. The number of colocalized puncta was normalized to the 3D volume.

For analysis of PV/VGAT colocalization in close proximity to Thy1-GFP excitatory cells in Neurolucida, images were processed as described above, excitatory cells were rendered using soma and tree tracing, then VGAT and PV boutons within 1 μm of the cell that were at least 0.15 μm3 in size were rendered using the puncta feature. Renderings were analyzed in Neurolucida 360 by selecting the soma or dendrites and analyzing the number of colocalized puncta near the selected soma or dendrite. The number of colocalized PV/VGAT puncta was normalized to the volume of the selected soma or dendrite.

Analysis of CB1R puncta was performed using ImageJ software (RRID:nif-0000-30467) with similar methods as previously described in Nguyen et al. 2020 (Nguyen et al., 2020). Z-stacks of equal size were collapsed into a single image by projection, converted to a tiff file, and background subtracted. Next, each image was threshold-adjusted using default auto threshold and converted into a binary image. The watershed function was used to segment overlapping puncta. ROIs were drawn around the SP and SR layers of the CA1 hippocampus and the number of puncta was counted using the particle analysis tool, where puncta of 0.5-10 μm2 in size were analyzed.

Analysis of EphB/PV puncta colocalization in the SP was performed in Neurolucida Software. Z-stacks were imported into Neurolucida, background subtracted, histogram equalized, and contrast was enhanced. Image stacks were trimmed in the Z plane to analyze stacks of an equal number of Z planes and contours were drawn around regions of interest (ROI) to be analyzed. 3D renderings of PV boutons of at least 0.15 μm3 and EphB puncta of at least 0.05 μm3 were generated in Neurolucida and then renderings were analyzed in Neurolucida 360 by selecting puncta within the ROI, measuring the total number of puncta and the number of colocalized puncta using the puncta feature, then normalizing to the 3D volume.

Analysis of EphB puncta on PV soma was performed in Image J as described above. Z-stacks of equal size were collapsed into a single image by projection, converted to a tiff file, and background subtracted. Each image was threshold-adjusted, converted into a binary image, the despeckle function was used to eliminate noise and the watershed function was used to segment overlapping puncta. ROIs were drawn around PV soma and the number of puncta per soma was counted using the particle analysis tool, where puncta of at least 0.1 μm2 in size were analyzed. The number of puncta was normalized to the area of each soma.

Analysis of EphB2 and PV immunofluorescence levels in PV interneurons was performed in ImageJ software. For EphB2 analysis, single image planes were separated by channel, ROIs were drawn around PV somata and then EphB2 mean fluorescence intensity levels within the ROIs were measured. Background signal was measured using a secondary only control and then was subtracted from the fluorescence intensity

measurement. For PV analysis, Z-stacks of equal size were collapsed into a single image by projection and converted to a tiff file. ROIs were drawn around PV soma and then PV mean fluorescence intensity levels within the ROIs were measured.

*2.3.6 Western blot analysis*

Hippocampal tissues from P28 control or KO mice were homogenized in RIPA lysis buffer (50 mM Tris-HCl, pH 7.4; 150 mM NaCl; 1 mM EDTA, pH 8.0; 1% Triton X-100; 0.1% SDS; 1% protease inhibitor cocktail (P8340, Sigma Millipore); 0.5 mM sodium orthovanadate) incubated for 1 h at 4°C. Samples were cleared by centrifugation at 12,000 g for 20 min at 4°C and added to 2× Laemmli Buffer (S3401, Sigma Millipore), boiled for 10 min, then run on an 8%-16% Tris-glycine Gel (XP08160, Invitrogen). Protein samples were transferred onto a nitrocellulose blotting membrane (10600007, GE Healthcare). Blots were blocked with 5% milk in TBS or for phosphorylated proteins 5% BSA in TBS (1 0mM Tris, 150 mM NaCl, pH 8.0), followed by immunostaining with mouse β-actin (1:1000, Santa Cruz Biotechnology, sc-47778, RRID:AB_626632), rabbit anti-Nrg1-type III (1 μg/ml, Abcam, ab23248, RRID:AB_2154667), rabbit anti-ErbB4 (1:1000, Cell Signaling Technology, 4795, RRID:AB_2099883), rabbit anti-ErbB4 (phospho Y1284) (1:1000, Abcam, ab109273, RRID:AB_10866384), or mouse CB1R (1 μg/mL, Immunogenes, NM_007726.3) diluted in 0.1% Tween 20/TBS (TBST) + 1% BSA at 4°C overnight. Blots were washed in TBST, 3x10 min. Then, blots were incubated with HRP-conjugated secondary antibodies donkey anti-mouse IgG (Jackson ImmunoResearch Laboratories, 715-035-150, RRID:AB_2340770) or HRP-conjugated goat anti-rabbit IgG (Jackson ImmunoResearch Laboratories, 111-035-003,

RRID:AB_2313567) diluted in TBST + 1% BSA. Following incubation with secondary antibodies, blots were washed in TBST, 3x10 min. Then, blots were incubated in Pierce ECL western Blotting Substrate (Thermo Fisher Scientific, 32106) and a signal was collected with Biorad ChemiDoc Imaging System (RRID:SCR_021693), with one image taken per min for a period of 20 min-1 h. Band intensity was analyzed by measuring the intensity of the band and subtracting the background intensity using FIJI.

*2.3.7 RNA analysis*

P28 mouse brains were dissected on ice in DEPC-treated PBS. Following dissection, total RNA was acutely isolated using Invitrogen PureLink RNA Mini Kit (ThermoFisher Scientific/Invitrogen, 12183020). Samples were lysed in RNA lysis buffer with β-mercaptoethanol (BME) added as described in the protocol provided by the kit. Tissue samples were homogenized in a lysis buffer using a pestle and then were passed through an 18-gauge needle. Following lysis, samples were centrifuged at 12,000 g for 2 min and the supernatants were transferred to fresh tubes. RNA isolation was then performed according to the manufacturer's instructions. Samples were eluted in nuclease free water, and RNA concentration and purity was determined using a Nanodrop spectrophotometer (RRID:SCR_016517). Samples were diluted to equal concentrations in nuclease free water. cDNA was synthesized using a High-Capacity cDNA Reverse Transcription Kit (Applied Biosystems, 4368814). qRT-PCR was performed using PowerSYBR Green PCR Master Mix (Applied Biosystems, 4367659) on Quantstudio 6 Flex System thermocycler (Applied Biosystem/Life Technologies, RRID:SCR_020239).

Data was normalized to GAPDH loading control and then analyzed using ΔΔCt method normalized to GAPDH housekeeping gene. Primer sequences are listed in supplemental materials (Fig. S2.5).

*2.3.8 Nanostring*

Half-brains were dissected and frozen in liquid nitrogen and stored in -80°C until use. RNAlater Ice (Invitrogen AM7030) was used to thaw samples according to manufacturer's instructions. Hippocampal tissue was dissected in DEPC-treated PBS on ice and then RNA isolation proceeded as described above. Samples were eluted in nuclease free water. To remove any residual salts or contaminants from buffers used during RNA isolation, RNA samples were further purified by ethanol precipitation as follows; 0.1 volumes of 0.3M Na-Acetate and 3 volumes of ice-cold 100% ethanol were added to the samples. Samples were incubated at -20°C overnight, centrifuged at 12,000 g, and then ethanol was removed. Samples were analyzed using Agilent 2100 Bioanalyzer/Advanced Analytics Fragment Analyzer (RRID:SCR_018043). RIN values above 7 were considered to be adequate for Nanostring profiling. RNA samples were analyzed using nCounter Mouse Glial Profiling Panel (Nanostring, XT-CSO-M-GLIAL-12) according to manufacturer's instructions. Briefly, 50 ng of unamplified RNA was hybridized with the reporter codeset at 65°C for 18 h. Samples were spun down, nuclease free water was added to the samples, and then the samples were loaded into the nCounter cartridge. The cartridge was run on the Nanostring nCounter SPRINT Profiler (RRID:SCR_021712). Data was exported and analyzed using Nanostring nSolver and

Advanced Analysis Software (RRID:SCR_021712). Normalized linear counts for all genes in the panel were used in fold change analysis of control and KO genes.

*2.3.9 Whole cell patch clamp recordings*

Animals were anesthetized with isoflurane, brains were dissected and 300 μm coronal sections were sliced in ice-cold sucrose containing ACSF containing (in mM) CaCl2 2.5, sucrose 196.6, KCl 2.5, MgSO4 1.3, NaH2PO4 1, NaHCO3 26.2, (D)-Glucose 11, Kyneuric acid 3, Na-Pyruvate 2, MOPS 3.5. Slices were incubated in ice cold sucrose ACSF for 30 min. Slices were then transferred to ACSF containing (in mM) NaCl 126, KCl 2.5, D-glucose 10, NaH2PO4 1.25, MgCl2 2, CaCl2 2, NaHCO3 26 and allowed to incubate for 45 min at room temperature. Slices were transferred to a recording chamber and continuously perfused with oxygenated ACSF at a flow rate of 1 ml/min at 31˚C and allowed to equilibrate to the chamber for at least 10 min.

Whole-cell patch experiments were conducted blind, with experimental procedures described in Castaneda-Castellanos, 2006 (Castañeda-Castellanos et al., 2006). Blind, whole-cell patch clamp recordings were obtained from CA1 pyramidal neurons using pipettes made from glass capillaries pulled by Narishige PC-10 vertical micropipette puller (Narishige, RRID:SCR_022057). Pipette resistance ranged from 3-5 mOhms and were filled with high-chloride internal solution containing (in mM) KCl 125, K-gluconate 10, MgCl2 2, EGTA 0.2, HEPES 10, Mg2ATP 2, Na2GTP 0.5, PO Creatine 10, QX-314 10, and 0.2% biocytin for postlabeling and was pH adjusted to 7.2 with KOH. CA1 hippocampal neurons were voltage clamped and held at -60 mV. Due to high-

chloride internal solution and negative holding potential, inhibitory currents were measured as inward currents. Pyramidal cells were voltage clamped at -60 mV and inhibitory postsynaptic currents were recorded in response to photoactivation.

PV interneurons were optically stimulated using a fiber-coupled LED light of 470 nm wavelength (Thorlabs, LEDD1B). A cannula was attached to the fiber-optic cable in order to submerge the light source into the bath and place the light source directly over the slice. Input-output curves were generated using a fixed duration of light pulse (5 ms) and increasing the intensity of the LED power. 12 sweeps with increasing intensity of the LED light source were used (starting at approximately 0.13 mW and increasing up to 4 mW of power) to photoactivate PV interneurons and to record IPSCs in pyramidal cells. 20 Hz stimulation was also used in order to analyze short-term plasticity, where oeIPSC amplitudes were measured from the original baseline prior to stimulation to the peak of each oeIPSC in the train. I used a 5 ms LED pulse followed by 45 ms of LED off at 100% LED power in this protocol. oeIPSCs were recorded using a HEKA EPC-9 amplifier (HEKA Elektronik), filtered at 1 kHz, and digitized at 10 kHz. Series resistance was compensated and was monitored throughout the experiment by delivering 5 mV voltage steps. Data was discarded if the series resistance changed >20% during the course of an experiment. Data was analyzed on HEKA Electronik software and statistical significance was analyzed using Prism 10 software (GraphPad Software, RRID:SCR_002798 ).

*2.3.10 PTZ Seizure Test*

Before testing, mice were housed in a room with a 12 h light/dark cycle with ad libitum access to food and water. The cages were transferred to the behavioral room for 30 min habituation prior to the test. Between tests, the cages were cleaned with 2%-3% acetic acid, 70% ethanol, and water to eliminate odor trails. Pentylenetetrazole (PTZ) (Sigma, P6500) was diluted in 0.9% sodium chloride injection diluent (Hospira Inc, NDC-0409-4888-03) to make a stock solution of 5 mg/ml PTZ. For each mouse, a 20 mg/kg dose was made in 50 µl saline, a 30 mg/kg dose was made in 50 µl saline, and a 40 mg/kg dose was made in 100 µl saline, based on the weight of the mouse. Each mouse received three doses of PTZ over the 5 h testing period that were delivered via IP injection. At time (t)=0 h mice received a 50 µl, 20 mg/kg dose of PTZ and were recorded for one hour. At t=2 h, mice received a 50 µl, 30 mg/kg dose of PTZ and were recorded for 1 h. At t=4 h, mice received a 100 µl, 40 mg/kg dose of PTZ and were recorded for 1 h. Data was analyzed based on the Racine seizure score as described in Shimada and Yamagata 2018 (Shimada and Yamagata, 2018). Videos were manually scored by an experimenter blind to the condition as follows: score 0 - absence of seizure activity; score 1 - immobilization, lying flat on abdomen; score 2 - head nodding, facial, forelimb, or hindlimb myoclonus; score 3 - continuous whole-body myoclonus, myoclonic jerks, tail held up stiffly; score 4 - tonic-clonic seizure, rearing and falling; score 5 - tonic-clonic seizure, loss of postural tone, wild rushing and jumping; score 6 - death.

*2.3.11 Behavior*

Home cage behaviors were analyzed as described by Reinhard, Rais et al. 2019 (Reinhard et al., 2019) with modifications. Mice were placed in new cages with fresh bedding and recorded for 30 min. Videos were manually scored by an experimenter blind to the condition. The video was paused at 10 s intervals for the first 10 min of the recording and the observer recorded if the mouse was performing any of the following: motion, rearing, digging, grooming, or scanning.

*2.3.12 Experimental Design and Statistical Analyses*

For PV/VGAT colocalization in the SP: Statistical analysis was performed using GraphPad Prism 10 software (RRID:SCR_002798). Astrocytic ephrin-B1 OE mice were analyzed by paired two-tailed t-tests, 5 male mice with 10 images per group. Astrocytic ephrin-B1 KO and CON mice were analyzed using a two-tailed t-test, 3 KO and 3 CON male mice per group with 6 images per group. PV-EphB2 control, heterozygous, and KO male and female mice were analyzed by Brown-Forsythe and Welch ANOVA test in GraphPad Prism 10 software (RRID:SCR_002798), n=5-13 mice per group, 19-46 images per group. PV-EphB2 KO+AAV-EfnB1 male and female mice were analyzed by paired two-tailed t-tests, n=22 images/group, 6 mice. For analysis of PV/VGAT near Thy1-GFP excitatory neurons: Statistical analysis was performed using GraphPad Prism 10 software (RRID:SCR_002798) using Welch-corrected two-tailed t-tests, 4 male mice per group, 13-18 images per group. For analysis of CB1 puncta in SP: Statistical analysis was performed using GraphPad Prism 10 software (RRID:SCR_002798) using two-tailed

t-tests, n=3-4 male mice per group, 9-15 images per group. For analysis of PV/EphB puncta in the SP: Statistical analysis was performed using GraphPad Prism 10 software (RRID:SCR_002798) using two-tailed t-test (CON/KO) or paired two-tailed t-test (OE mice), 3-4 male mice per group, 8-16 images per group. For analysis of EphB puncta on PV somata: Statistical analysis was performed using GraphPad Prism 10 software (RRID:SCR_002798) using two-tailed t-test (CON/KO) or paired two-tailed t-test (OE mice), 3-4 male mice per group, 21-25 PV interneurons per group. PV and EphB2 intensity in PV interneurons: Statistical analysis was performed using GraphPad Prism 10 software (RRID:SCR_002798). Paired two-tailed t-test (OE) and two-tailed t-test (CON/KO) were used for analysis of PV intensity in PV interneurons of astrocytic ephrin-B1 OE (3 OE male mice per group with 19-27 cells per group) and KO mice (4 male mice per group with 23-24 cells per group). Brown-Forsythe and Welch ANOVA with Dunnett's multiple comparisons test were used for analysis of PV intensity in PV interneurons of PV-EphB2 control, heterozygous, or KO male and female mice (72-165 cells per group, 4-13 mice per group). Welch's t-test was used for analysis of EphB2 levels in PV interneurons of PV-EphB2 KO and control male and female mice (n=3-4 mice per group, 50-57 cells per group). Western Blot: Statistical analysis was performed with unpaired two-tailed t-test using GraphPad Prism 10 software (RRID:SCR_002798), n=3-4 male mice per group. pRT-PCR: Statistical analysis performed in GraphPad Prism 10 software using two-tailed t-test or two-tailed t-test with Welch correction, n=3-4 male mice per group. Nanostring: Normalized linear counts for all genes in the panel were used in fold change analysis of control and KO genes. Statistical analysis performed in

GraphPad Prism 10 software using two-tailed t-test or two-tailed t-test with Welch correction, n=3-4 male mice per group. Electrophysiology: Unpaired Student's two-tailed t-test was used to analyze peak oeIPSC amplitude and Two-way ANOVA with Sidak's multiple comparisons post-hoc test was used to analyze oeIPSC amplitude against LED power, oeIPSCs over 20 Hz trains, and paired pulse ratios. AAV-EfnB1/AAV-TdTomato male and female mice: 8-11 cells per group, 7-8 mice per group. PV/EphB2 KO/CON male and female mice: 18 cells per group, 7-9 mice per group. PV/EphB2 KO+AAV-EfnB1/PV/EphB2 KO+AAV-TdTomato male and female mice: 9-12 cells per group, 5-6 mice per group. PTZ seizures: Statistical analysis was performed using GraphPad Prism 10 software. Latency to tonic-clonic seizure was analyzed by two-tailed t-test, seizure duration was analyzed with two-tailed t-test or Mann-Whitney test, and the number of seizure events was analyzed with Mann-Whitney test, 8-12 male mice per group. Home cage behaviors: Statistical analysis was performed using GraphPad Prism 10 software using Mann-Whitney tests, 12 male mice per group.

## 2.4 Results

### *2.4.1 Astrocytic ephrin-B1 promotes functional connectivity between PV and pyramidal cells.*

To test if astrocytes regulate the development of functional inhibitory connections between PV interneurons and pyramidal neurons via EphB receptor signaling, I overexpressed the EphB receptor ligand, ephrin-B1, in astrocytes during the early

postnatal P14-P28 developmental period. I overexpressed ephrin-B1 in hippocampal astrocytes of P14 male and female mice by injecting AAV7.GfaABC1D.ephrin-B1.SV40 (AAV-EfnB1) into the hippocampus, while vehicle-injected controls received AAV7.GfaABC1D.tdTomato.SV40 (AAV-TdTomato)(Fig. 2.1A). PV->PC connectivity was tested at P28+/-2D using whole-cell voltage clamp electrophysiology in combination with an optogenetic approach to selectively activate PV-expressing interneurons. PV interneurons expressing ChR2-YFP were optogenetically activated using 470 nm LED light and optically evoked, gabazine-sensitive inhibitory postsynaptic currents (oeIPSCs) were recorded in CA1 pyramidal cells of astrocytic ephrin-B1 OE mice and vehicle-injected control mice (Fig. 2.1B, Fig. S2.2). Input-Output (IO) curves were generated by delivering LED light pulses with increasing LED power at a fixed pulse length and the maximum responses were analyzed to measure peak oeIPSC amplitude (Fig. 2.1C-E). I observed a significant effect of LED power and interaction of genotype and LED power (Fig. 2.1D; Extended Data Two-Way ANOVA, Sidak's multiple comparisons test, $F(11,231)=2.684$, $p=0.0029$). In addition, overexpression of ephrin-B1 in astrocytes significantly increased the peak oeIPSC amplitude, suggesting that astrocytic ephrin-B1 positively regulates PV->PC functional connectivity (Fig. 2.1E, Extended Data; t-test, $t(21)=2.303$, $p=0.0316$). To test if astrocytic ephrin-B1 also affects short-term plasticity at PV->PC synapses, PV interneurons were optically stimulated with a 20 Hz train of ten LED light pulses at maximal LED power (Fig. 2.1F). I observed a significant increase in the average oeIPSC amplitude during the first two stimulations in the OE group, consistent with the increased strength of the functional connections between PV

interneurons and CA1 PCs following the overexpression of astrocytic ephrin-B1 (Fig. 2.1G; Extended Data; Two-Way ANOVA, $F(1,17)=4.221$, $p=0.0556$; Sidak's multiple comparisons post-hoc test, $p<0.0001$, $p= 0.0237$). However, the increase in oeIPSC amplitude was not accompanied by any significant difference in the paired pulse ratio (PPR) of the oeIPSCs, calculated as a ratio of the oeIPSC amplitude for each pulse to the first oeIPSC amplitude (Fig. 2.1H; Extended Data; Two-Way ANOVA, Sidak's multiple comparisons post-hoc test, $F(1,17)=0.3607$, $p=0.5560$), suggesting no differences in release probability. My data suggest that the observed increase in the strength of PV->PC connectivity following overexpression of ephrin-B1 in astrocytes is most likely a result of increased PV->PC synapse number or their strength.

*2.4.2 Astrocytic ephrin-B1 boosts the development of PV-specific presynaptic inhibitory sites.*

To test if levels of astrocytic ephrin-B1 affect the development of structural PV-positive inhibitory synapses during the P14-P28 period, I analyzed the density of PV-positive inhibitory presynaptic sites in the pyramidal (SP) layer of the CA1 hippocampus with immunostaining. Astrocytic ephrin-B1 was overexpressed in hippocampal astrocytes at P14 (Fig. 2.1A), and analysis was done at P28 with the contralateral, uninjected side used as a control. To delete ephrin-B1 from astrocytes, ephrin-B1 floxed mice expressing ERT2-Cre under the GFAP promoter were injected with 5 IP doses of tamoxifen starting at P14 and tamoxifen-injected controls lacking floxed ephrin-B1 were used as the controls. At P28, PV-positive presynaptic sites were detected with antibodies against PV

and vesicular GABA transporter (VGAT) in brain slices from mice overexpressing astrocytic ephrin-B1, lacking astrocytic ephrin-B1, and their respective controls (Fig. 2.1I-J). Overexpression of astrocytic ephrin-B1 increased the number of PV/VGAT colocalized puncta in the SP (Fig. 2.1K; Extended Data; paired t-test, $t(4)=2.789$, $p=0.049$), whereas deletion of astrocytic ephrin-B1 reduced the number of PV/VGAT colocalized puncta in the SP (Fig. 1L; Extended Data; t-test, $t(10)=2.841$, $p=0.0175$; Fig. 2.1O). Interestingly, PV intensity was not significantly different in OE (Fig. 2.1M; Extended Data; t-test, $t(44)=1.616$, $p=0.1132$) or KO groups (Fig. 2.1N; Extended Data; t-test, $t=(45)1.247$, $p=0.2187$). The data suggest that astrocytic ephrin-B1 positively regulates the establishment of PV-positive presynaptic sites in the CA1 hippocampus during development.

*2.4.3 Deletion of astrocytic ephrin-B1 impairs Nrg-ErbB4 signaling.*

If the number of PV-positive synaptic sites and the strength of PV->PC connectivity are affected by the level of ephrin-B1 in astrocytes, then I would also expect changes in Nrg1-ErbB4 signaling, which has been implicated in basket and chandelier cell connectivity with excitatory cells (Vullhorst et al., 2009; Fazzari et al., 2010; del Pino et al., 2013; Yang et al., 2013; Exposito-Alonso et al., 2020). Therefore, I next examined mRNA and protein levels of Nrg1 and ErbB4 in the P28 hippocampus following ephrin-B1 deletion from P14 astrocytes using qRT-PCR, Nanostring, and western blot analysis. Deletion of astrocytic ephrin-B1 did not affect mRNA levels of Nrg-1 (Fig. 2.2A; Extended Data, t-test, Welch correction, $t(3.288)=0.5067$, $p=0.6444$) or

ErbB4 (Fig. 2.2A; Extended Data, t-test, t(4)=1.217, p=0.2906). Protein levels of Nrg1 (Fig. 2.2B-C; Extended Data; t-test, t(6)=0.1659, p=0.8737) and ErbB4 (Fig. 2.2D-E; Extended Data; t-test, t(4)=1.027, p=0.3625) were also unchanged, however the active, phosphorylated form of ErbB4 was significantly reduced following deletion of astrocytic ephrin-B1 (Fig. 2.2D-E; Extended Data; t-test, t(4)=3.526, p=0.0243), suggesting that loss of astrocytic ephrin-B1 impaired Nrg-ErbB4 signaling. As Nrg-ErbB4 signaling also plays a role in establishing connections between pyramidal cells and CCK basket cells, which express CB1R in their axon terminals, I also analyzed CB1R mRNA and protein levels. Although I found CB1R mRNA levels to be significantly increased in KO mice compared to controls (Fig. 2.2A; Extended Data, t-test, t(6)=3.442, p=0.0138), there was no difference at the protein level (Fig. 2.2B-C; Extended Data; t-test, t(6)=0.1607, p=0.8776). My data suggest that the changes in Nrg-ErbB4 signaling is most likely a result of altered PV->PC but not CCK->PC connectivity.

### *2.4.4 Inhibitory innervation of CA1 pyramidal neurons by PV interneurons but not CCK cells is reduced following developmental deletion of astrocytic ephrin-B1.*

To examine if somatic innervation of CA1 pyramidal cells was specifically disrupted by the deletion of ephrin-B1 in astrocytes, I analyzed the innervation of soma and dendrites of CA1 pyramidal cells by PV and CCK cells. PV-positive presynaptic sites onto GFP-expressing CA1 pyramidal neurons were detected using immunostaining against VGAT and PV. I observed a significant reduction in the number of colocalized PV/VGAT presynaptic sites on both SO dendrites (Fig. 2.2K; Extended Data; Welch-

corrected t test, t(21.21)=2.277, p=0.0332) and somata (Fig. 2.2L; Extended Data; Welch-corrected t test, t(17.37)=2.290, p=0.0348) of CA1 pyramidal neurons in the hippocampus of P28 ephrin-B1 KO mice compared to controls. To address whether the connectivity between CB1R-expressing CCK-positive basket cells and the somata of CA1 pyramidal cells was also affected by loss of astrocytic ephrin-B1, CB1R puncta were detected with immunofluorescence staining and the number of CB1R puncta was analyzed in the SP layer of the CA1 hippocampus. There was no significant difference in the number of CB1R puncta in the SP (Fig. 2.2O; Extended Data; t-test, t(5)=0.0202, p=0.9847). The data indicate that developmental deletion of astrocytic ephrin-B1 reduces the number of PV-positive structural synapses formed onto both SO dendrites and somata of CA1 excitatory neurons and suggests that PV->PC but not CCK->PC connectivity is regulated by levels of astrocytic ephrin-B1.

*2.4.5 Deletion of astrocytic ephrin-B1 increases seizure susceptibility and repetitive behaviors.*

To assess whether alterations in PV mediated inhibition of CA1 pyramidal neurons led to functional changes in astrocytic ephrin-B1 KO mice, I examined their susceptibility to seizures induced by pentylenetetrazole (PTZ), a $GABA_A$ receptor antagonist (Fig. 2.3A). Indeed, P48 mice lacking astrocytic ephrin-B1 were more susceptible to PTZ induced seizures and exhibited robust seizures in response to PTZ at a 30 mg/kg dose, while only 25% of the controls seized during the duration of the test. The latency to seizure was also significantly reduced in KO mice (Fig. 2.3B; Extended Data;

t-test, t(18)=4.439, p=0.0003), while the duration (Fig. 2.3C; Extended Data; t-test, t(16)=2.166, p=0.0458) and maximum seizure score (Fig. 2.3D; Extended Data; Mann-Whitney test, DoF(18), MWU=17, p=0.0044) were significantly increased compared to controls. The increased maximum score was due to an increase in the number of stage 4 (Fig. 2.3F; Extended Data; Mann-Whitney test, DoF(16), MWU=20, p=0.0359) and stage 5 events in KO mice compared to controls (Fig. 2.3F; Extended Data; Mann-Whitney test, DoF(18), MWU=16, p=0.0044). In addition, I found that astrocytic ephrin-B1 KO mice showed a significant increase in digging behavior (Fig. 2.3J; Extended Data; Mann-Whitney test, DoF(21), MWU=16.5, p=0.0013), which can be interpreted as repetitive behavior. Together, the data suggest that impaired inhibition following the deletion of astrocytic ephrin-B1 is most likely responsible for increased susceptibility, duration, and severity of PTZ induced seizures, as well as exacerbated repetitive behaviors.

*2.4.6 Astrocytic ephrin-B1 controls localization of EphB in PV boutons but not PV soma.*

To test whether astrocytic ephrin-B1 controls PV->PC connectivity through regulating EphB signaling in PV interneurons, I tested if changes in astrocytic ephrin-B1 levels would affect EphB receptor localization using immunofluorescence staining against PV and pan-EphB (EphB1-4, Fig. 2.4A-B). Although neither overexpression (Fig. 4C; Extended Data; paired t-test, t(3)=0.4911, p=0.6570) nor deletion (Fig. 2.4F; Extended Data; t-test, t(5)=0.0064, p=0.9951) of astrocytic ephrin-B1 affected the total number of EphB puncta in the SP layer of the CA1 hippocampus, levels of astrocytic ephrin-B1 influenced the association of the EphB immunoreactive puncta with PV

boutons (Fig. 2.4D,G). Overexpression of astrocytic ephrin-B1 reduced PV/EphB colocalization in the SP layer compared to the contralateral side of the same brain slice (Fig. 2.4D; Extended Data; paired t-test, $t(3)=4.052$, $p=0.0271$), while deletion of astrocytic ephrin-B1 increased PV/EphB colocalization compared to controls (Fig. 2.4G; Extended Data; t-test, $t(5)=5.677$, $p=0.0024$). Analysis of EphB receptors on the somata of PV interneurons did not show any significant changes in EphB-positive puncta number in OE mice (Fig. 2.4E; Extended Data; paired t-test, $t(2)=0.4047$, $p=0.7249$) and in KO mice (Fig. 2.4H; Extended Data; Welch's t-test, $t(2.611)=3.058$, $p=0.0781$). Altogether, the results show that levels of astrocytic ephrin-B1 did not significantly alter EphB receptor localization on the somata of PV interneurons, but instead specifically affected its localization in PV boutons. Reduced levels of EphB/PV colocalization in presynaptic boutons coincided with increased PV->PC connectivity in OE mice and increased EphB/PV colocalization in presynaptic boutons coincided with reduced PV->PC connectivity in KO mice. Therefore, I hypothesize that EphB signaling in PV boutons negatively regulates the establishment of inhibitory PV->PC contacts, and astrocytic ephrin-B1 controls PV->PC connectivity by directly regulating the localization of the EphB receptors in PV boutons but not on PV somata.

### *2.4.7 Deletion of EphB2 from PV interneurons enhances PV->PC functional connectivity.*

To test the hypothesis that EphB signaling in PV boutons negatively regulates PV->PC connectivity, I generated a mouse line in which EphB2 receptor was specifically

targeted in PV interneurons (PV-EphB2 KO mice) by crossing PV-Cre and EphB2-floxed mice (Fig. 2.5A,B; Fig. S2.4). Brain slices from P28 control and PV-EphB2 KO mice were immunolabeled against PV and EphB2. I observed a significant reduction in the levels of EphB2 immunoreactivity in PV interneurons (Fig. 2.5C; Extended Data; Welch's t-test, $t(96.88)=3.817$, $p=0.0002$). The presence of residual immunoreactivity may be due to a non-specific detection of other EphB receptors in PV interneurons. As before, I used whole-cell voltage clamp electrophysiology in combination with optogenetics to measure PV specific oeIPSCs in CA1 pyramidal cells of control and PV-EphB2 KO mice at P28±2D. PV interneurons expressing ChR2-YFP, but lacking both copies of EphB2 were optogenetically stimulated using 470 nm LED light and responses were recorded in CA1 pyramidal cells. Deletion of EphB2 from PV interneurons significantly increased the oeIPSC amplitude as a function of increased LED power (Fig. 2.5D,E; Extended Data; Two-Way ANOVA, Genotype difference: $F(1,34)=4.484$, $p=0.0416$; LED-Genotype interaction: $F(11,374)=2.946$, $p=0.0009$, Sidak's multiple comparisons post-hoc test, $*p<0.05$). The peak oeIPSC amplitude was also significantly increased in PV-EphB2 KO mice compared to controls (Fig. 2.5F; Extended Data; t-test, $t(34)=2.188$, $p=0.0357$). The data indicate that deletion of EphB2 from PV interneurons enhances the strength of PV->PC functional connectivity. The significant enhancement of oeIPSC amplitude was also observed in PV-EphB2 KO mice during the first stimulation in a 20 Hz train (Fig. 2.5H; Extended Data; Two-Way ANOVA, Genotype difference: $F(1,34)=1.741$, $p=0.195$, Stim: $F(9,306)=93.98$, $p<0.0001$, Interaction: $F(9,306)=2.473$, $p=0.0098$, Sidak's multiple comparisons post-hoc test, $*p<0.05$), but I observed no

differences in PPR between the groups (Fig. 2.5I; Extended Data; Two-Way ANOVA, Genotype difference: $F(1,34)=0.4691$, $p=0.4980$, Stim: $F(8,272)=121.8$, $p<0.0001$, interaction: $F(8, 272)=1.767$, $p=0.0836$, Sidak's multiple comparisons post-hoc test), suggesting that deletion of EphB2 from PV interneurons enhanced functional PV->PC connectivity without changing the presynaptic release probability, most likely due to an increased number or strength of PV->PC synapses.

*2.4.8 Deletion of EphB2 receptors from PV interneurons enhances PV->PC structural connectivity.*

To test if levels of EphB2 in PV interneurons affect the number of PV-positive inhibitory synapses during P14-P28 period, I analyzed the density of PV-positive inhibitory presynaptic sites in the pyramidal (SP) layer of the CA1 hippocampus by immunolabeling hippocampal slices against PV and VGAT (Fig. 2.5J-L). Deletion of one or both copies of EphB2 in PV interneurons was sufficient to increase PV immunoreactivity in PV interneurons (Fig. 2.5M; Extended Data; Brown-Forsythe and Welch ANOVA; $F(2.0,202.7)=13.5$, $p<0.0001$; Dunnett's multiple comparisons test, CON-HET: $p=0.0012$, CON-KO: $p<0.0001$, **$p<0.01$, ****$p<0.0001$). As PV expression is activity dependent and thought to correlate with PV cell activity and maturation (Donato et al., 2013; Page et al., 2019), PV interneuron activity or maturation may be negatively regulated by EphB2 expression in PV interneurons. Mice lacking both copies of EphB2 in PV interneurons also showed a significant increase in the number of PV/VGAT presynaptic sites in the SP compared to controls, while deletion of one copy

of EphB2 in PV interneurons had no significant effect (Fig. 2.5N; Extended Data; Brown-Forsythe and Welch ANOVA; F(2.0,32.24)=1.837, p=0.1756; Dunnett's multiple comparisons test, CON-HET: p=0.5407, CON-KO: p=0.0486, *p<0.05). The results suggest that EphB2 signaling in PV interneurons may negatively regulate PV->PC connectivity and that loss of both copies of EphB2 gene is sufficient to promote the development of PV->PC synapses.

*2.4.9 Astrocytic ephrin-B1 overexpression does not further enhance PV->PC connectivity in mice lacking EphB2 in PV interneurons.*

If astrocytic ephrin-B1 regulates PV->PC connectivity through controlling EphB2 signaling in PV boutons, I expect that overexpression of astrocytic ephrin-B1 in mice lacking EphB2 in PV interneurons should not further enhance PV->PC connectivity. To test this hypothesis, I performed whole-cell voltage clamp electrophysiology recordings to measure PV-specific oeIPSCs in CA1 pyramidal cells of PV-EphB2 KO mice injected with AAV-ephrin-B1 to overexpress ephrin-B1 in astrocytes or AAV-TdTomato control vector. PV interneurons were optogenetically stimulated, and responses were recorded in CA1 pyramidal cells. IO curves were generated as described previously and maximum responses were used to measure peak oeIPSCs (Fig. 2.6A-C). I observed a significant effect of LED power but no effects of genotype or interaction of genotype and LED power (Fig. 2.6B; Extended Data; Two-Way ANOVA, Genotype: F(1,20)=1.409, p=0.2492, LED power: F(2.460,49.19)=104.1, p<0.0001, interaction: F(11, 220)=0.3973, p=0.9561, Sidak's multiple comparisons post-hoc test). There was also no significant

difference in the peak oeIPSC amplitude between the groups (Fig. 2.6C; Extended Data; t-test, $t(20)=0.7851$, $p=0.4461$). The data suggests that astrocytic ephrin-B1 OE did not further enhance the strength of PV->PC functional connections in ephrin-B1-injected PV-EphB2 KO compared to control-injected PV-EphB2 KO group. Overexpression of astrocytic ephrin-B1 in mice lacking EphB2 in PV interneurons also did not affect oeIPSC amplitude over a 20 Hz train (Fig. 2.6E; Extended Data; Two-Way ANOVA, Genotype: $F(1,17)=1.936$, $p=0.1821$, Stim: $F(9,153)=96.12$, $p<0.0001$, interaction: $F(9,153)=0.8606$, $P=0.5619$, Sidak's multiple comparisons post-hoc test). Interestingly, there was a trend towards increased paired pulse ratio and a significant interaction between stimulus number and genotype (Fig. 2.6F; Extended Data; Two-Way ANOVA, Genotype: $F(1,17)=3.294$, $p=0.0872$, Stim: $F(2.958,50.28)=102.3$, $p<0.0001$, interaction: $F(8,136)=2.293$, $p=0.0246$, Sidak's multiple comparisons post-hoc test), suggesting that the two groups may exhibit differences in short-term synaptic dynamics. PV->PC synapses of PV-EphB2 KO mice overexpressing astrocytic ephrin-B1 were able to maintain their oeIPSC amplitudes over the train, suggesting that they may have reduced release probability at PV->PC synapses compared to vehicle-injected controls. Analysis of structural PV/VGAT presynaptic sites by immunolabeling also did not reveal any significant difference between ephrin-B1 overexpressing PV-EphB2 KO and the contralateral control side of the same brain slice (Fig. 2.6K; Extended Data; paired t-test, $t(21)=0.9448$, $p=0.3555$). These data support the hypothesis that astrocytic ephrin-B1 controls PV->PC connectivity by negatively regulating EphB receptor signaling in PV boutons, allowing for more inhibitory connections to form between PV and PC cells.

## 2.5 Discussion

Here I report two major findings: (1) astrocytes regulate the strength of functional connections between PV and pyramidal cells during a critical developmental period of inhibitory circuit assembly in the hippocampus; and (2) the role of ephrin-B/EphB receptor signaling in the development of these connections. More specifically, I show that the strength of PV->PC connectivity was affected by the levels of ephrin-B1 in astrocytes. Overexpression of ephrin-B1 in astrocytes led to a significant increase in the amplitude of PV specific oeIPSCs recorded in pyramidal cells with no significant difference in the PPR. The enhancement of oeIPSC amplitude following overexpression of astrocytic ephrin-B1 can be explained by an increased number of synapses or increased GABA receptor number or function. Although activation of the EphB receptor with its ligand ephrin-B was reported to regulate AMPAR and NMDAR clustering and function, its effects on GABA receptors have not been observed (Dalva et al., 2000; Takasu et al., 2002; Kayser et al., 2006). In addition, the analysis of mRNA levels of multiple GABA receptors showed no changes in their levels in ephrin-B1 KO mice (Fig. S2.3). My findings suggest the astrocytic ephrin-B1 is regulating EphB receptors at the presynaptic site of inhibitory synapses, as I observe the increased number of PV/VGAT presynaptic sites following astrocytic ephrin-B1 OE but reduced in astrocytic ephrin-B1 KO. The reduction in PV/VGAT presynaptic sites in ephrin-B1 KO also coincided with a decrease in VGAT/Gephyrin inhibitory synapses on SO dendrites and PC somata in the CA1 hippocampus (Nguyen et al., 2020), suggesting that the observed changes in PV-

positive presynaptic sites are most likely responsible for reduced inhibition. These observations that both the strength and number of PV->PC synapses are positively regulated by the levels of astrocytic ephrin-B1 provide further evidence that the development of PV-positive inhibitory synapses is tightly regulated by astrocytes through EphB receptor signaling.

One receptor that is critical for synaptic wiring of PV and CCK-positive basket and chandelier cells is ErbB4 (del Pino et al., 2013; del Pino et al., 2017; Favuzzi et al., 2019; Exposito-Alonso et al., 2020). Earlier in development, ErbB4 expression in MGE-derived interneurons assists their migration to the cortex and hippocampus (Flames et al., 2004). Intriguingly, it has also been shown that ErbB4 and EphB work together to guide cortical and striatal interneurons to their final destination. ErbB4 acts as a chemoattractant for migration of cortical and striatal interneurons, however striatal interneurons also co-express EphB, which acts as a repellent factor, preventing striatal interneurons from entering the cortex (Villar-Cerviño et al., 2015). These two signaling pathways could similarly play opposing roles in developing synapses if they are co-expressed by the same neuron. Although, I found no changes in the protein and mRNA levels of Nrg-1 and ErbB4 following deletion of astrocytic ephrin-B1, ErbB4 phosphorylation was decreased in mice lacking astrocytic ephrin-B1. This change may reflect reduced excitatory drive onto PV interneurons, as we previously reported (Nguyen et al., 2020), or reduced CCK innervation of pyramidal cells, as more recent data suggest that Nrg-1/ErbB4 signaling regulates CCK->PC connectivity, while Nrg-3/ErbB4 signaling regulates PC->PV connectivity (Vullhorst et al., 2009; Yang et al., 2013;

Exposito-Alonso et al., 2020). Therefore, in addition to PV->PC connectivity, I also analyzed CCK->PC connectivity. However, the effects of astrocytic ephrin-B1 seem specific to PV interneurons, as I did not detect changes in CB1R-positive CCK terminals in the pyramidal layer of CA1 hippocampus or overall protein levels of CB1R in astrocytic ephrin-B1 KO mice. Interestingly, EphB2 and EphB1 receptors, which are major ephrin-B1 binding partners, are expressed in PV but not in CCK interneurons, which could explain why levels of astrocytic ephrin-B1 seem to preferentially influence PV interneurons (Harris et al., 2018). While I observed a reduction in perisomatic innervation of PC by PV interneurons following ephrin-B1 KO in astrocytes, both AIS and perisomatic innervation were measured when analyzing PV->PC connectivity in SP layers of CA1 hippocampus. Further studies will investigate whether the effects of astrocytic ephrin-B1 on PV->PC connectivity are limited to perisomatic innervation of pyramidal cells by PV basket cells or if AIS innervation by PV chandelier cells is also affected.

E/I imbalance is hypothesized to drive pathological phenotypes exhibited in NDDs (Rubenstein and Merzenich, 2003). More specifically, impaired inhibition is thought to underlie the development of hyperactive neuronal networks in NDDs such as ASD and epilepsy (Sohal and Rubenstein, 2019; Tang et al., 2021). Dysfunctions of PV interneurons, including reduced density of PV interneurons, reduced PV expression, impaired PNN formation, and reduced activity of PV interneurons have been observed in individuals with ASD, suggesting that PV interneurons may critically regulate E/I balance and that they may play an important role in the pathogenesis of NDDs (Lawrence

et al., 2010; Hashemi et al., 2016; Contractor et al., 2021). My data shows that deletion of astrocytic ephrin-B1 increases susceptibility to PTZ induced seizures, providing further evidence of the involvement of ephrin-B/EphB signaling in regulating inhibition in vivo. I speculate that the reduction in PV->PC connectivity most likely contributes to this impaired inhibition. I also found that mice lacking ephrin-B1 in astrocytes exhibit repetitive digging behavior, in addition to previously observed impaired social behaviors in these mice (Nguyen et al., 2020). Impaired social behaviors and restrictive, repetitive behaviors are currently two of the major diagnostic criteria for ASD (Association), additionally ASD individuals present with epilepsy at disproportionate rates compared to the normal population (Spence and Schneider, 2009; Tuchman and Cuccaro, 2011). Importantly, de novo mutations in the gene encoding EphB2 receptors have been reported to be risk factors for the development of ASD and is identified as a strong candidate with score 2 in SFARI database (Kong et al., 2012; Sanders et al., 2012; Abrahams et al., 2013; Yang et al., 2013). Therefore, I believe the results of my study illustrate a novel mechanism responsible for proper inhibitory circuit development, which when impaired can result in ASD phenotypes.

I find that levels of astrocytic ephrin-B1 influence the localization of EphB receptor clusters in PV boutons but not on the somata of PV interneurons. It is intriguing that the levels of astrocytic ephrin-B1 influence the localization of EphB receptors in a compartment specific manner. The compartment specific nature of this regulation is a rather significant finding, as presynaptic vs postsynaptic EphB signaling may regulate diverse and or opposing functions in neuronal development and synaptic maintenance.

For example, postsynaptic EphB receptors play important roles in recruiting and stabilizing AMPA/NMDARs in excitatory postsynaptic membranes in dendrites and also regulate dendritic filopodial motility, spine morphogenesis, and dendritic spine maturation, thereby coordinating excitatory synaptic development (Dalva et al., 2000; Sloniowski and Ethell, 2012). As I saw the most robust effects of astrocytic ephrin-B1 on the localization of the EphB receptor in PV boutons, I believe ,y work suggests that astrocytic ephrin-B1 regulates PV->PC connectivity by limiting the repulsive trans-synaptic interactions between EphB expressing PV boutons and ephrin-B expressing soma or AIS of pyramidal cells. Additionally, since astrocytic ephrin-B1 interferes with trans-synaptic ephrin-B/EphB receptor interactions, I would expect ephrin-B1 KO in astrocytes to increase clustering of NMDAR and AMPAR in excitatory PC->PV synapses, enhancing excitatory drive onto PV interneurons and increasing inhibition. However, we see a decrease in inhibition of pyramidal cells following ephrin-B1 KO in astrocytes (Nguyen et al., 2020), supporting my hypothesis that EphB expression in PV boutons but not somata of PV interneurons regulate their synaptic connectivity.

Here I propose a new mechanism of astrocyte-mediated regulation of inhibitory synapse assembly by neutralizing EphB receptor signaling in PV-positive presynaptic boutons. My observations that a reduction in EphB receptor association with PV boutons following the overexpression of astrocytic ephrin-B1 or genetic deletion of EphB2 from PV interneurons both enhance the assembly of PV presynaptic sites are consistent with the adverse role of EphB receptor in inhibitory synapse development. To examine the role of EphB signaling in PV interneurons, I used PV-cre promoter to drive cre-lox

mediated deletion of floxed EphB2 receptors. As ephrin/EphB signaling has also been implicated in the migration of Dlx1/2 expressing inhibitory interneurons during embryonic development (Talebian et al., 2017), it is important to note that PV expression begins around P10-12 and gradually increases until about the third postnatal week (Seto-Ohshima et al., 1990; Lecea et al., 1995; Yang et al., 2013), timing EphB2 deletion during the P14-P21 period, well after PV interneuron migration to the hippocampus occurs (Tricoire et al., 2011; Pelkey et al., 2017). If EphB2 plays a role in promoting excitatory innervation of PV interneurons I would expect reduced activity of PV interneurons following its deletion. However, similar to overexpressing astrocytic ephrin-B1, I found that deletion of EphB2 from PV boutons increases PV specific oeIPSCs recorded in pyramidal cells. My findings suggest that EphB2 negatively regulates PV->PC contact formation and most likely acts as a repulsive cue for inhibitory synapse development. It is supported by the fact that disrupting trans-synaptic ephrin-B/EphB2 interactions by removing EphB2 is sufficient to trigger an increase in PV->PC connectivity. This is also in line with other published work showing that ectopic expression of EphB4 in PV interneurons reduced perisomatic innervation by PV interneurons in the visual cortex (Baohan et al., 2016). Interestingly, this group found that under normal conditions, Pten suppresses EphB4 expression but that loss of a single copy of Pten increased EphB4 expression and impaired PV->PC connection probability, without affecting PC->PV connectivity. This is consistent with my finding that EphB receptor levels are regulated in PV boutons and are important for PV->PC connectivity but may be less important for PC->PV connectivity (Baohan et al., 2016). I hypothesized

that astrocytic ephrin-B1 regulated PV->PC connectivity by impairing repulsive trans-synaptic EphB/Ephrin-B signaling. Consistent with my hypothesis, I found that overexpression of ephrin-B1 in astrocytes did not further enhance PV->PC connectivity in mice lacking EphB2 in PV interneurons. Interestingly, it has been shown that EphB2 signaling kinetics dictate whether or not a stable contact will form so that large amounts of EphB2 signaling very quickly will mediate repulsion, however slower, more gradual EphB2 signaling facilitates adhesion (Mao et al., 2018). It is possible that removal of one EphB receptor or interruption of some but not all trans-synaptic EphB/Ephrin-B signaling by astrocytes works through a mechanism that simply slows down the EphB signaling kinetics within the PV bouton, encouraging contact formation.

In summary, I show that astrocytes utilize ephrin-B1 to regulate PV->PC connectivity through interfering with repulsive trans-synaptic ephrin-B/EphB signaling. My study implicates EphB2 signaling as an important developmental cue for inhibitory synapse development between PV interneurons and pyramidal cells. Disruption of this regulatory mechanism leads to impaired inhibition in vivo as evidenced by increased seizure susceptibility and the presence of repetitive behaviors. As PV interneuron dysfunction is implicated in the pathogenesis of ASD (Rubenstein and Merzenich, 2003; Ali Rodriguez et al., 2018; Sohal and Rubenstein, 2019; Contractor et al., 2021), and EphB2 has been reported to be a strong risk factor for the development of ASD (Sanders et al., 2012), EphB signaling in PV interneurons can also serve as an important and powerful therapeutic target for correcting impaired inhibition in NDDs. Future studies

can address whether aberrant EphB2 signaling in PV interneurons underlies the development of pathological ASD phenotypes in NDDs.

## REFERENCES FOR CHAPTER TWO


Abrahams BS, Arking DE, Campbell DB, Mefford HC, Morrow EM, Weiss LA, Menashe I, Wadkins T, Banerjee-Basu S, Packer A (2013) SFARI Gene 2.0: a community-driven knowledgebase for the autism spectrum disorders (ASDs). Mol Autism 4:36.

Ali Rodriguez R, Joya C, Hines RM (2018) Common Ribs of Inhibitory Synaptic Dysfunction in the Umbrella of Neurodevelopmental Disorders. Front Mol Neurosci 11:132.

Allen NJ, Eroglu C (2017) Cell Biology of Astrocyte-Synapse Interactions. Neuron 96:697-708.

Association AP Diagnostic and Statistical Manual of Mental Disorders.

Augusto-Oliveira M, Arrifano GP, Takeda PY, Lopes-Araújo A, Santos-Sacramento L, Anthony DC, Verkhratsky A, Crespo-Lopez ME (2020) Astroglia-specific contributions to the regulation of synapses, cognition and behaviour. Neurosci Biobehav Rev 118:331-357.

Baohan A, Ikrar T, Tring E, Xu X, Trachtenberg JT (2016) Pten and EphB4 regulate the establishment of perisomatic inhibition in mouse visual cortex. Nat Commun 7:12829.

Castañeda-Castellanos DR, Flint AC, Kriegstein AR (2006) Blind patch clamp recordings in embryonic and adult mammalian brain slices. Nat Protoc 1:532-542.

Clarke LE, Barres BA (2013) Emerging roles of astrocytes in neural circuit development. Nature Reviews Neuroscience 14:311-321.

Contractor A, Ethell IM, Portera-Cailliau C (2021) Cortical interneurons in autism. Nature Neuroscience 24:1648-1659.

Contractor A, Rogers C, Maron C, Henkemeyer M, Swanson GT, Heinemann SF (2002) Trans-synaptic Eph receptor-ephrin signaling in hippocampal mossy fiber LTP. Science 296:1864-1869.

Dalva MB, Takasu MA, Lin MZ, Shamah SM, Hu L, Gale NW, Greenberg ME (2000) EphB Receptors Interact with NMDA Receptors and Regulate Excitatory Synapse Formation. Cell 103:945-956.

del Pino I, Brotons-Mas JR, Marques-Smith A, Marighetto A, Frick A, Marín O, Rico B (2017) Abnormal wiring of CCK+ basket cells disrupts spatial information coding. Nature Neuroscience 20:784-792.

del Pino I, García-Frigola C, Dehorter N, Brotons-Mas Jorge R, Alvarez-Salvado E, Martínez de Lagrán M, Ciceri G, Gabaldón María V, Moratal D, Dierssen M, Canals S, Marín O, Rico B (2013) Erbb4 Deletion from Fast-Spiking Interneurons Causes Schizophrenia-like Phenotypes. Neuron 79:1152-1168.

Donato F, Rompani SB, Caroni P (2013) Parvalbumin-expressing basket-cell network plasticity induced by experience regulates adult learning. Nature 504:272-276.

Elmariah SB, Oh EJ, Hughes EG, Balice-Gordon RJ (2005) Astrocytes Regulate Inhibitory Synapse Formation via Trk-Mediated Modulation of Postsynaptic GABA<sub>A</sub> Receptors. The Journal of Neuroscience 25:3638-3650.

Ethell IM, Irie F, Kalo MS, Couchman JR, Pasquale EB, Yamaguchi Y (2001) EphB/syndecan-2 signaling in dendritic spine morphogenesis. Neuron 31:1001-1013.

Exposito-Alonso D, Osório C, Bernard C, Pascual-García S, del Pino I, Marín O, Rico B (2020) Subcellular sorting of neuregulins controls the assembly of excitatory-inhibitory cortical circuits. eLife 9:e57000.

Favuzzi E, Deogracias R, Marques-Smith A, Maeso P, Jezequel J, Exposito-Alonso D, Balia M, Kroon T, Hinojosa AJ, E FM, Rico B (2019) Distinct molecular programs regulate synapse specificity in cortical inhibitory circuits. Science 363:413-417.

Fazzari P, Paternain AV, Valiente M, Pla R, Luján R, Lloyd K, Lerma J, Marín O, Rico B (2010) Control of cortical GABA circuitry development by Nrg1 and ErbB4 signalling. Nature 464:1376-1380.

Filice F, Janickova L, Henzi T, Bilella A, Schwaller B (2020) The Parvalbumin Hypothesis of Autism Spectrum Disorder. Front Cell Neurosci 14:577525.

Flames N, Long JE, Garratt AN, Fischer TM, Gassmann M, Birchmeier C, Lai C, Rubenstein JL, Marín O (2004) Short- and long-range attraction of cortical GABAergic interneurons by neuregulin-1. Neuron 44:251-261.

Harris KD, Hochgerner H, Skene NG, Magno L, Katona L, Bengtsson Gonzales C, Somogyi P, Kessaris N, Linnarsson S, Hjerling-Leffler J (2018) Classes and continua of hippocampal CA1 inhibitory neurons revealed by single-cell transcriptomics. PLoS Biol 16:e2006387.

Hashemi E, Ariza J, Rogers H, Noctor SC, Martínez-Cerdeño V (2016) The Number of Parvalbumin-Expressing Interneurons Is Decreased in the Prefrontal Cortex in Autism. Cerebral Cortex 27:1931-1943.

Henderson JT, Georgiou J, Jia Z, Robertson J, Elowe S, Roder JC, Pawson T (2001) The receptor tyrosine kinase EphB2 regulates NMDA-dependent synaptic function. Neuron 32:1041-1056.

Henkemeyer M, Itkis OS, Ngo M, Hickmott PW, Ethell IM (2003) Multiple EphB receptor tyrosine kinases shape dendritic spines in the hippocampus. Journal of Cell Biology 163:1313-1326.

Hughes EG, Elmariah SB, Balice-Gordon RJ (2010) Astrocyte secreted proteins selectively increase hippocampal GABAergic axon length, branching, and synaptogenesis. Mol Cell Neurosci 43:136-145.

Hussain NK, Thomas GM, Luo J, Huganir RL (2015) Regulation of AMPA receptor subunit GluA1 surface expression by PAK3 phosphorylation. Proceedings of the National Academy of Sciences 112:E5883-E5890.

Kayser MS, McClelland AC, Hughes EG, Dalva MB (2006) Intracellular and Trans-Synaptic Regulation of Glutamatergic Synaptogenesis by EphB Receptors. The Journal of Neuroscience 26:12152-12164.

Klein R (2012) Eph/ephrin signalling during development. Development 139:4105-4109.

Kong A et al. (2012) Rate of de novo mutations and the importance of father's age to disease risk. Nature 488:471-475.

Lawrence YA, Kemper TL, Bauman ML, Blatt GJ (2010) Parvalbumin-, calbindin-, and calretinin-immunoreactive hippocampal interneuron density in autism. Acta Neurol Scand 121:99-108.

Lecea Ld, del Ri´o JA, Soriano E (1995) Developmental expression of parvalbumin mRNA in the cerebral cortex and hippocampus of the rat. Molecular Brain Research 32:1-13.

Lim BK, Matsuda N, Poo M-m (2008) Ephrin-B reverse signaling promotes structural and functional synaptic maturation in vivo. Nature Neuroscience 11:160-169.

Liu Q-Y, Schaffner AE, Li Y-X, Dunlap V, Barker JL (1996) Upregulation of GABA<sub>A</sub> Current by Astrocytes in Cultured Embryonic Rat Hippocampal Neurons. The Journal of Neuroscience 16:2912-2923.

Mao YT, Zhu JX, Hanamura K, Iurilli G, Datta SR, Dalva MB (2018) Filopodia Conduct Target Selection in Cortical Neurons Using Differences in Signal Kinetics of a Single Kinase. Neuron 98:767-782.e768.

Moeller ML, Shi Y, Reichardt LF, Ethell IM (2006) EphB receptors regulate dendritic spine morphogenesis through the recruitment/phosphorylation of focal adhesion kinase and RhoA activation. Journal of Biological Chemistry 281:1587-1598.

Nguyen AQ, Sutley S, Koeppen J, Mina K, Woodruff S, Hanna S, Vengala A, Hickmott PW, Obenaus A, Ethell IM (2020) Astrocytic Ephrin-B1 Controls Excitatory-Inhibitory Balance in Developing Hippocampus. The Journal of Neuroscience 40:6854-6871.

Nolt MJ, Lin Y, Hruska M, Murphy J, Sheffler-Colins SI, Kayser MS, Passer J, Bennett MVL, Zukin RS, Dalva MB (2011) EphB Controls NMDA Receptor Function and Synaptic Targeting in a Subunit-Specific Manner. The Journal of Neuroscience 31:5353-5364.

Page CE, Shepard R, Heslin K, Coutellier L (2019) Prefrontal parvalbumin cells are sensitive to stress and mediate anxiety-related behaviors in female mice. Scientific Reports 9:19772.

Pasquale EB (2008) Eph-ephrin bidirectional signaling in physiology and disease. Cell 133:38-52.

Pelkey KA, Chittajallu R, Craig MT, Tricoire L, Wester JC, McBain CJ (2017) Hippocampal GABAergic Inhibitory Interneurons. Physiological Reviews 97:1619-1747.

Petrelli F, Pucci L, Bezzi P (2016) Astrocytes and Microglia and Their Potential Link with Autism Spectrum Disorders. Front Cell Neurosci 10:21.

Reinhard SM, Rais M, Afroz S, Hanania Y, Pendi K, Espinoza K, Rosenthal R, Binder DK, Ethell IM, Razak KA (2019) Reduced perineuronal net expression in Fmr1 KO mice auditory cortex and amygdala is linked to impaired fear-associated memory. Neurobiol Learn Mem 164:107042.

Rubenstein JL, Merzenich MM (2003) Model of autism: increased ratio of excitation/inhibition in key neural systems. Genes Brain Behav 2:255-267.

Sanders SJ et al. (2012) De novo mutations revealed by whole-exome sequencing are strongly associated with autism. Nature 485:237-241.

Seto-Ohshima A, Aoki E, Semba R, Emson PC, Heizmann CW (1990) Appearance of parvalbumin-specific immunoreactivity in the cerebral cortex and hippocampus of the developing rat and gerbil brain. Histochemistry 94:579-589.

Sheffler-Collins SI, Dalva MB (2012) EphBs: an integral link between synaptic function and synaptopathies. Trends Neurosci 35:293-304.

Shimada T, Yamagata K (2018) Pentylenetetrazole-Induced Kindling Mouse Model. JoVE:e56573.

Sloniowski S, Ethell IM (2012) Looking forward to EphB signaling in synapses. Semin Cell Dev Biol 23:75-82.

Sohal VS, Rubenstein JLR (2019) Excitation-inhibition balance as a framework for investigating mechanisms in neuropsychiatric disorders. Molecular Psychiatry 24:1248-1257.

Spence SJ, Schneider MT (2009) The Role of Epilepsy and Epileptiform EEGs in Autism Spectrum Disorders. Pediatric Research 65:599-606.

Takasu MA, Dalva MB, Zigmond RE, Greenberg ME (2002) Modulation of NMDA receptor-dependent calcium influx and gene expression through EphB receptors. Science 295:491-495.

Talebian A, Britton R, Ammanuel S, Bepari A, Sprouse F, Birnbaum SG, Szabó G, Tamamaki N, Gibson J, Henkemeyer M (2017) Autonomous and non-autonomous roles for ephrin-B in interneuron migration. Developmental Biology 431:179-193.

Tan CX, Eroglu C (2021) Cell adhesion molecules regulating astrocyte-neuron interactions. Curr Opin Neurobiol 69:170-177.

Tang X, Jaenisch R, Sur M (2021) The role of GABAergic signalling in neurodevelopmental disorders. Nature Reviews Neuroscience 22:290-307.

Tricoire L, Pelkey KA, Erkkila BE, Jeffries BW, Yuan X, McBain CJ (2011) A Blueprint for the Spatiotemporal Origins of Mouse Hippocampal Interneuron Diversity. The Journal of Neuroscience 31:10948-10970.

Tuchman R, Cuccaro M (2011) Epilepsy and Autism: Neurodevelopmental Perspective. Current Neurology and Neuroscience Reports 11:428-434.

Villar-Cerviño V, Kappeler C, Nóbrega-Pereira S, Henkemeyer M, Rago L, Nieto MA, Marín O (2015) Molecular mechanisms controlling the migration of striatal interneurons. J Neurosci 35:8718-8729.

Vullhorst D, Neddens J, Karavanova I, Tricoire L, Petralia RS, McBain CJ, Buonanno A (2009) Selective expression of ErbB4 in interneurons, but not pyramidal cells, of the rodent hippocampus. J Neurosci 29:12255-12264.

Yang J-M, Zhang J, Chen X-J, Geng H-Y, Ye M, Spitzer NC, Luo J-H, Duan S-M, Li X-M (2013) Development of GABA Circuitry of Fast-Spiking Basket Interneurons in the Medial Prefrontal Cortex of erbb4-Mutant Mice. The Journal of Neuroscience 33:19724-19733.

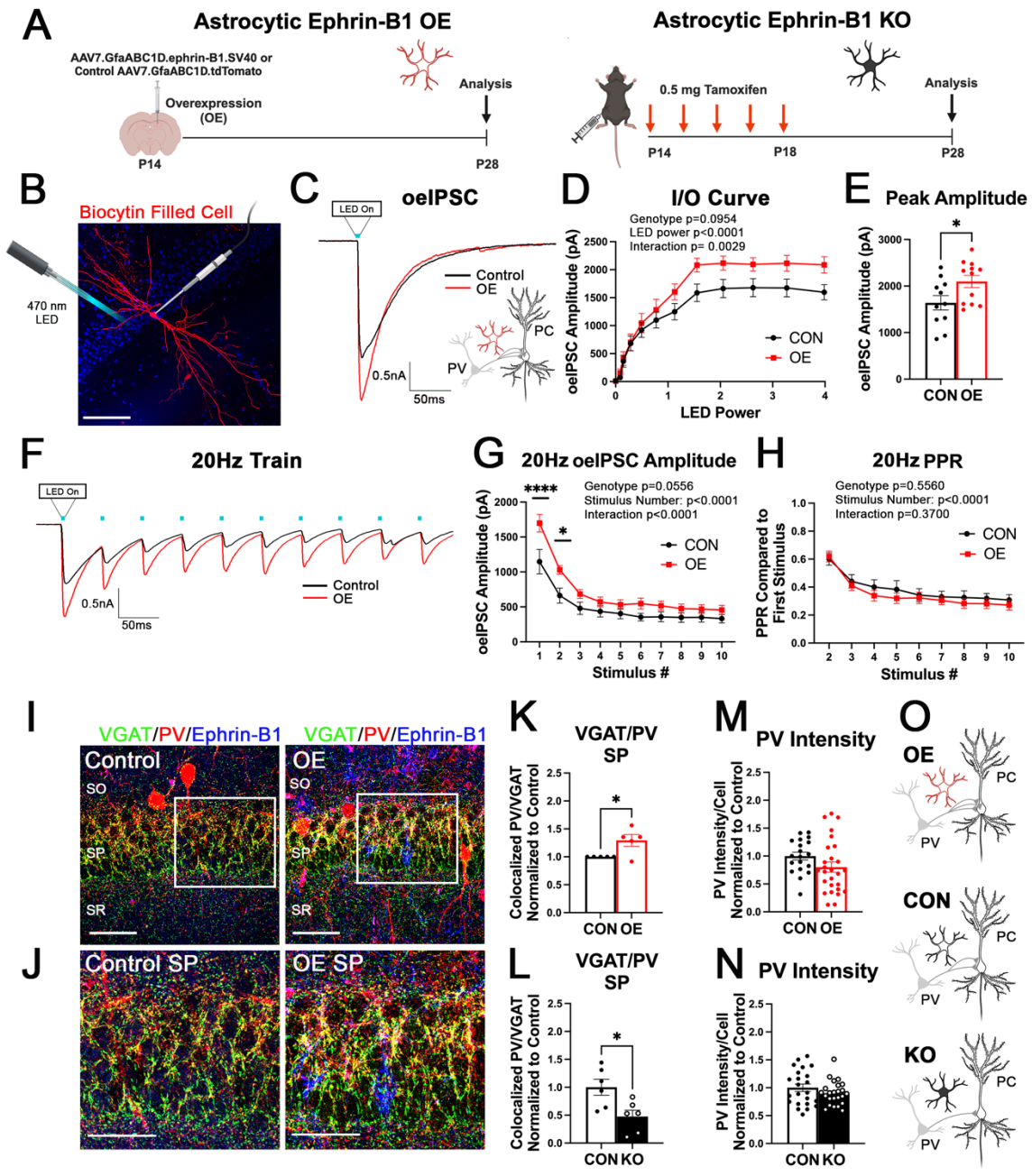
A
Astrocytic Ephrin-B1 OE
AAV7.GfaABC1D.ephrin-B1.SV40 or
Control AAV7.GfaABC1D.tdTomato
Overexpression
(OE)
Analysis
P14
P28
Astrocytic Ephrin-B1 KO
0.5 mg Tamoxifen
Analysis
P14
P18
P28
B
Biocytin Filled Cell
470 nm
LED
C
oeIPSC
LED On
Control
OE
PC
PV
0.5nA
50ms
D
I/O Curve
Genotype p=0.0954
LED power p<0.0001
Interaction p= 0.0029
oeIPSC Amplitude (pA)
CON
OE
LED Power
E
Peak Amplitude
oeIPSC Amplitude (pA)
CON OE
F
20Hz Train
LED On
Control
OE
0.5nA
50ms
G
20Hz oeIPSC Amplitude
****
*
Genotype p=0.0556
Stimulus Number: p<0.0001
Interaction p<0.0001
oeIPSC Amplitude (pA)
CON
OE
Stimulus #
H
20Hz PPR
Genotype p=0.5560
Stimulus Number: p<0.0001
Interaction p=0.3700
PPR Compared to First Stimulus
CON
OE
Stimulus #
I
VGAT/PV/Ephrin-B1
VGAT/PV/Ephrin-B1
Control
OE
SO
SP
SR
J
Control SP
OE SP
K
VGAT/PV SP
Colocalized PV/VGAT Normalized to Control
CON OE
L
VGAT/PV SP
Colocalized PV/VGAT Normalized to Control
CON KO
M
PV Intensity
PV Intensity/Cell Normalized to Control
CON OE
N
PV Intensity
PV Intensity/Cell Normalized to Control
CON KO
O
OE
PC
PV
CON
PC
PV
KO
PC
PV

**Figure 2.1: Astrocytic ephrin-B1 overexpression (OE) increases PV->PC connectivity. (A)** Experimental timeline. **(B)** Representative image of a biocytin filled pyramidal cell in the CA1 hippocampus, labeled with streptavidin (red) following whole cell recording. Scale bar, 100 μm. **(C)** Representative current traces of the oeIPSC recorded from PC in hippocampal slices of OE and vehicle-injected mice (control) following the activation of PV interneurons expressing ChR2 with 400 nm LED light. **(D)** Input-output (IO) curve shows the average oeIPSC amplitude in OE and control groups plotted against LED power. There is a significant effect of LED power and interaction of genotype and LED power (11-12 cells per group, 7-8 mice per group, 2-way ANOVA). **(E)** Graph shows the average peak amplitude of the last five stimulations in the IO curve. Ephrin-B1 OE group shows a significant increase in the peak oeIPSC amplitude (11-12 cells per group, 7-8 mice per group, t-test, *$p<0.05$). **(F)** Representative traces of the oeIPSCs in control and OE groups, generated during stimulation with a 20 Hz train of ten LED pulses. **(G)** Graph shows the average oeIPSC amplitude in control and OE during each LED pulse within a 20 Hz train. There is a significant increase in the average oeIPSC amplitude in response to the first two stimuli in OE compared to the control group (8-9 cells per group, 7-8 mice per group, 2-way ANOVA, *$p<0.05$, ****$p<0.0001$). **(H)** Graph shows the average oeIPSCs normalized to the first stimulus in the 20 Hz train to assess short-term plasticity with no significant effect of genotype or interaction (8-9 cells per group, 7-8 mice per group, 2-way ANOVA). **(I)** Confocal images of brain slices from control and OE mice immunolabeled against VGAT (green), PV (red), and ephrin-B1 (blue), scale bar 50 μm. **(J)** Magnified images showing the SP

layer in control and OE slices, scale bar 25 μm. **(K,L)** Graphs show the average number of colocalized PV/VGAT puncta in the OE group normalized to the contralateral uninjected side, and in KO group normalized to the respective control. OE group shows a significant increase and KO group shows a reduction in PV/VGAT colocalized puncta in the SP layer of the CA1 hippocampus (5 OE mice per group with 10 images per group; 3 KO and 3 control mice per group with 6 images per group paired t-test (OE) or t-test (KO) *$p<0.05$, **$p<0.01$, ***$p<0.001$). **(M,N)** Graphs show the intensity of PV within PV interneurons of OE **(M)** and KO mice **(N)**. Intensity of PV in PV interneurons was not affected by OE or KO (3 OE mice per group with 19-27 cells per group and 4 mice per group with 23-24 cells per group, t-test). **(O)** Drawing depicts differences in PV->PC connectivity between ephrin-B1 OE, control and ephrin-B1 KO groups. All data are represented as mean ± SEM. Graphics created with Biorender.com.

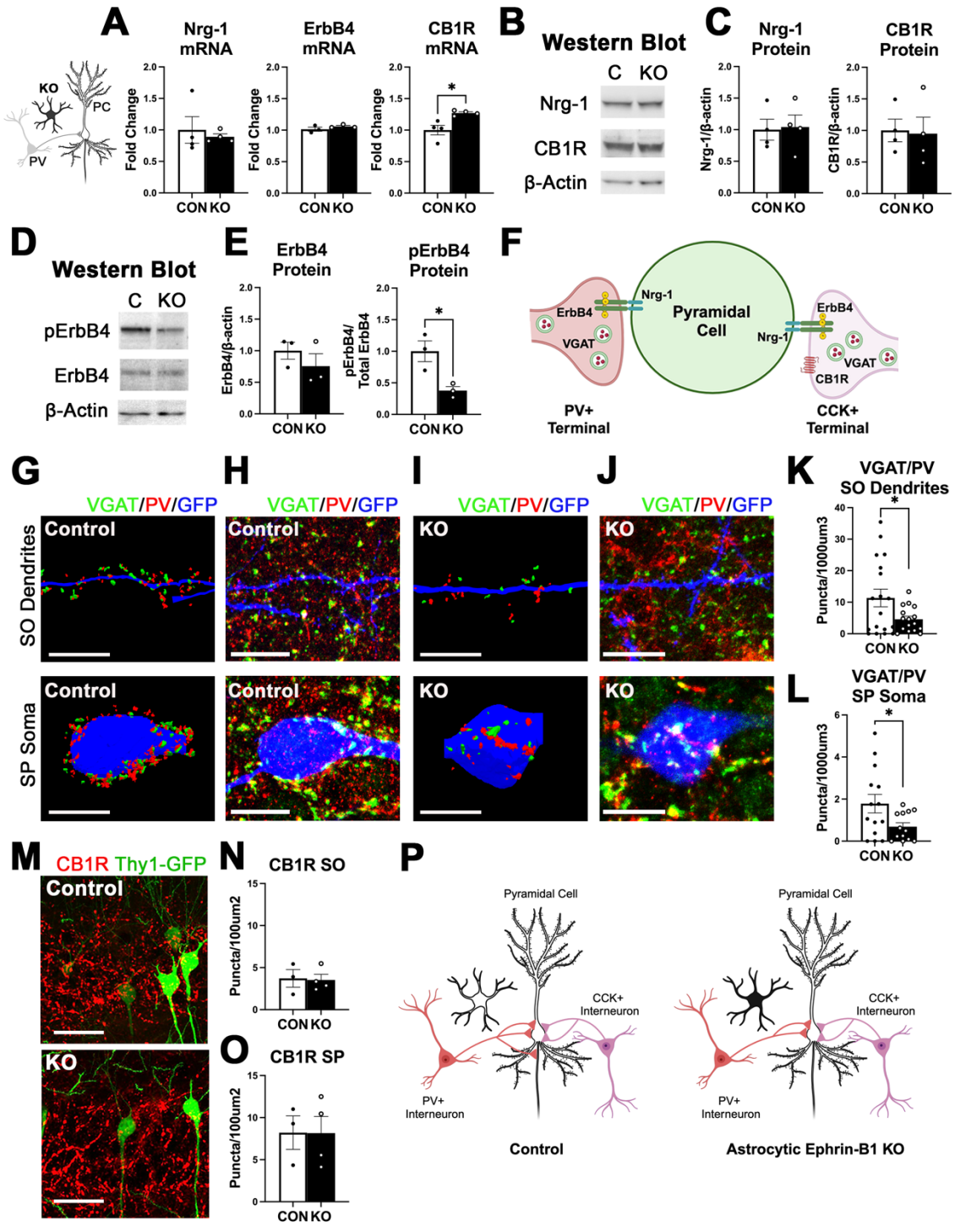
A
Nrg-1 mRNA
ErbB4 mRNA
CB1R mRNA
KO
PC
PV
Fold Change
CON KO
B
Western Blot
C KO
Nrg-1
CB1R
β-Actin
C
Nrg-1 Protein
CB1R Protein
Nrg-1/β-actin
CB1R/β-actin
D
Western Blot
C KO
pErbB4
ErbB4
β-Actin
E
ErbB4 Protein
pErbB4 Protein
ErbB4/β-actin
pErbB4/ Total ErbB4
F
ErbB4
Nrg-1
VGAT
Pyramidal Cell
CB1R
PV+ Terminal
CCK+ Terminal
G
H
I
J
VGAT/PV/GFP
SO Dendrites
SP Soma
Control
KO
K
VGAT/PV SO Dendrites
Puncta/1000um3
L
VGAT/PV SP Soma
M
CB1R Thy1-GFP
N
CB1R SO
Puncta/100um2
O
CB1R SP
P
Pyramidal Cell
CCK+ Interneuron
PV+ Interneuron
Control
Astrocytic Ephrin-B1 KO

**Figure 2.2: Deletion of astrocytic ephrin-B1 reduces PV perisomatic innervation of CA1 pyramidal neurons.** **(A)** Graphs show mRNA levels of Nrg-1, ErbB4 and CB1R in control and KO mice, analyzed by RT-qPCR or Nanostring. Deletion of astrocytic ephrin-B1 increased levels of CB1R mRNA but did not affect mRNA levels of Nrg-1 or ErbB4 (n=3-4 mice/group t-test, *p<0.05). **(B)** Western blot of Nrg-1, CB1R, and β-Actin in control and astrocytic ephrin-B1 KO mice. **(C)** Graphs show quantification of Nrg-1 and CB1R protein levels normalized to β-Actin (n=4 mice/group, t-test). **(D)** Western blot of ErbB4, phosphorylated ErbB4, and β-Actin in control and KO mice. **(E)** Graphs show quantification of ErbB4 protein levels normalized to β-actin, and phosphorylated ErbB4 normalized to total ErbB4. Although deletion of astrocytic ephrin-B1 did not affect total levels of ErbB4, KO mice showed a significant decrease in phosphorylated ErbB4 protein levels (n=3 mice/group, t-test, *p<0.05). **(F)** Graphic showing innervation of CA1 pyramidal cells by PV and CCK interneurons. **(G-J)** Neurolucida 3D renderings **(G,I)** of confocal images **(H,J)** showing VGAT (green) and PV (red) immunostaining in close proximity to SO dendrites or somata of CA1 excitatory pyramidal neurons labeled with GFP (blue). Scale bar, 10 μm. **(K-L)** Graphs represent the average colocalized PV/VGAT puncta within 1 μm of SO dendrites **(K)** or somata **(L)** of GFP expressing CA1 excitatory neurons in control and astrocytic ephrin-B1 KO mice. KO mice show a significantly reduced density of colocalized PV/VGAT puncta on SO dendrites and somata of excitatory neurons (4 mice per group, 13-18 images per group, t-test, *p<0.05). **(M)** Images of brain slices immunostained with CB1R and GFP expressing excitatory neurons. **(N-O)** Graphs represent the number of CB1R puncta in

the SO **(N)** and SP **(O)** of control and KO mice. There was no difference in the number of CB1R puncta between the groups (n=3-4 mice/group, 9-15 images/group, t-test). **(P)** Drawing depicts the changes in PV- and CCK-positive innervation of PC following deletion of astrocytic ephrin-B1. All data are represented as mean ± SEM. Graphics created with Biorender.com.

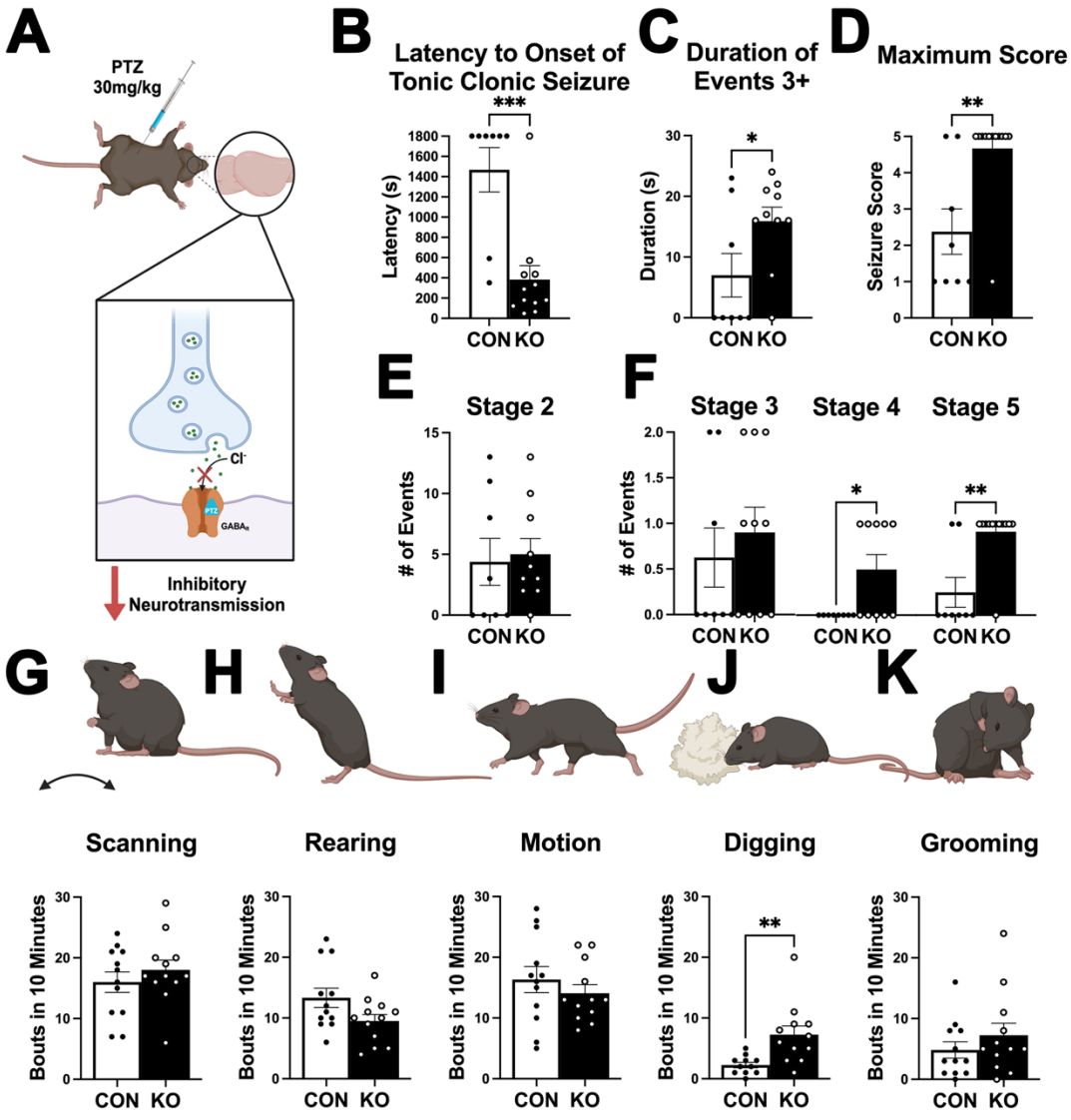
A
PTZ
30mg/kg
Cl-
PTZ
GABAR
Inhibitory
Neurotransmission
B
Latency to Onset of
Tonic Clonic Seizure
***
Latency (s)
CON KO
C
Duration of
Events 3+
*
Duration (s)
CON KO
D
Maximum Score
**
Seizure Score
CON KO
E
Stage 2
# of Events
CON KO
F
Stage 3
Stage 4
Stage 5
# of Events
*
**
CON KO
CON KO
CON KO
G
H
I
J
K
Scanning
Rearing
Motion
Digging
Grooming
Bouts in 10 Minutes
**
CON KO
CON KO
CON KO
CON KO
CON KO

**Figure 2.3: Deletion of astrocytic ephrin-B1 leads to increased seizure susceptibility and repetitive behaviors. (A)** Diagram shows seizure testing paradigm and the mechanism of action of pentylenetetrazole (PTZ). **(B)** Graph shows the latency to onset of tonic-clonic seizure in control and KO mice following injection of 30 mg/kg PTZ at P48+/-2D. Astrocytic ephrin-B1 deletion reduced the latency to onset of tonic-clonic seizure following PTZ treatment, indicating that KO mice were more susceptible to PTZ induced seizure (n=8-12 mice/group, t-test, ***p<0.001). **(C)** The duration of events stage 3+ and maximum seizure score achieved **(D)** as measured by racine seizure scale were increased following deletion of astrocytic ephrin-B1, indicating that deletion of astrocytic ephrin-B1 increased the severity of PTZ induced seizures (n=8-12 mice/group, t-test or Mann-Whitney test, *p<0.05, **p<0.01). **(E-F)** Graphs show the number of seizure events of stage 2-5 as measured by the Racine seizure scale. KO mice show increased numbers of events at stages 4 and 5 compared to control mice (n=8-12 mice/group, Mann-Whitney test, *p<0.05, **p<0.01). **(G-K)** Graphs show analysis of common home cage behaviors represented as the number of scanning, grooming, motion, digging, and grooming bouts in 10 min. KO mice displayed an increased number of digging bouts compared to control mice at P28 **(J**; n=12 animals per group, t-test, **p<0.01). All data are represented as mean ± SEM. Graphics created with Biorender.com.

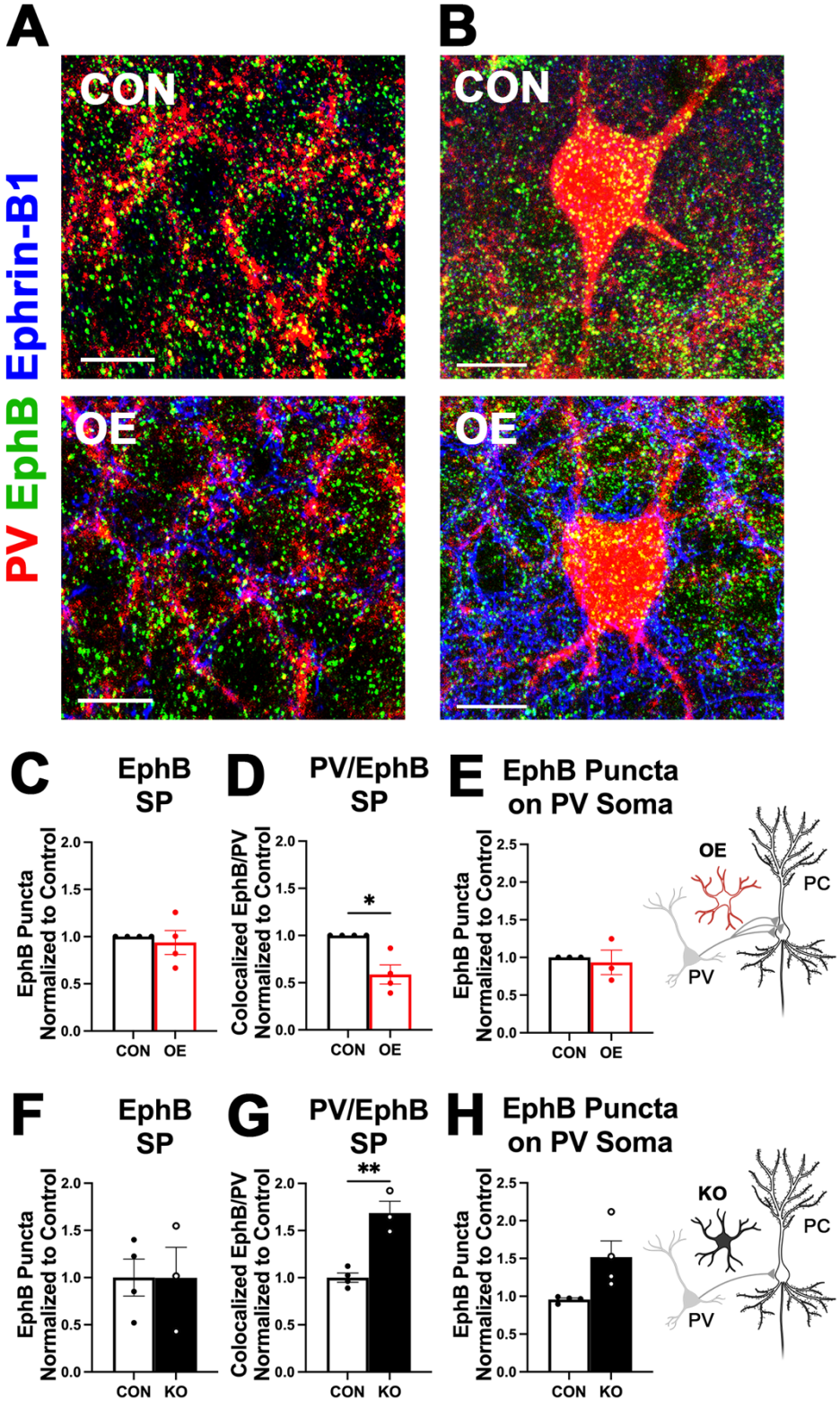
A
B
CON
CON
OE
OE
PV EphB Ephrin-B1
C
EphB SP
EphB Puncta Normalized to Control
CON OE
D
PV/EphB SP
Colocalized EphB/PV Normalized to Control
*
CON OE
E
EphB Puncta on PV Soma
EphB Puncta Normalized to Control
CON OE
OE
PC
PV
F
EphB SP
EphB Puncta Normalized to Control
CON KO
G
PV/EphB SP
Colocalized EphB/PV Normalized to Control
**
CON KO
H
EphB Puncta on PV Soma
EphB Puncta Normalized to Control
CON KO
KO
PC
PV

**Figure 2.4: Astrocytic ephrin-B1 levels control localization of EphB in PV boutons but not in the soma of PV interneurons. (A-B)** Confocal images of brain slices from astrocytic ephrin-B1 OE side and the contralateral control side of the same brain slice (CON) showing PV (red), pan-EphB (green), and ephrin-B1 (blue) immunofluorescence labeling in the SP layer of CA1 hippocampus **(A)** and on PV soma **(B)**. Scale bar, 10 μm. **(C-H)** Graphs represent the number of EphB puncta in the pyramidal layer **(C,F)**, the number of colocalized PV/EphB puncta in the pyramidal layer **(D,G)**, or the number of EphB puncta on PV soma **(E,H)** in OE mice normalized to the contralateral side of the same brain slice (CON) **(C-E)** and KO mice normalized to tamoxifen injected controls lacking ERT2-cre (CON) **(F-H)**. Overexpression **(C)** or deletion **(F)** of astrocytic ephrin-B1 did not affect the total number of EphB puncta in the SP (n=3-4 mice per group, 8-16 images per group, t-test or paired t-test (OE mice), $p>0.05$). The number of PV/EphB2 colocalized puncta in the SP was significantly reduced in OE group **(D),** but increased in KO group **(G)** compared to their respective controls (n=3-4 mice per group, 8-16 images per group, t-test or paired t-test (OE mice),*$p<0.05$, **$p<0.01$). The number of EphB puncta on the soma of PV interneurons was unchanged in both OE mice **(E)** and KO mice **(H)** (n=3-4 mice per group, 21-25 PV interneurons per group, t-test or paired t-test (OE mice). All data are represented as mean ± SEM. Graphics created with Biorender.com.

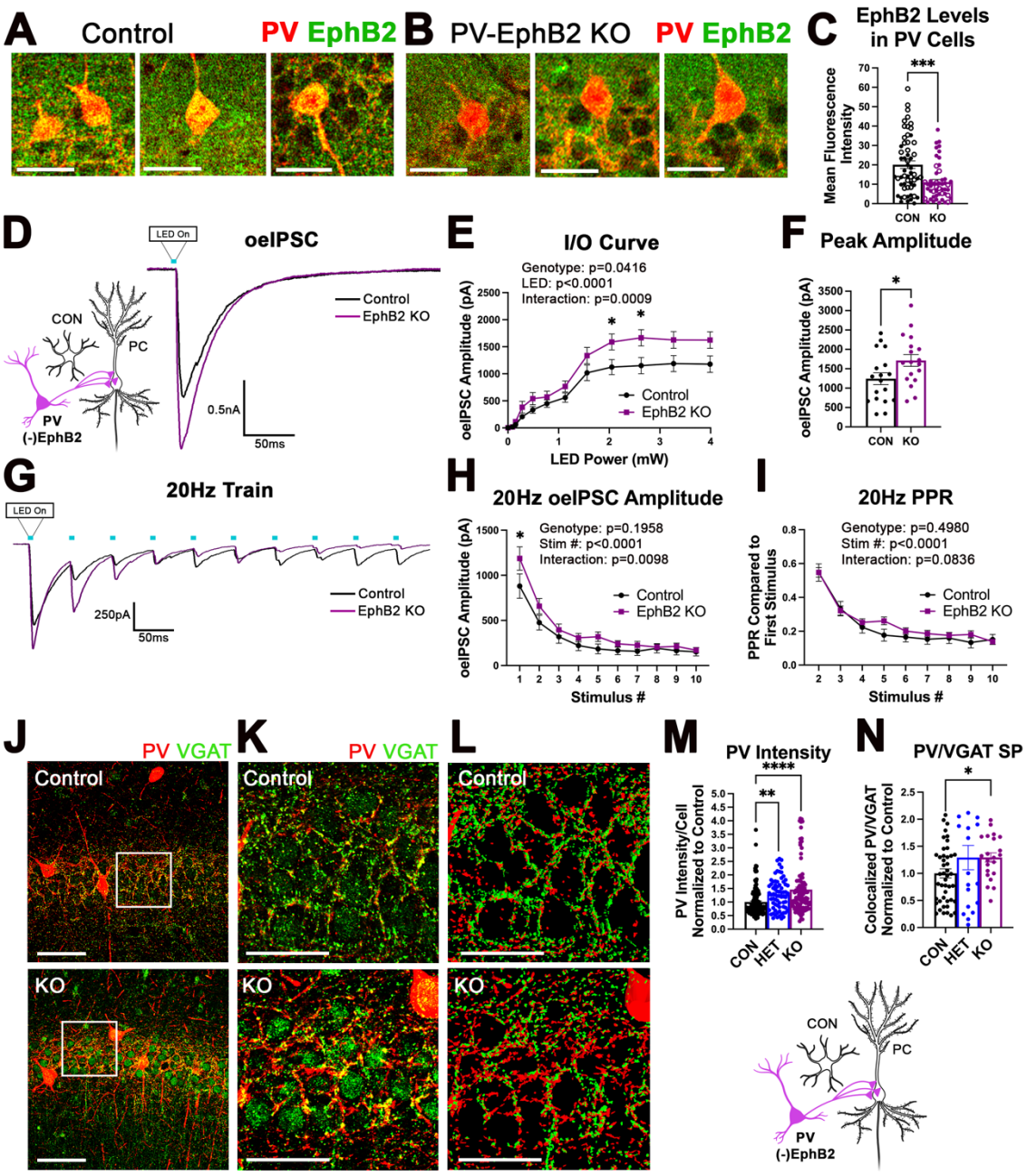
A
Control
PV EphB2
B
PV-EphB2 KO
PV EphB2
C
EphB2 Levels in PV Cells
Mean Fluorescence Intensity
***
CON KO
D
oeIPSC
LED On
CON
PC
PV
(-)EphB2
Control
EphB2 KO
0.5nA
50ms
E
I/O Curve
Genotype: p=0.0416
LED: p<0.0001
Interaction: p=0.0009
oeIPSC Amplitude (pA)
LED Power (mW)
Control
EphB2 KO
F
Peak Amplitude
oeIPSC Amplitude (pA)
CON KO
G
20Hz Train
LED On
250pA
50ms
Control
EphB2 KO
H
20Hz oeIPSC Amplitude
Genotype: p=0.1958
Stim #: p<0.0001
Interaction: p=0.0098
oeIPSC Amplitude (pA)
Stimulus #
I
20Hz PPR
Genotype: p=0.4980
Stim #: p<0.0001
Interaction: p=0.0836
PPR Compared to First Stimulus
Stimulus #
J
PV VGAT
Control
KO
K
PV VGAT
Control
KO
L
Control
KO
M
PV Intensity
****
**
PV Intensity/Cell Normalized to Control
CON HET KO
N
PV/VGAT SP
*
Colocalized PV/VGAT Normalized to Control
CON HET KO
CON
PC
PV
(-)EphB2

**Figure 2.5: Deletion of EphB2 receptor from PV interneurons enhances PV->PC connectivity. (A,B)** Confocal images of PV (red) and EphB2 (green) immunolabeling in brain slices from control **(A)** and PV-EphB2 KO mice **(B)**. Scale bar, 25 μm. **(C)** Graph shows quantification of EphB2 immunofluorescence levels in PV interneurons of control and PV-EphB2-/- KO mice. Deletion of EphB2 from PV interneurons significantly reduced the EphB2 immunofluorescence intensity levels in PV interneurons (n=3-4 mice per group, 50-57 cells per group, Welch's t-test, ***p<0.001). **(D)** Representative current traces of the oeIPSCs recorded from excitatory CA1 pyramidal cells of mice lacking EphB2 in PV interneurons (PV-EphB2 KO) and control mice. **(E)** IO curve shows the average oeIPSC amplitudes in PV-EphB2 KO and control mice plotted against LED power. 2-way ANOVA showed a significant effect of genotype, LED power, and interaction between genotype and LED power (18 cells per group, 7-9 mice per group, 2-way ANOVA (sphericity assumed, Sidak's post hoc test), *p<0.05). **(F)** Graph shows the average peak oeIPSC amplitude in PV-EphB2 KO and control mice with a significant increase in PV-EphB2 KO group (18 cells per group, 7-9 mice per group, t-test, *p<0.05). **(G)** Representative traces of oeIPSCs from control and PV-EphB2 KO groups during a 20 Hz train of ten LED pulses. **(H)** Graph shows the average oeIPSC amplitude in control and PV-EphB2 KO cells during each LED pulse within a 20 Hz train. PV-EphB2 KO cells showed a significant increase in the average oeIPSC amplitude during the first stimulus. **(I)** Graph shows the average oeIPSCs normalized to the first stimulus in the 20 Hz train to assess the plasticity with no significant effect of genotype or interaction (18 cells per group, 7-9 mice per group, 2-way ANOVA, sphericity assumed,

Sidak's post hoc test). **(J,K)** Confocal images of control and PV-EphB2 KO brain slices immunolabeled against VGAT (green), and PV (red), scale bar 50 μm or 25 μm. **(L)** Neurolucida renderings of confocal images pictured in **(J,K).** Scale bar, 25 μm. **(M)** Graph shows the average PV intensity in control, PV-EphB2+/-, and PV-EphB2-/- KO mice normalized to control. PV intensity was increased in mice lacking one or both copies of EphB2 (72-165 cells/group, 4-13 mice/group, Brown-Forsythe and Welch ANOVA test, Dunnett's multiple comparisons test, **p<0.01, ****p<0.0001). **(N)** Graph shows the average number of colocalized PV/VGAT puncta in the SP layer of the CA1 hippocampus of control, PV-EphB2+/-, and PV-EphB2-/- KO mice normalized to control. PV-EphB2-/- KO mice showed a significant increase in the number of PV/VGAT colocalized puncta compared to controls (n=5-13 mice per group, 19-46 images per group, Brown-Forsythe and Welch ANOVA test, Dunnett's multiple comparisons test, *p<0.05). All data are represented as mean ± SEM. Graphics created with Biorender.com.

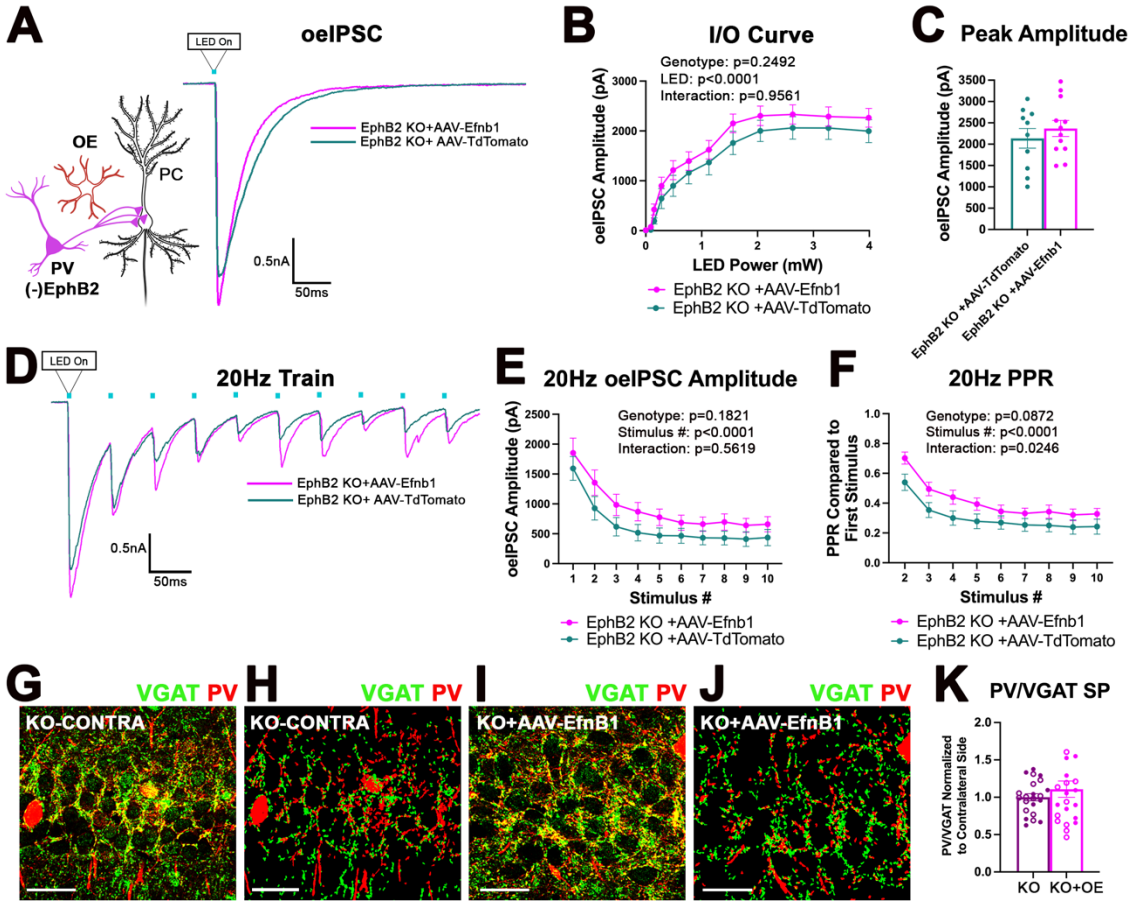
A
oeIPSC
LED On
OE
PC
PV
(-)EphB2
EphB2 KO+AAV-Efnb1
EphB2 KO+ AAV-TdTomato
0.5nA
50ms
B
I/O Curve
Genotype: p=0.2492
LED: p<0.0001
Interaction: p=0.9561
oeIPSC Amplitude (pA)
LED Power (mW)
EphB2 KO +AAV-Efnb1
EphB2 KO +AAV-TdTomato
C
Peak Amplitude
oeIPSC Amplitude (pA)
EphB2 KO +AAV-TdTomato
EphB2 KO +AAV-Efnb1
D
LED On
20Hz Train
EphB2 KO+AAV-Efnb1
EphB2 KO+ AAV-TdTomato
0.5nA
50ms
E
20Hz oeIPSC Amplitude
Genotype: p=0.1821
Stimulus #: p<0.0001
Interaction: p=0.5619
oeIPSC Amplitude (pA)
Stimulus #
EphB2 KO +AAV-Efnb1
EphB2 KO +AAV-TdTomato
F
20Hz PPR
Genotype: p=0.0872
Stimulus #: p<0.0001
Interaction: p=0.0246
PPR Compared to First Stimulus
Stimulus #
EphB2 KO +AAV-Efnb1
EphB2 KO +AAV-TdTomato
G
VGAT PV
KO-CONTRA
H
VGAT PV
KO-CONTRA
I
VGAT PV
KO+AAV-EfnB1
J
VGAT PV
KO+AAV-EfnB1
K
PV/VGAT SP
PV/VGAT Normalized to Contralateral Side
KO
KO+OE

**Figure 2.6: Astrocytic ephrin-B1 overexpression does not further enhance PV->PC connectivity in mice lacking EphB2 in PV interneurons. (A)** Representative current traces of oeIPSCs recorded from excitatory CA1 pyramidal cells of mice overexpressing astrocytic ephrin-B1 but lacking EphB2 in PV interneurons (PV-EphB2 KO+AAV-EfnB1) and vehicle-injected mice lacking EphB2 in PV interneurons (PV-EphB2 KO+AAV-TdT). **(B)** Input-output (IO) curve shows the average oeIPSC amplitude in PV-EphB2 KO+AAV-EfnB1 and in PV-EphB2 KO+AAV-TdT mice plotted against LED power. Overexpression of astrocytic ephrin-B1 in mice lacking EphB2 in PV interneurons did not significantly change the oeIPSC amplitude compared to control mice (n=10-12 cells per group, 5-6 mice per group, 2-way ANOVA (sphericity not assumed, Sidak post hoc test). **(C)** Graph shows the average peak amplitude achieved during generation of the IO curve. oeIPC amplitudes recorded in CA1 PCs of PV-EphB2 KO mice overexpressing astrocytic ephrin-B1 were not significantly different from those recorded in PCs of PV-EphB2 KO mice injected with control AAV-TdT (n=11-12 cells per group, 5-6 mice per group, t-test). **(D)** Representative traces of the oeIPSCs from PV-EphB2 KO+AAV-EfnB1 and PV-EphB2 KO+AAV-TdT cells, generated during stimulation with a 20 Hz train of ten LED pulses. **(E)** Graph shows the average oeIPSC amplitude in PV-EphB2 KO+AAV-EfnB1 and PV-EphB2 KO+AAV-TdT cells during each LED pulse within a 20 Hz train. There was no significant genotype or interaction effect. **(F)** Graph shows the average oeIPSCs normalized to the first stimulus in the 20 Hz train to assess the plasticity with no significant effect of genotype, however there was a significant interaction effect (**E-F**, 9-10 cells per group, 5-6 mice per group, 2-way

ANOVA). **(G-J)** Confocal images **(G,I)** and Neurolucida renderings **(H,J)** of brain slices from EphB2 KO+AAV-EfnB1 mice (KO+OE) and the contralateral uninjected side (KO) of the same brain slice immunolabeled against VGAT (green) and PV (red), scale bar 25 μm. **(K)** Graph shows the number of PV/VGAT colocalized puncta in the SP normalized to the contralateral side of the same brain slice. Overexpression of astrocytic ephrin-B1 in mice lacking EphB2 in PV interneurons did not affect the number of PV/VGAT presynaptic sites (n=22 images/group, 6 mice, paired t-test). All data are represented as mean ± SEM. Graphics created with Biorender.com.

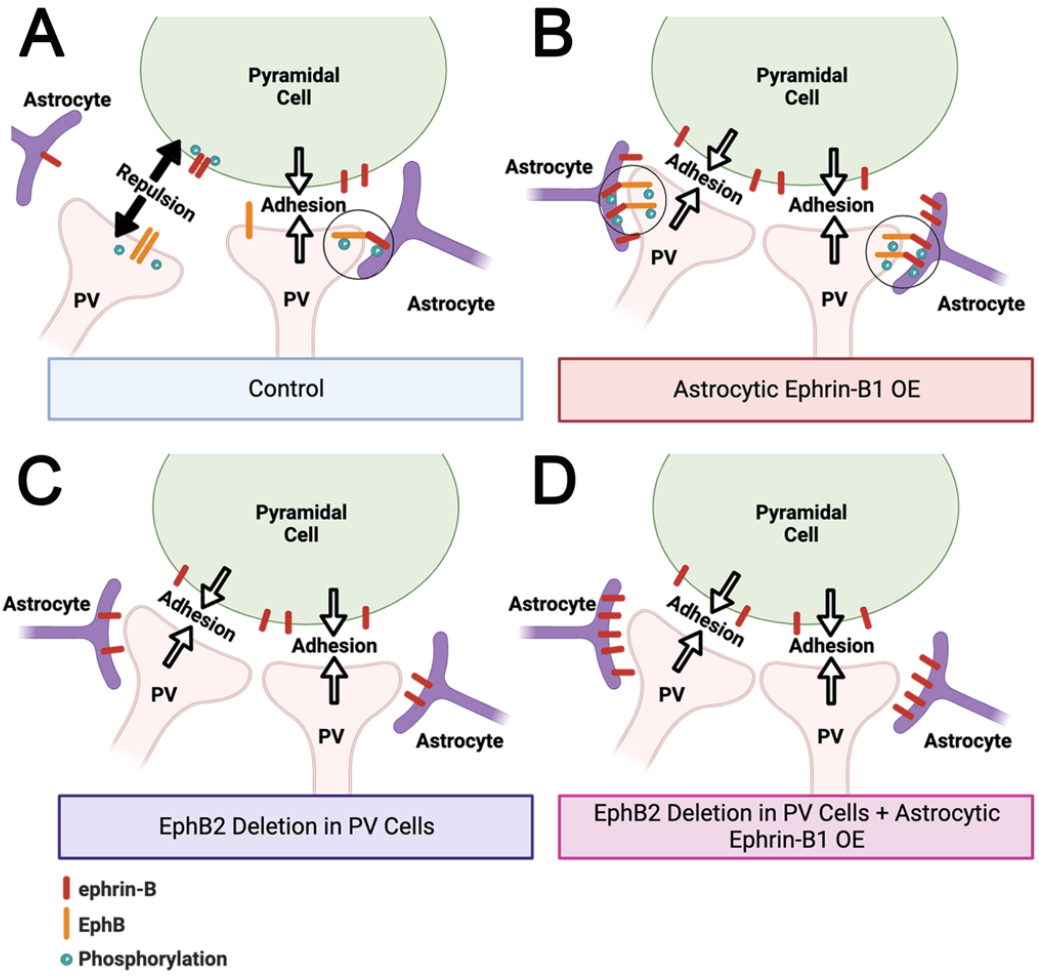
A
Astrocyte
Pyramidal Cell
Repulsion
Adhesion
PV
PV
Astrocyte
Control
B
Pyramidal Cell
Astrocyte
Adhesion
Adhesion
PV
PV
Astrocyte
Astrocytic Ephrin-B1 OE
C
Pyramidal Cell
Astrocyte
Adhesion
Adhesion
PV
PV
Astrocyte
EphB2 Deletion in PV Cells
D
Pyramidal Cell
Astrocyte
Adhesion
Adhesion
PV
PV
Astrocyte
EphB2 Deletion in PV Cells + Astrocytic Ephrin-B1 OE
ephrin-B
EphB
Phosphorylation

**Figure 2.7: Astrocytic ephrin-B1 controls PV->PC connectivity through regulating EphB receptor signaling in PV boutons. (A)** Control astrocytes expressing normal levels of ephrin-B1 compete with pyramidal cell ephrin-B1 for EphB in PV boutons. This interaction facilitates adhesion and formation of PV->PC synapses by preventing repulsion between EphB-expressing PV boutons and ephrin-B1 expressing pyramidal cell soma and allows a limited number of PV->PC connections to form. **(B)** Overexpression of astrocytic ephrin-B1 further enhances the ability of astrocytes to interact with EphB in PV boutons, preventing the repulsion between EphB-expressing PV boutons and ephrin-B1 expressing pyramidal cells, and boosting PV->PC connectivity. **(C)** Loss of EphB2 in PV interneurons also increases PV->PC connectivity. **(D)** Overexpression of ephrin-B1 in astrocytes surrounding PV interneurons lacking EphB2 does not further enhance PV->PC connectivity, suggesting that astrocytes do indeed regulate PV->PC connectivity by preventing the repulsion between EphB-expressing PV boutons and ephrin-B1 expressing pyramidal cells. Graphics created with Biorender.com.

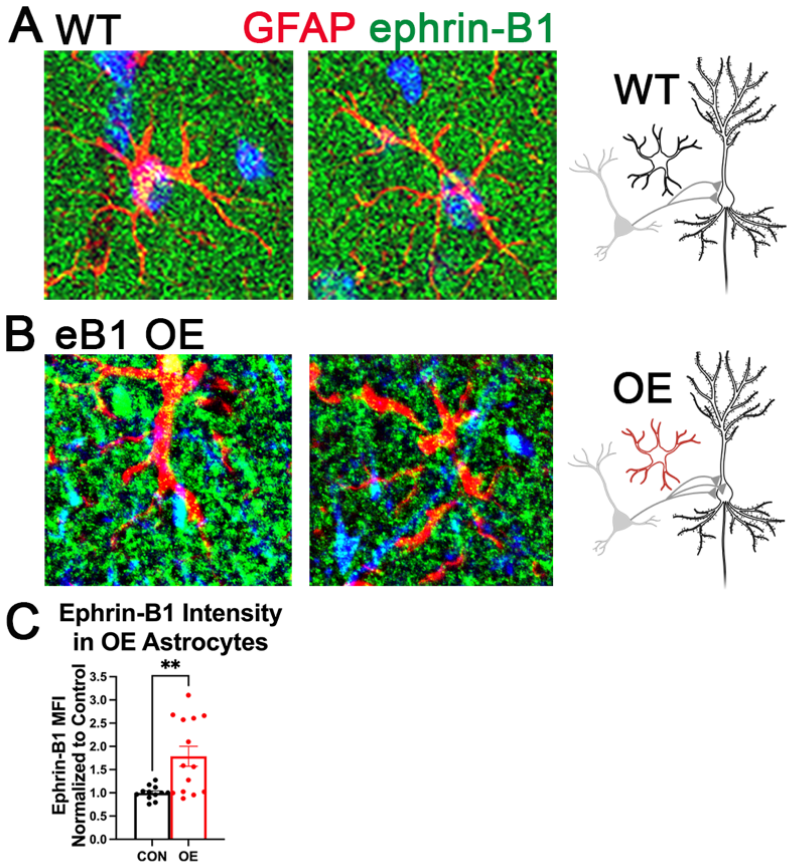


**Figure S2.1: Overexpression of Astrocytic Ephrin-B1 increases levels of ephrin-B1 in astrocytes. (A,B)** Confocal images showing immunolabeling of ephrin-B1 (green) and GFAP (red) in control **(A)** and OE **(B)** astrocytes. **(C)** Graph shows the quantification of ephrin-B1 mean fluorescence intensity levels in GFAP+ astrocytes of OE astrocytes normalized to the intensity of astrocytes from the contralateral, un-injected side of the same brain slice. OE significantly increases ephrin-B1 intensity in astrocytes (n=3 mice, 12-14 images, paired t-test, t=3.629, df=10, p= 0.0046).

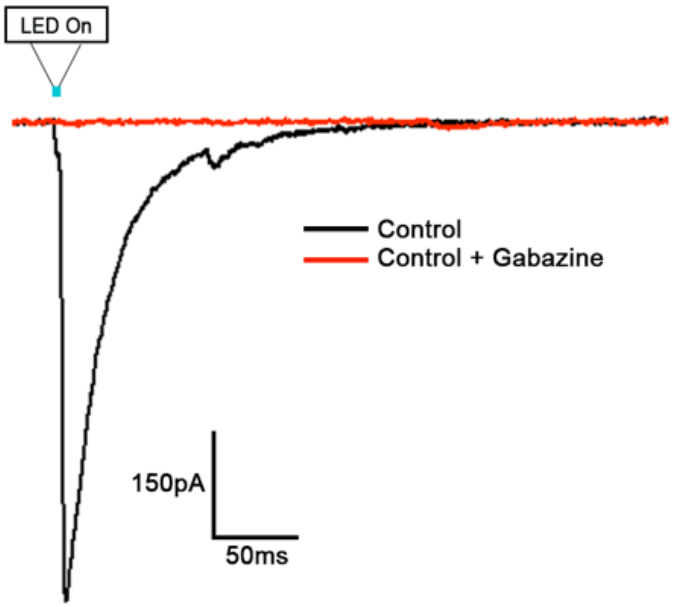


**Figure S2.2: Gabazine wash-in eliminates PV specific oeIPSCs**. Black line shows the optically evoked inhibitory currents recorded in a CA1 pyramidal cell prior to application of Gabazine. The red line shows the current response to optical stimulation after bath-application of 10μM Gabazine. Bath application of gabazine successfully abolished oeIPCs, indicating that the currents were inhibitory.

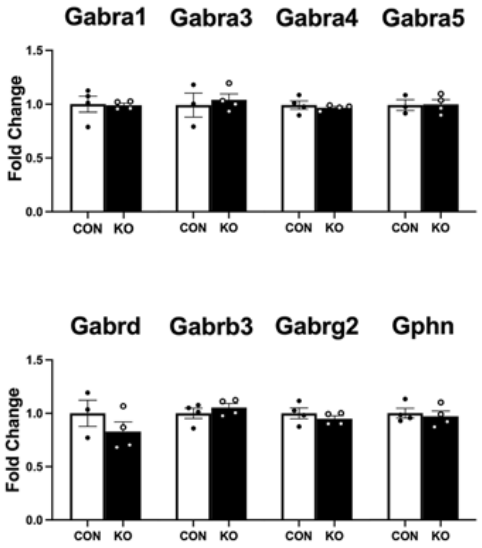


**Figure S2.3: Deletion of astrocytic ephrin-B1 does not influence RNA expression of GABA receptors or gephyrin.** mRNA levels of GABA receptors were analyzed with nanostring analysis. None of the GABA receptors or gephyrin analyzed showed any significant difference following developmental deletion of astrocytic ephrin-B1 (n=3-4 mice/group, t-test).

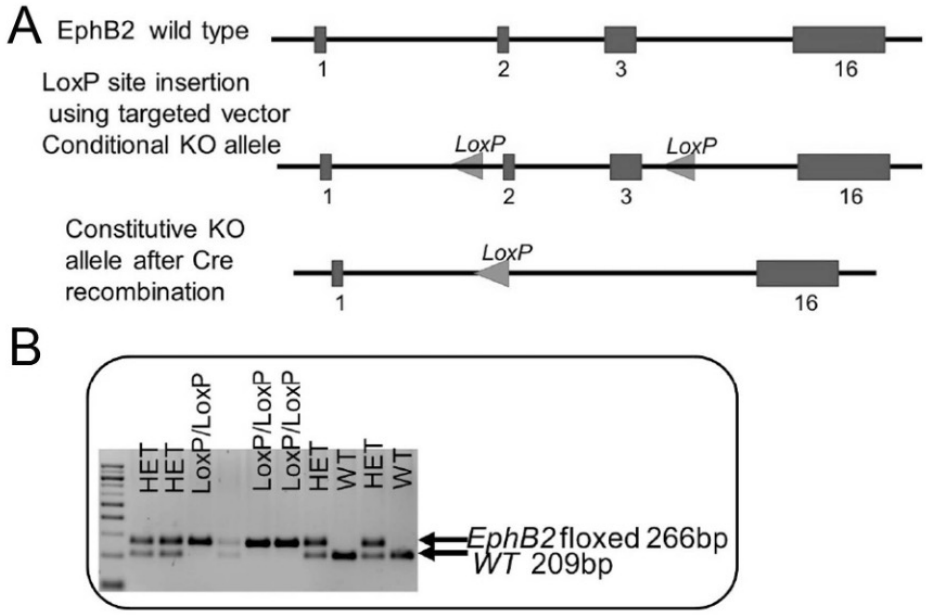


**Figure S2.4: The generation of EphB2 floxed mice.** (A) Schematics of the generation of EphB2floxed mice for conditional deletion of EphB2 using a Cre driver. Exons 2 and 3 were selected as a conditional knockout region by inserting the loxP site upstream of exon 2 and downstream of exon3. Deletion of this region should result in the loss of the ligand binding domain of EphB2 receptor. (B) Representative genotypes showing the WT band (209 bp), the heterozygous (HET), and the homozygous EphB2floxed band (266 bp).

| Gene | Forward Sequence | Reverse Sequence | Method |
|---|---|---|---|
| GAPDH | AGGTCGGTGTGAACGGATTTG | TGTAGACCATGTAGTTGAGGTCA | qRT-PCR |
| ErbB4 | TGCCATAAGTCTTGCACTGG | CGTAGGGTCCATAGCACCTG | qRT-PCR |
| Nrg1 | | | Nanostring |
| CB1R | | | Nanostring |

**Table S2.5**: Primer sequences used for RT-PCR analysis.

# CHAPTER THREE

## Astrocytic Ephrin-B1 Regulates Oligodendrocyte Development and Myelination

A version of this chapter was submitted for publication in the ASN Neuro (Sutley-Koury et al., ASN Neuro 2024 under review)

## 3.1 Abstract

Astrocytes have been implicated in oligodendrocyte development and myelination, however, the mechanisms by which astrocytes regulate oligodendrocytes remain unclear. My findings suggest a new mechanism that regulates astrocyte-mediated oligodendrocyte development through ephrin-B/EphB receptor signaling. Using a mouse model, I examined the role of astrocytic ephrin-B1 signaling in oligodendrocyte development by deleting ephrin-B1 specifically in astrocytes during the postnatal days (P)14-P28 period and used mRNA analysis, immunohistochemistry, and mouse behaviors to study its effects on oligodendrocytes and myelination. I found that deletion of astrocytic ephrin-B1 downregulated many genes associated with oligodendrocyte development, myelination, and lipid metabolism in the hippocampus and the corpus callosum. Additionally, I observed a reduced number of omyligodendrocytes and impaired myelination in the corpus callosum of astrocyte-specific ephrin-B1 KO mice. Finally, my data show that these mice exhibit a clasping phenotype, which is indicative of reduced motor strength, most likely due to impaired myelination. My studies provide new evidence that astrocytic ephrin-B1 positively regulates oligodendrocyte development and myelination, potentially through astrocyte-oligodendrocyte interactions.

## 3.2 Introduction

Astrocytes and oligodendrocytes are two major macro glial cell types in the CNS. Astrocytes perform a number of critical functions including synapse formation and elimination, synaptic plasticity, ion homeostasis, neurotransmission, as well as regulate the innate and adaptive immune responses (Liddelow and Barres, 2017; Khakh and Deneen, 2019). The primary function of oligodendrocytes is generation of the myelin sheath around axons of CNS neurons (De Robertis et al., 1958; Baumann and Pham-Dinh, 2001). Although astrocytes and oligodendrocytes play distinct roles in supporting neuronal functions, there are active interactions between these cell types. Astrocytes are suggested to be important regulators of oligodendrocyte development and function (Clemente et al., 2013). Astrocyte-secreted factors such as platelet derived growth factor (PDGF) and leukemia inhibitory factor-like (LIF) protein are required for proper oligodendrocyte development and survival (Raff et al., 1988; Gard et al., 1995). Additionally, astrocyte-secreted factors regulate oligodendrocyte differentiation and myelination (Richardson et al., 1988; Ishibashi et al., 2006). Not only do astrocytes regulate oligodendrocytes through secreted factors, but they also influence oligodendrocyte metabolism through gap junction coupling, allowing for direct transfer of metabolites, as well as electrical coupling between the cells (Kleopa et al., 2004; Kamasawa et al., 2005; Stadelmann et al., 2019). My findings suggest a new mechanism that regulates astrocyte-mediated oligodendrocyte development through ephrin-B/EphB receptor signaling.

Neuronal Ephs and ephrins regulate a number of neurodevelopmental processes including axon guidance, cell migration, and synapse maturation. The trans-synaptic functions of Ephs and ephrins are particularly well studied in excitatory synapses where Ephs and ephrins regulate dendritic spine formation, AMPAR and NMDAR trafficking and localization, and synaptic plasticity (Dalva et al., 2000; Ethell et al., 2001; Contractor et al., 2002; Henkemeyer et al., 2003; Kayser et al., 2006; Moeller et al., 2006; Sloniowski and Ethell, 2012). We previously observed that astrocytes express ephrin-B1, and that ephrin-B1 in astrocytes regulates both excitatory and inhibitory synapse development in the CA1 hippocampus (Nguyen et al., 2020). Here I propose a new role for astrocytic ephrin-B1 signaling in oligodendrocyte development that has not been previously described. Oligodendrocyte precursor cells (OPCs) express several Ephs and ephrins, including EphA2, -A4, -B1, and -B2, and ephrin-A1, -A5, -B1, -B2, and -B3 (Linneberg et al., 2015). Moreover, EphA4 and EphB1 mRNA and protein levels in particular significantly increase as OPCs mature into oligodendrocytes (Linneberg et al., 2015). The same group also showed that EphB forward signaling in oligodendrocytes impaired myelination, while ephrin-B reverse signaling in oligodendrocytes enhanced myelination, supporting a role for ephrin-B/EphB in regulating oligodendrocyte differentiation and myelination (Linneberg et al., 2015). Additionally, myelinating oligodendrocytes were shown to express ephrin-B3, which acts as an inhibitor of neurite outgrowth during development, by interacting with Eph receptors in cortical neurons (Benson et al., 2005). Furthermore, both ephrin-B and ephrin-A signaling in OPCs controls OPC adhesion and migration (Chatzopoulou et al., 2004). Treatment of OPCs

with ephrin-Bs showed that ephrin-B1 and -B3 inhibit OPC differentiation in culture by activating EphA4 signaling in OPCs, leading to inhibition of focal adhesion (FAK), which was previously described as a positive regulator of OPC development and myelination (Forrest et al., 2009; Syed et al., 2016). These results were further corroborated by another group showing that EphA4 signaling in oligodendrocytes prevented axo-glial contact formation and myelination (Harboe et al., 2018). Together, these findings support a role for Eph/ephrin signaling in oligodendrocyte development and myelination, however the contributions of astrocyte specific ephrin-B1 in regulating these processes has not been previously described.

The goal of this study was to determine the role of ephrin-B/EphB receptor signaling in astrocyte-oligodendrocyte communications and oligodendrocyte development. I targeted the postnatal day (P)14-P28 period of oligodendrocyte development and myelination and examined the role of ephrin-B/EphB signaling by deleting ephrin-B1 from astrocytes. I observed a significant downregulation in genes implicated in oligodendrocyte differentiation and myelination using Nanostring mRNA analysis and reduced myelination in the corpus callosum using immunohistochemical assays. In addition, I report impaired motor strength in these mice showing clasping phenotype most likely due to impaired myelination. My findings provide new evidence for the role of astrocytic ephrin-B1 in regulating oligodendrocyte development and myelination, potentially through astrocyte-oligodendrocyte interactions.

## 3.3 Methods

### *3.3.1 Ethics statement.*

Mouse studies were performed according to National Institutes of Health and Institutional Animal Care and Use Committee at the University of California Riverside guidelines; animal welfare assurance #A3439-01 is on file with the Office of Laboratory Animal Welfare. Mice were maintained in an Association for Assessment and Accreditation of Laboratory Animal Care-accredited facility under 12 h light/dark cycle and fed standard mouse chow.

### *3.3.2 Mice*

In order to evaluate the effects of astrocytic ephrin-B1 deletion on myelination, and oligodendrocyte development, I used two mouse lines: (1) ERT2-Cre$^{GFAP}$*ephrin-B1*$^{flox/y}$ KO mice were generated by breeding female *ephrin-B1*$^{flox/flox}$ (129S-*Efnb1* $^{flox}$/J, RRID:IMSR_JAX:007664) mice with male ERT2-Cre$^{GFAP}$ (B6.Cg-Tg(*GFAP*-cre/ERT2)505Fmv/J, RRID:IMSR_JAX: 012849) mice. Ephrin-B1$^{flox/y}$ mice that did not express ERT2-CreGFAP were used as controls (2) Rosa-CAG-LSL-tdTomato reporter mice (CAG-tdTomato; RRID:IMSR_JAX:007909) were bred with ERT2-Cre$^{GFAP+/+}$ (B6.Cg-Tg(*GFAP*-cre/ERT2)505Fmv/J RRID:IMSR_JAX:012849) mice to generate tdTomatoERT2-Cre$^{GFAP}$ mice first. Then, male tdTomatoERT2-Cre$^{GFAP}$ mice were crossed with female *ephrin-B1*$^{flox/flox}$ to obtain tdTomatoERT2-Cre$^{GFAP}$*ephrin-B1*$^{flox/y}$ KO male mice. For controls, tdTomatoERT2-Cre$^{GFAP}$ male mice were crossed with

control female ephrin-B1$^{+/+}$ mice to generate tdTomatoERT2-Cre$^{GFAP}$ control male mice, resulting in tdTomato expression in astrocytes (used for nanostring/mRNA analysis). Both control and KO mice were treated with tamoxifen at P14 intraperitoneally (0.5 mg in 5 mg/ml of 1:9 ethanol/sunflower seed oil solution) once a day for 5 consecutive days and analysis was performed at P28.

*3.3.3 Immunohistochemistry*

Immunohistochemistry was performed as previously described in (Nguyen et al., 2020). Animals were anesthetized with isoflurane and transcardially perfused with 0.1M PBS followed by fixation with 4% paraformaldehyde (PFA) in 0.1 M PBS, pH 7.4. Brains were postfixed for 2 h in 4% PFA in 0.1 M PBS. 100 μm coronal brain slices were obtained via vibratome sectioning. Samples were washed in PBS, permeabilized in 0.3% Triton in PBS for 30 min, blocked for 2 h in 15% normal goat serum (NGS) in 0.1 M PBS. Primary and secondary antibodies were diluted in PBS. Samples were incubated in primary antibodies for 2 h at room temperature and then overnight at 4°C. Chicken anti-myelin basic protein (MBP) (1:500, EMD Millipore, AB9348, RRID:AB_2140366) was used to detect myelin and rabbit anti-Olig2 (1:500, EMD Millipore, AB9610, RRID:AB_570666) was used to identify oligodendrocytes. Following incubation with primary antibody, samples were washed with PBS, then incubated with secondary antibodies for 2 h at room temperature. Primary antibodies were recognized with the following secondary antibodies: Donkey anti-rabbit 488 IgG (1:500, Invitrogen, A-21206, RRID:AB_2535792) and goat anti-chicken 647 (1:500, Invitrogen, A-21449,

RRID:AB_2535866). Samples were then washed in PBS and then mounted on coverslips with Vectashield antifade mounting medium with Dapi (Vector Laboratories, H-2000).

*3.3.4 Confocal Imaging and Analysis*

Confocal images of coronal brain slices containing the stratum oriens (SO), stratum pyramidal (SP), and stratum radiatum (SR) of the dorsal CA1 hippocampus or corpus callosum (CC) were taken using a Zeiss LSM 880 inverted laser scanning microscope. High resolution optical sections were acquired with a 20x air objective (0.8 NA), 1x zoom at 1 μm step intervals, (1024x1024) pixel format to measure myelin basic protein (MBP) intensity, the number of Olig2+ oligodendrocytes, and Olig2+ intensity. Identical conditions were used to acquire and process all samples for analysis.

For analysis of MBP intensity, Z-stacks of equal size were collapsed into a single image by projection and converted to a tiff file, images were separated by channel and regions of interest (ROIs) were drawn around the area to be measured. For CC measurement the ROI was drawn around the CC and for the hippocampus, ROIs contained SO, SP, and SR layers. Any cortical areas in the image were excluded from the measurements. Mean fluorescence intensity levels within the ROIs were measured. Background signal was measured using a secondary antibody only control and then was subtracted from the fluorescence intensity measurement. Statistical analysis was performed using GraphPad Prism 10 software (RRID:SCR_002798) using a two-tailed student's t-test.

For analysis of Olig2+ cell density, Z-stacks of equal size were collapsed into a single image by projection, converted to a tiff file, separated by channel, and background subtracted. Each image was threshold-adjusted, converted into a binary image, the despeckle function was used to eliminate noise and the watershed function was used to segment overlapping cells. Particle analysis was used to count the number of cells per image and to generate ROIs around the counted cells. Images were re-opened, separated by channel, and the ROIs were applied to the Olig2 channel. Mean fluorescence intensity levels within the ROIs were measured. Background signal was measured using a secondary antibody only control and then was subtracted from the fluorescence intensity measurement. Statistical analysis was performed using GraphPad Prism 10 software (RRID:SCR_002798) using a two-tailed student's t-test.

*3.3.4 Nanostring*

Half-brains were dissected and frozen in liquid nitrogen and stored in -80°C. RNAlater Ice (Invitrogen AM7030) was used to thaw samples according to manufacturer's instructions. After thawing in RNAlater Ice, hippocampal tissue was dissected in DEPC-treated PBS on ice. Following dissection, total RNA was isolated using Invitrogen PureLink RNA Mini Kit (ThermoFisher Scientific/Invitrogen, 12183020). Samples were lysed in RNA lysis buffer with β-mercaptoethanol (BME) added as described in the protocol provided by the kit. Tissue samples were homogenized in a lysis buffer provided by the kit using a pestle and then were passed through an 18-gauge needle. Following lysis, samples were centrifuged at 12,000 g for 2 min and the

supernatants were transferred to fresh tubes. RNA isolation was then performed according to the manufacturer's instructions. Samples were eluted in nuclease free water. To remove any residual salts or contaminants from buffers used during RNA isolation, RNA samples were further purified by ethanol precipitation as follows; 0.1 volumes of 0.3M Na-Acetate and 3 volumes of ice-cold 100% ethanol were added to the samples. Samples were incubated at -20°C overnight, centrifuged at 12,000 g, and then ethanol was removed, the pellet was dried, and samples were reconstituted in nuclease free water. RNA concentration and purity was determined using a Nanodrop spectrophotometer (RRID:SCR_016517), then samples were analyzed using Agilent 2100 Bioanalyzer/Advanced Analytics Fragment Analyzer (RRID:SCR_018043). RIN values above 7 were considered to be adequate for Nanostring profiling. RNA samples were analyzed using nCounter Mouse Glial Profiling Panel (Nanostring, XT-CSO-M-GLIAL-12) according to manufacturer's instructions. Briefly, 50 ng of unamplified RNA was hybridized with the reporter codeset at 65°C for 18 h. Samples were spun down, nuclease free water was added to the samples, and then the samples were loaded into the nCounter cartridge. The cartridge was run on the Nanostring nCounter SPRINT Profiler (RRID:SCR_021712). Data was exported and analyzed using Nanostring nSolver and Advanced Analysis Software (RRID:SCR_021712). Normalized linear counts for all genes in the panel were used to graph fold changes of control and KO genes. Statistical analysis was performed in the Nanostring online advanced analysis differential expression module using the differential expression algorithm described in the advanced

analysis manual (nCounter Advanced Analysis 2.0 User Manual, MAN-10030-03). The Bonferroni correction was used to correct for the high number of multiple comparisons.

*3.3.5 qRT-PCR analysis*

P28 mouse brains were dissected on ice in DEPC-treated PBS. Following dissection, total RNA was acutely isolated as described above. Samples were eluted in nuclease free water, and RNA concentration and purity was determined using a Nanodrop spectrophotometer (RRID:SCR_016517). Samples were diluted to equal concentrations in nuclease free water. cDNA was synthesized using a High-Capacity cDNA Reverse Transcription Kit (Applied Biosystems, 4368814). qRT-PCR was performed using PowerSYBR Green PCR Master Mix (Applied Biosystems, 4367659) on Quantstudio 6 Flex System thermocycler (Applied Biosystem/Life Technologies, RRID:SCR_020239). Data was normalized to GAPDH loading control and then analyzed using ΔΔCt method normalized to GAPDH housekeeping gene. Statistical analysis performed in GraphPad Prism 10 software using two-tailed student's t-test. Primer sequences are listed in supplemental materials (Table S1).

*3.3.6 Clasping*

Before testing, mice were housed in a room with a 12 h light/dark cycle with ad libitum access to food and water. Cages were transferred to the behavioral room 30 min prior to testing for habituation. Clasping behavior was assessed with methods similar to previously described (Guyenet et al., 2010). Briefly, mice were held by the base of the

tail and were video recorded as they were suspended in the air for one minute. The presence of a clasping phenotype was scored by an experimenter blind to the condition as follows: 0 - hindlimbs were consistently splayed away from the abdomen, 1 – one hindlimb was retracted toward the abdomen, 2 – both hindlimbs were retracted toward the abdomen, and 3 – both hindlimbs were retracted toward the abdomen and touched the abdomen. Statistical analysis performed in GraphPad Prism 10 software using Mann-Whitney test and Log-rank (Mantel-Cox) test.

## 3.4 Results

### *3.4.1 Deletion of astrocytic ephrin-B1 affected expression of genes associated with astrocyte metabolism, calcium signaling and reactive state.*

In order to assess whether developmental deletion of astrocyte specific ephrin-B1 alters the expression of glial genes, I performed Nanostring analysis on RNA isolated from brain tissues including hippocampus and CC of P28 control and KO male mice using the Nanostring Glial Profiling Panel. Of the 74 differentially expressed genes, 13 were associated with astrocytes (Fig. 3.1B). Vimentin, an intermediate filament expressed in astrocytes (Schnitzer et al., 1981), was significantly reduced (Fig. 3.1C, p= 0.0106), while GFAP was unchanged (p=0.506). Genes encoding for *Chil1* (p=0.0457) and *Serpina3n* (Fig. 3.1C, p=0.000191), both of which are secreted by reactive astrocytes (Escartin et al., 2021), were also found to be reduced in KO animals, suggesting that deletion of astrocytic ephrin-B1 may reduce the inflammatory response and or reactivity

of astrocytes. *Serpina3n* is a serine protease inhibitor which is secreted into the extracellular matrix (Escartin et al., 2021). Enzymes associated with metabolism in astrocytes were also affected by KO such as, *Aldh1l1* (Fig. 3.1C, p= 0.0033) which was reduced in KO mice and *Aldh1a1* (Fig. 3.1C, p= 0.00615), which was increased in KO mice (Anthony and Heintz, 2007; Kwak et al., 2020). The transcription factor *Rfx4*, which was shown to be enriched in astrocytes was also reduced in KO mice (Fig. 3.1C, 0.00242). Two genes associated with calcium signaling in astrocytes, *Cpne2* (Fig. 3.1C, p= 0.00879) and *Gmp6* (Fig. 3.1C, p= 0.000642) were increased in KO animals (Creutz et al., 1998; Mukobata et al., 2002). The most significantly regulated gene I detected via Nanostring analysis was the *Slc8a1* gene (Fig. 3.1C, p= 3.47E-06), encoding the NCX sodium-calcium exchanger (Rose et al., 2020). Although this gene is not specific to astrocytes and is expressed in neurons, it is also expressed in astrocytes and plays an important role in sodium/calcium buffering in astrocytes (Rose et al., 2020). Astrocyte calcium signaling has been implicated in astrocyte functions such as release of gliotransmitters, which could have a profound impact on neuronal function (Bazargani and Attwell, 2016; Goenaga et al., 2023). Interestingly I found that expression of the cell surface receptor *Amigo-2*, which is associated with A1-polarized reactive astrocytes (Kim et al., 2024) was significantly increased (Fig. 3.1C, p= 0.0209), while the cell surface receptor *Fcgrt* (Stamou et al., 2018) was modestly reduced (Fig. 3.1C, p= 0.0464). A full table of the statistical analysis and levels of all genes assayed via Nanostring analysis can be found in the supplementary materials (Extended Data Table 1).

*3.4.2 Developmental deletion of ephrin-B1 in astrocytes impairs expression of oligodendrocyte- and myelin-associated genes.*

Nanostring analysis revealed that deletion of astrocytic ephrin-B1 during the P14-P28 developmental period also affected expression of a significant number of oligodendrocyte- and myelin-associated genes. I observed a broad downregulation of genes associated with oligodendrocyte differentiation, myelination, and lipid metabolism (Fig. 3.2B-D). mRNA levels of several transcription factors implicated in oligodendrocyte differentiation were reduced in KO mice, including *Sox10* and *Dlx1* (Fig. 3.2B, *Sox10*: p= 0.000113; *Dlx1*: p= 0.0352), suggesting a possible reduction in oligodendrocytes or impaired oligodendrocyte maturation in KO mice (Stolt et al., 2002; Petryniak et al., 2007; Pozniak et al., 2010; Kuhn et al., 2019). I found that genes encoding the major protein components of the myelin sheath including myelin basic protein (*MBP*) and proteolipid protein 1 (*Plp1*) (Kuhn et al., 2019) were also significantly reduced in KO mice (Fig. 3.2C, *MBP*: p= 0.00327; *Plp1*: p= 0.00115). Furthermore, I detected a reduced mRNA expression of genes involved in lipid metabolism in KO mice (Fig. 3.2D). Of particular interest, I found reduced *Ugt8a* and *Fa2h* mRNA levels (Fig. 3.2D, *Ugt8a*: p= 0.00877; *Fa2h*: p= 0.000862), encoding the enzymes involved in sphingolipid synthesis, which are abundant in the myelin sheath (Coetzee et al., 1998; Marcus et al., 2000; Maldonado et al., 2008; Eckhardt, 2023). The reduction in genes encoding the components of the myelin sheath and enzymes regulating lipid metabolism may suggest that myelination is likely impaired following deletion of astrocytic ephrin-B1. Interestingly, I found that expression of connexin-32 (Cx32), a connexin found in

oligodendrocytes and involved in coupling oligodendrocytes and astrocytes (Altevogt and Paul, 2004; Kleopa et al., 2004; Kamasawa et al., 2005; Stadelmann et al., 2019), was also downregulated in KO mice (Fig. 3.2E, p= 0.00151). I further investigated the levels of two connexins expressed in astrocytes, Cx30, which forms gap junctions with oligodendrocyte Cx32 (Altevogt and Paul, 2004; Kleopa et al., 2004; Kamasawa et al., 2005), and Cx43 using qRT-PCR and found that KO mice showed reduced levels of Cx30 (Fig. 3.2E, Extended Data Table 2; t-test, t(4)=2.980, p=0.0407), but not Cx43 (Fig. 3.2E, Extended Data Table 2; t-test, t(4)=1.005, p=0.3719). Reduced mRNA levels of Cx32 and Cx30 in KO mice could indicate impaired astrocyte-oligodendrocyte communication.

*3.4.3 Loss of astrocytic ephrin-B1 impaired myelination and reduced the number of oligodendrocytes in the CC but not the hippocampus.*

Because I found such marked reductions in nearly all oligodendrocyte- and myelin-related genes assessed via nanostring, I next assessed whether myelination or oligodendrocyte development was impaired by developmental deletion of astrocytic ephrin-B1. To analyze myelin levels , I performed immunolabeling against MBP, one of the main proteins of the myelin sheath (Stadelmann et al., 2019), and analyzed the fluorescence intensity in both the CC and the CA1 hippocampus of CON and KO mice. I found reduced MBP fluorescence intensity in the CC (Fig. 3.3B, Extended Data; t-test, t(6)=3.197, p= 0.0187) but not the CA1 hippocampus of KO mice (Fig. 3.3E, Extended Data; t-test, t(6)=0.6161, p=0.5605). The reduced MBP intensity in the CC indicates that

KO mice show impaired myelination. The overall MBP immunolabeling was much lower in the hippocampus than the CC, most likely contributing to our inability to detect any differences between CON and KO mice. Next, I analyzed whether there were any differences in the oligodendrocyte development. I visualized Olig2 positive (+) oligodendrocytes using immunofluorescence labeling and counted the number of Olig2+ cells in the CC and CA1 hippocampus of CON and KO mice. Developmental deletion of astrocytic ephrin-B1 significantly reduced the number of Olig2+ cells in the CC (Fig. 3.3C, Extended Data; t-test, $t(14)=3.656$, $p= 0.0026$), and resulted in a trend towards reduced numbers in the hippocampus (Fig. 3.3F, Extended Data; t-test, $t(29)=1.764$, $p=0.0883$). My results suggest that oligodendrocyte maturation or survival is impaired in KO mice, leading to the deficits in myelination.

*3.4.4 Astrocytic ephrin-B1 KO mice exhibit a clasping phenotype.*

In order to determine whether the observed reduction in oligodendrocytes and myelin expression resulted in functional impairments in vivo, I subjected P28 CON and KO mice to a clasping test. A clasping phenotype where mice retract their hindlimbs toward the abdomen when suspended by the tail, has been observed in mouse models of EAE and the presence of a clasping phenotype can be a sign of decreased motor strength due to hypomyelination or demyelination (Cahill et al., 2019; Bhaskaran et al., 2023). I found that developmental deletion of astrocytic ephrin-B1 resulted in a clasping phenotype that was significantly increased compared to controls at all time points assessed (Fig 3.4A-C, Extended Data; t= 10 s: Mann-Whitney test, DoF= 29, $p= 0.0066$;

t= 30 s: Mann-Whitney test, DoF= 29, p= 0.0008; t= 60 s: Mann-Whitney test, DoF= 29, p= 0.0065). Indeed, KO mice showed an increased probability of developing the clasping phenotype over the course of the test compared to controls (Fig 3.4D, Extended Data; Log-rank test, p= 0.0048). The presence of the clasping phenotype in KO mice suggests reduced motor strength most likely as a result of the observed deficits in oligodendrocyte development and myelination.

### 3.5 Discussion

Here I provide new evidence that astrocytes regulate oligodendrocyte development and myelination during development through ephrin-B1 signaling. My study reports that the astrocyte-specific deletion of ephrin-B1 during P14-P28 developmental period leads to (1) dysregulation of both astrocyte- and oligodendrocyte-related genes; (2) impaired oligodendrocyte development and myelination; (3) clasping phenotype, indicative of reduced motor strength.

I found that developmental deletion of astrocytic ephrin-B1 led to dysregulated expression of several genes associated with reactive astrocytosis (Fig. 3.1B-C). Of particular interest, genes encoding proteins secreted by reactive astrocytes, *Chil1* and *Serpina3n*, were found to be significantly reduced in KO animals (Fig. 3.1C). *Chil1* (*Chi3l1*, YKL-40) plays a role in cell growth, proliferation, and survival, inflammatory response, as well as regulating synthesis and degradation of the extracellular matrix through inhibiting type 1 collagen and hyaluronic acid degradation and regulating the

activity of MMPs (Zhao et al., 2020). Increased levels of *Chi3l1* in the cerebrospinal fluid (CSF) have been observed in Alzheimer's disease (AD) and multiple sclerosis (MS) (Craig-Schapiro et al., 2010; Floro et al., 2022). Recently, *Chi3l1* overexpression was shown to reduce hippocampal neurogenesis and impair hippocampal dependent learning in mice (Jiang et al. 2023), while knockdown in astrocytes increased phagocytosis of pHrodo beads and Aβ42 peptides in culture (Lananna et al., 2020). *Serpina3n* has been shown to be increased in many neuroinflammatory contexts, including AD, stroke, TBI, and TLE (Norton et al., 2021; Ma et al., 2022; Zhang et al., 2022; Liu et al., 2023). *Serpina3n* was found to be upregulated following the kainate (KA)-induced seizure model and was shown to mediate immune responses in astrocytes (Liu et al., 2023). While its overexpression increased expression of multiple cytokines, silencing of Serpina3n reduced cytokine expression and NFκB signaling (Liu et al., 2023). Dysregulation of these genes may suggest that astrocyte reactivity and immune response are altered in ephrin-B1 KO mice.

Additionally, I observed that genes associated with calcium signaling in astrocytes were significantly upregulated, such as *Gpm6a* and *Cpne2* (Fig. 3.1C). In neurons, Gpm6a has been implicated in NGF-mediated $Ca^{2+}$ influx (Mukobata et al., 2002). In addition, *Gpm6a* was shown to bind to many synaptic proteins, and of interest to this study, was also found to bind to Plp, one of the major myelin proteins (Aparicio et al., 2020). *Gpm6a* expression has been detected in subsets of astrocytes in a mouse model of TBI, however the function of Gpm6a remains to be explored (Choi et al., 2013). Interestingly, the most significantly regulated gene I detected via Nanostring analysis was

the Slc8a1 gene (Fig. 3.1C), encoding NCX sodium-calcium exchanger. Expression of this transporter in astrocytes is hypothesized to convert sodium transients induced by excitatory neuronal activity into astrocyte calcium signals through reverse transport of calcium through the exchanger (Rose et al., 2020). The increased expression of *Slc8a1* in KO animals, therefore, could suggest that astrocytes are more responsive to excitatory neuronal activity and are able to initiate calcium signaling in response to more modest neuronal activity. Astrocyte calcium signaling is also known to induce the release of gliotransmitters such as D-serine, adenosine, ATP, and GABA, therefore alterations in astrocyte calcium signaling could have profound effects on neurotransmission and neuronal excitability (Bazargani and Attwell, 2016; Goenaga et al., 2023).

Most importantly, I found that genes associated with oligodendrocyte development, myelination, and lipid metabolism were all significantly decreased in KO animals (Fig. 3.2B-D). For example, mRNA levels of *Dlx1*, a negative regulator of oligodendroglial versus neuronal specification during development (Petryniak et al., 2007) were reduced in KO mice (Fig. 3.2B). Furthermore, mRNA levels of *Sox10*, one of the major drivers of oligodendrocyte differentiation and a transcription factor required for oligodendrocytes to acquire a myelinating phenotype was also significantly reduced in KO animals (Fig. 3.2B) (Stolt et al., 2002; Pozniak et al., 2010; Kuhn et al., 2019), suggesting that oligodendrocyte development was altered in KO mice. Only mature oligodendrocytes acquire the ability to myelinate axons and begin expressing myelin proteins such as Plp, MBP, MAG, and Mog, therefore the reduced mRNA levels of all of these genes also suggest impaired oligodendrocyte maturation in KO mice as well as

reduced myelination (Kuhn et al. 2019). I also detected decreases in several genes associated with lipid metabolism (Fig. 3.2D), including cholesterol, ceramide, and sphingolipid metabolism, all of which are major components of the myelin sheath (Coetzee et al., 1998; Marcus et al., 2000; Maldonado et al., 2008; Chrast et al., 2011; Stadelmann et al., 2019; Poitelon et al., 2020; Ho et al., 2022; Eckhardt, 2023). Altogether, Nanostring mRNA analysis revealed marked downregulation of many oligodendrocyte, myelin, and lipid metabolism genes in KO animals, which suggests a supportive role for astrocytic ephrin-B1 in oligodendrocyte development and myelination during development.

To address whether the changes in oligodendrocyte and myelin related genes resulted in changes in oligodendrocyte development or myelination at the protein level, I used immunofluorescence staining to detect the number of oligodendrocytes and the MBP levels in the corpus callosum, one of the largest white matter tracts in the brain, and the hippocampus (Fig. 3.3). In support of my gene expression data, I found that both the number of oligodendrocytes and the MBP levels were reduced in the CC of KO mice (Fig. 3.3A-C), supporting the mRNA changes detected by Nanostring analysis and suggesting that oligodendrocyte development and myelination were impaired in KO mice. The changes were less robust in the hippocampus possibly due to the fact that there were fewer oligodendrocytes in the hippocampus than the CC. The data supports that astrocytic ephrin-B1 regulates oligodendrocyte development and myelination during the P14-P28 developmental period. To test if the observed deficits in oligodendrocyte numbers and myelination resulted in functional impairments in vivo, I tested whether KO

mice exhibited a clasping phenotype, indicative of reduced motor strength due to impaired myelination. Indeed, developmental deletion of astrocytic ephrin-B1 resulted in an increase in clasping behavior (Fig. 3.4). Previous studies showed that demyelination induced by EAE and Sod2 deletion in motor neurons resulted in clasping behavior, suggesting that the observed clasping phenotype can be attributed to poor myelination (Cahill et al., 2019; Bhaskaran et al., 2023).

Astrocytes and oligodendrocytes are functionally coupled through pairs of connexin (Cx) gap junction proteins, allowing for electrical coupling, spatial buffering, and transfer of metabolites between the cells (Stadelmann et al., 2019). Astrocytes express Cx30 and Cx43, while oligodendrocytes express Cx47 and Cx32 and astrocyte-oligodendrocyte gap junctions are composed of Cx47/Cx43 or Cx32/Cx30 pairs, where Cx32/30 channels are localized to the outer layer of myelin sheaths, while Cx47/Cx43 channels are more often localized to oligodendrocyte somata (Altevogt and Paul, 2004; Kleopa et al., 2004; Kamasawa et al., 2005; Stadelmann et al., 2019). Interestingly, Nanostring analysis revealed that mRNA levels of Cx-32 were reduced in KO animals (Fig. 3.2E). Further qPCR analysis revealed that mRNA levels of the partner for Cx32 expressed on astrocytes, Cx30, was also significantly reduced in KO animals (Fig. 3.2E). However, mRNA levels of Cx43 were not affected by developmental deletion of astrocytic ephrin-B1 (Fig. 3.2E). These findings are intriguing because they suggest that impaired astrocyte-oligodendrocyte communication likely occurs at the myelin sheath but not necessarily at the oligodendrocyte soma in our model. Other groups showed that double deletion of Cx47/Cx30 impaired myelin formation and resulted in thinner myelin

sheaths (Tress et al. 2012; Menichella et al. 2003), therefore downregulation of Cx32/30 in KO mice could explain the observed impairments in myelination. It was also shown that lipid synthesis in astrocytes is required for proper myelination (Camargo et al., 2017) and that cholesterol transfer from astrocytes to oligodendrocytes regulates oligodendrocyte survival and remyelination (Molina-Gonzalez et al., 2023). Since gap junctions allow for metabolite transfer between astrocytes and oligodendrocytes, it is conceivable that the observed impairments in myelination and lipid metabolism in KO animals can be at least partially explained by the downregulation of Cx32 and Cx30. Future studies should address whether impaired coupling between astrocytes and oligodendrocytes is responsible for the observed deficits and if restoring levels of Cx32 in oligodendrocytes and/or Cx30 in astrocytes would improve astrocyte-oligodendrocyte communication and rescue the deficits in oligodendrocyte development and myelination in KO mice.

My study shows for the first time that astrocytes contribute to oligodendrocyte development and myelination through ephrin-B1 signaling. Deletion of astrocytic ephrin-B1 reduced gene expression levels of genes associated with oligodendrocyte development, myelin, and lipid metabolism, led to reduced numbers of oligodendrocytes and reduced levels of myelination, resulting in a clasping phenotype. Future studies can address whether impaired ephrin-B1 expression in astrocytes is associated with demyelinating diseases such as MS. Astrocytic ephrin-B1 may be an important therapeutic target to promote remyelination and oligodendrocyte survival in demyelinating diseases.

REFERENCES FOR CHAPTER THREE

Altevogt BM, Paul DL (2004) Four Classes of Intercellular Channels between Glial Cells in the CNS. The Journal of Neuroscience 24:4313-4323.

Anthony TE, Heintz N (2007) The folate metabolic enzyme ALDH1L1 is restricted to the midline of the early CNS, suggesting a role in human neural tube defects. Journal of Comparative Neurology 500:368-383.

Aparicio GI, Formoso K, León A, Frasch AC, Scorticati C (2020) Identification of Potential Interacting Proteins With the Extracellular Loops of the Neuronal Glycoprotein M6a by TMT/MS. Frontiers in Synaptic Neuroscience 12.

Baumann N, Pham-Dinh D (2001) Biology of Oligodendrocyte and Myelin in the Mammalian Central Nervous System. Physiological Reviews 81:871-927.

Bazargani N, Attwell D (2016) Astrocyte calcium signaling: the third wave. Nature Neuroscience 19:182-189.

Benson MD, Romero MI, Lush ME, Lu QR, Henkemeyer M, Parada LF (2005) Ephrin-B3 is a myelin-based inhibitor of neurite outgrowth. Proceedings of the National Academy of Sciences 102:10694-10699.

Bhaskaran S, Kumar G, Thadathil N, Piekarz KM, Mohammed S, Lopez SD, Qaisar R, Walton D, Brown JL, Murphy A, Smith N, Saunders D, Beckstead MJ, Plafker S, Lewis TL, Towner R, Deepa SS, Richardson A, Axtell RC, Van Remmen H (2023) Neuronal deletion of MnSOD in mice leads to demyelination, inflammation and progressive paralysis that mimics phenotypes associated with progressive multiple sclerosis. Redox Biology 59:102550.

Cahill LS, Zhang MA, Ramaglia V, Whetstone H, Sabbagh MP, Yi TJ, Woo L, Przybycien TS, Moshkova M, Zhao FL, Rojas OL, Gomes J, Kuerten S, Gommerman JL, Sled JG, Dunn SE (2019) Aged hind-limb clasping experimental autoimmune encephalomyelitis models aspects of the neurodegenerative process seen in multiple sclerosis. Proceedings of the National Academy of Sciences 116:22710-22720.

Camargo N, Goudriaan A, van Deijk A-LF, Otte WM, Brouwers JF, Lodder H, Gutmann DH, Nave K-A, Dijkhuizen RM, Mansvelder HD, Chrast R, Smit AB, Verheijen MHG (2017) Oligodendroglial myelination requires astrocyte-derived lipids. PLOS Biology 15:e1002605.

Chatzopoulou E, Ikenaka K, Kagawa T, Lebras B, Lemkine G, Prestoz L, Spassky N, Thomas J-L, Zalc B (2004) Control of axonophilic migration of oligodendrocyte precursor cells by Eph–ephrin interaction. Neuron Glia Biology 1:73-83.

Choi KM, Kim JY, Kim Y (2013) Distribution of the Immunoreactivity for Glycoprotein M6B in the Neurogenic Niche and Reactive Glia in the Injury Penumbra Following Traumatic Brain Injury in Mice. Exp Neurobiol 22:277-282.

Chrast R, Saher G, Nave K-A, Verheijen MHG (2011) Lipid metabolism in myelinating glial cells: lessons from human inherited disorders and mouse models. Journal of Lipid Research 52:419-434.

Clemente D, Ortega MC, Melero-Jerez C, De Castro F (2013) The effect of glia-glia interactions on oligodendrocyte precursor cell biology during development and in demyelinating diseases. Frontiers in Cellular Neuroscience 7.

Coetzee T, Dupree JL, Popko B (1998) Demyelination and altered expression of myelin-associated glycoprotein isoforms in the central nervous system of galactolipid-deficient mice. J Neurosci Res 54:613-622.

Contractor A, Rogers C, Maron C, Henkemeyer M, Swanson GT, Heinemann SF (2002) Trans-synaptic Eph receptor-ephrin signaling in hippocampal mossy fiber LTP. Science 296:1864-1869.

Craig-Schapiro R, Perrin RJ, Roe CM, Xiong C, Carter D, Cairns NJ, Mintun MA, Peskind ER, Li G, Galasko DR, Clark CM, Quinn JF, D'Angelo G, Malone JP, Townsend RR, Morris JC, Fagan AM, Holtzman DM (2010) YKL-40: A Novel Prognostic Fluid Biomarker for Preclinical Alzheimer's Disease. Biological Psychiatry 68:903-912.

Creutz CE, Tomsig JL, Snyder SL, Gautier MC, Skouri F, Beisson J, Cohen J (1998) The copines, a novel class of C2 domain-containing, calcium-dependent, phospholipid-binding proteins conserved from Paramecium to humans. J Biol Chem 273:1393-1402.

Dalva MB, Takasu MA, Lin MZ, Shamah SM, Hu L, Gale NW, Greenberg ME (2000) EphB receptors interact with NMDA receptors and regulate excitatory synapse formation. Cell 103:945-956.

De Robertis E, Gerschenfeld HM, Wald F (1958) Cellular mechanism of myelination in the central nervous system. J Biophys Biochem Cytol 4:651-656.

Eckhardt M (2023) Fatty Acid 2-Hydroxylase and 2-Hydroxylated Sphingolipids: Metabolism and Function in Health and Diseases. Int J Mol Sci 24.

Escartin C et al. (2021) Reactive astrocyte nomenclature, definitions, and future directions. Nat Neurosci 24:312-325.

Ethell IM, Irie F, Kalo MS, Couchman JR, Pasquale EB, Yamaguchi Y (2001) EphB/syndecan-2 signaling in dendritic spine morphogenesis. Neuron 31:1001-1013.

Floro S, Carandini T, Pietroboni AM, De Riz MA, Scarpini E, Galimberti D (2022) Role of Chitinase 3–like 1 as a Biomarker in Multiple Sclerosis. Neurology Neuroimmunology & Neuroinflammation 9:e1164.

Forrest AD, Beggs HE, Reichardt LF, Dupree JL, Colello RJ, Fuss B (2009) Focal adhesion kinase (FAK): A regulator of CNS myelination. Journal of Neuroscience Research 87:3456-3464.

Gard AL, Burrell MR, Pfeiffer SE, Rudge JS, Williams WC, II (1995) Astroglial control of oligodendrocyte survival mediated by PDGF and Leukemia Inhibitory Factor-like protein. Development 121:2187-2197.

Goenaga J, Araque A, Kofuji P, Herrera Moro Chao D (2023) Calcium signaling in astrocytes and gliotransmitter release. Frontiers in Synaptic Neuroscience 15.

Guyenet SJ, Furrer SA, Damian VM, Baughan TD, La Spada AR, Garden GA (2010) A simple composite phenotype scoring system for evaluating mouse models of cerebellar ataxia. J Vis Exp.

Harboe M, Torvund-Jensen J, Kjaer-Sorensen K, Laursen LS (2018) Ephrin-A1-EphA4 signaling negatively regulates myelination in the central nervous system. Glia 66:934-950.

Henkemeyer M, Itkis OS, Ngo M, Hickmott PW, Ethell IM (2003) Multiple EphB receptor tyrosine kinases shape dendritic spines in the hippocampus. Journal of Cell Biology 163:1313-1326.

Ho WY, Hartmann H, Ling S-C (2022) Central nervous system cholesterol metabolism in health and disease. IUBMB Life 74:826-841.

Ishibashi T, Dakin KA, Stevens B, Lee PR, Kozlov SV, Stewart CL, Fields RD (2006) Astrocytes promote myelination in response to electrical impulses. Neuron 49:823-832.

Kamasawa N, Sik A, Morita M, Yasumura T, Davidson KGV, Nagy JI, Rash JE (2005) Connexin-47 and connexin-32 in gap junctions of oligodendrocyte somata, myelin sheaths, paranodal loops and Schmidt-Lanterman incisures: Implications for ionic homeostasis and potassium siphoning. Neuroscience 136:65-86.

Kayser MS, McClelland AC, Hughes EG, Dalva MB (2006) Intracellular and trans-synaptic regulation of glutamatergic synaptogenesis by EphB receptors. J Neurosci 26:12152-12164.

Khakh BS, Deneen B (2019) The Emerging Nature of Astrocyte Diversity. Annu Rev Neurosci 42:187-207.

Kim J, Yoo ID, Lim J, Moon J-S (2024) Pathological phenotypes of astrocytes in Alzheimer's disease. Experimental & Molecular Medicine.

Kleopa KA, Orthmann JL, Enriquez A, Paul DL, Scherer SS (2004) Unique distributions of the gap junction proteins connexin29, connexin32, and connexin47 in oligodendrocytes. Glia 47:346-357.

Kuhn S, Gritti L, Crooks D, Dombrowski Y (2019) Oligodendrocytes in Development, Myelin Generation and Beyond. Cells 8.

Kwak H, Koh W, Kim S, Song K, Shin J-I, Lee JM, Lee EH, Bae JY, Ha GE, Oh J-E (2020) Astrocytes control sensory acuity via tonic inhibition in the thalamus. Neuron 108:691-706. e610.

Lananna BV, McKee CA, King MW, Del-Aguila JL, Dimitry JM, Farias FHG, Nadarajah CJ, Xiong DD, Guo C, Cammack AJ, Elias JA, Zhang J, Cruchaga C, Musiek ES (2020) Chi3l1/YKL-40 is controlled by the astrocyte circadian clock and regulates neuroinflammation and Alzheimer’s disease pathogenesis. Science Translational Medicine 12:eaax3519.

Liddelow SA, Barres BA (2017) Reactive Astrocytes: Production, Function, and Therapeutic Potential. Immunity 46:957-967.

Linneberg C, Harboe M, Laursen LS (2015) Axo-Glia Interaction Preceding CNS Myelination Is Regulated by Bidirectional Eph-Ephrin Signaling. ASN Neuro 7:1759091415602859.

Liu C, Zhao X-M, Wang Q, Du T-T, Zhang M-X, Wang H-Z, Li R-P, Liang K, Gao Y, Zhou S-Y, Xue T, Zhang J-G, Han C-L, Shi L, Zhang L-W, Meng F-G (2023) Astrocyte-derived SerpinA3N promotes neuroinflammation and epileptic seizures by activating the NF-κB signaling pathway in mice with temporal lobe epilepsy. Journal of Neuroinflammation 20:161.

Ma X, Niu X, Zhao J, Deng Z, Li J, Wu X, Wang B, Zhang M, Zhao Y, Guo X, Sun P, Huang T, Wang J, Song J (2022) Downregulation of Sepina3n Aggravated Blood–Brain Barrier Disruption after Traumatic Brain Injury by Activating Neutrophil Elastase in Mice. Neuroscience 503:45-57.

Maldonado EN, Alderson NL, Monje PV, Wood PM, Hama H (2008) FA2H is responsible for the formation of 2-hydroxy galactolipids in peripheral nervous system myelin<sup>s⃞</sup>. Journal of Lipid Research 49:153-161.

Marcus J, Dupree JL, Popko B (2000) Effects of galactolipid elimination on oligodendrocyte development and myelination. Glia 30:319-328.

Moeller ML, Shi Y, Reichardt LF, Ethell IM (2006) EphB receptors regulate dendritic spine morphogenesis through the recruitment/phosphorylation of focal adhesion kinase and RhoA activation. J Biol Chem 281:1587-1598.

Molina-Gonzalez I et al. (2023) Astrocyte-oligodendrocyte interaction regulates central nervous system regeneration. Nature Communications 14:3372.

Mukobata S, Hibino T, Sugiyama A, Urano Y, Inatomi A, Kanai Y, Endo H, Tashiro F (2002) M6a acts as a nerve growth factor-gated Ca2+ channel in neuronal differentiation. Biochemical and Biophysical Research Communications 297:722-728.

Nguyen AQ, Sutley S, Koeppen J, Mina K, Woodruff S, Hanna S, Vengala A, Hickmott PW, Obenaus A, Ethell IM (2020) Astrocytic Ephrin-B1 Controls Excitatory-Inhibitory Balance in Developing Hippocampus. The Journal of Neuroscience 40:6854-6871.

Norton ES, Da Mesquita S, Guerrero-Cazares H (2021) SERPINA3 in glioblastoma and Alzheimer's disease. Aging (Albany NY) 13:21812-21813.

Petryniak MA, Potter GB, Rowitch DH, Rubenstein JLR (2007) Dlx1 and Dlx2 Control Neuronal versus Oligodendroglial Cell Fate Acquisition in the Developing Forebrain. Neuron 55:417-433.

Poitelon Y, Kopec AM, Belin S (2020) Myelin Fat Facts: An Overview of Lipids and Fatty Acid Metabolism. Cells 9.

Pozniak CD, Langseth AJ, Dijkgraaf GJ, Choe Y, Werb Z, Pleasure SJ (2010) Sox10 directs neural stem cells toward the oligodendrocyte lineage by decreasing Suppressor of Fused expression. Proc Natl Acad Sci U S A 107:21795-21800.

Raff MC, Lillien LE, Richardson WD, Burne JF, Noble MD (1988) Platelet-derived growth factor from astrocytes drives the clock that times oligodendrocyte development in culture. Nature 333:562-565.

Richardson WD, Pringle N, Mosley MJ, Westermark B, Dubois-Dalcg M (1988) A role for platelet-derived growth factor in normal gliogenesis in the central nervous system. Cell 53:309-319.

Rose CR, Ziemens D, Verkhratsky A (2020) On the special role of NCX in astrocytes: Translating Na+-transients into intracellular Ca2+ signals. Cell Calcium 86:102154.

Schnitzer J, Franke WW, Schachner M (1981) Immunocytochemical demonstration of vimentin in astrocytes and ependymal cells of developing and adult mouse nervous system. J Cell Biol 90:435-447.

Sloniowski S, Ethell IM (2012) Looking forward to EphB signaling in synapses. Semin Cell Dev Biol 23:75-82.

Stadelmann C, Timmler S, Barrantes-Freer A, Simons M (2019) Myelin in the Central Nervous System: Structure, Function, and Pathology. Physiological Reviews 99:1381-1431.

Stamou M, Grodzki AC, van Oostrum M, Wollscheid B, Lein PJ (2018) Fc gamma receptors are expressed in the developing rat brain and activate downstream signaling molecules upon cross-linking with immune complex. J Neuroinflammation 15:7.

Stolt CC, Rehberg S, Ader M, Lommes P, Riethmacher D, Schachner M, Bartsch U, Wegner M (2002) Terminal differentiation of myelin-forming oligodendrocytes depends on the transcription factor Sox10. Genes Dev 16:165-170.

Syed YA, Zhao C, Mahad D, Möbius W, Altmann F, Foss F, Sentürk A, Acker-Palmer A, Lubec G, Lilley K, Franklin RJM, Nave K-A, Kotter MRN (2016) Antibody-mediated neutralization of myelin-associated EphrinB3 accelerates CNS remyelination. Acta Neuropathologica 131:281-298.

Zhang Y, Chen Q, Chen D, Zhao W, Wang H, Yang M, Xiang Z, Yuan H (2022) SerpinA3N attenuates ischemic stroke injury by reducing apoptosis and neuroinflammation. CNS Neuroscience & Therapeutics 28:566-579.

Zhao T, Su Z, Li Y, Zhang X, You Q (2020) Chitinase-3 like-protein-1 function and its role in diseases. Signal Transduction and Targeted Therapy 5:201.

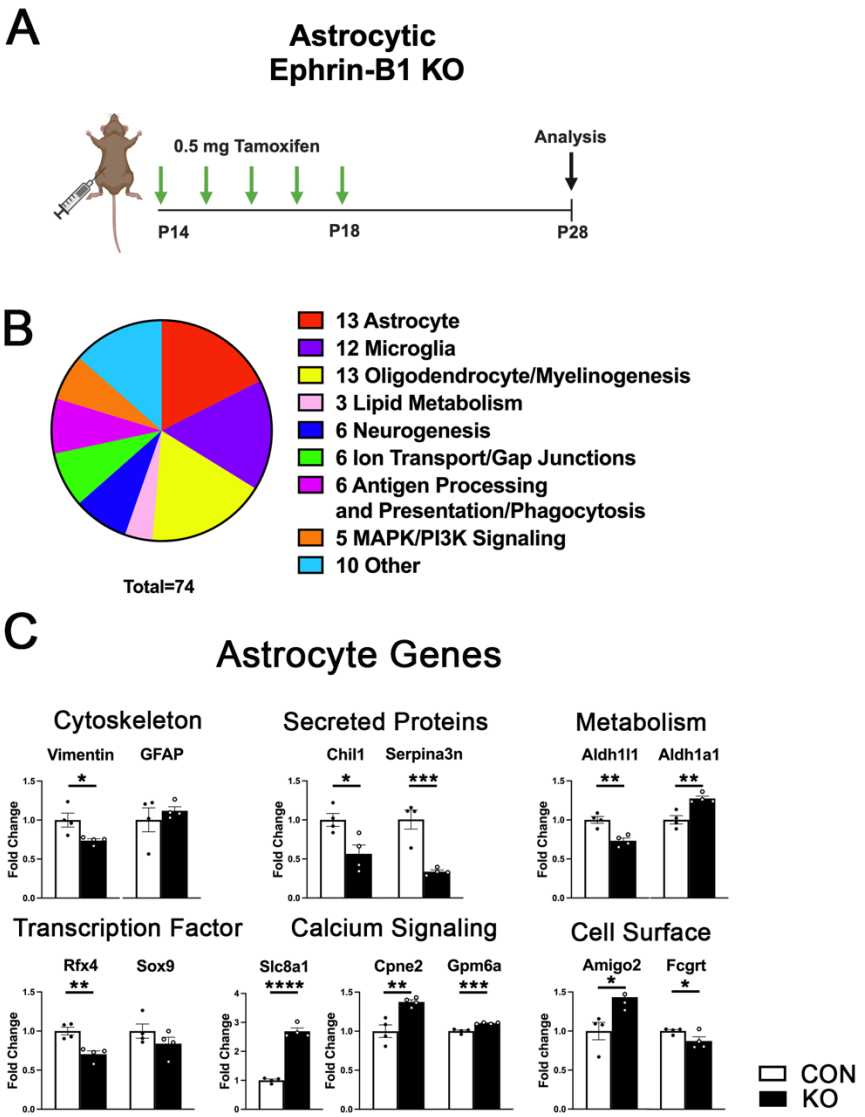
A
Astrocytic
Ephrin-B1 KO
0.5 mg Tamoxifen
Analysis
P14
P18
P28
B
13 Astrocyte
12 Microglia
13 Oligodendrocyte/Myelinogenesis
3 Lipid Metabolism
6 Neurogenesis
6 Ion Transport/Gap Junctions
6 Antigen Processing
and Presentation/Phagocytosis
5 MAPK/PI3K Signaling
10 Other
Total=74
C
Astrocyte Genes
Cytoskeleton
Vimentin
GFAP
Secreted Proteins
Chil1
Serpina3n
Metabolism
Aldh1l1
Aldh1a1
Transcription Factor
Rfx4
Sox9
Calcium Signaling
Slc8a1
Cpne2
Gpm6a
Cell Surface
Amigo2
Fcgrt
Fold Change
CON
KO

**Figure 3.1: Deletion of astrocytic ephrin-B1 alters astrocyte-associated gene expression.** A) Graphic depicts the astrocyte specific ephrin-B1 knockout (KO) model and experimental timeline. B) Graph shows the number of differentially expressed genes by category. Glial genes including astrocytes, oligodendrocytes, and microglia as well as myelin and lipid metabolism associated genes showed many significant differences following deletion of astrocytic ephrin-B1 KO. C) Graphs show mRNA levels astrocyte-associated genes which were differentially expressed following astrocytic ephrin-B1 KO (n=4 mice/group t-test, *$p<0.05$, **$p<0.01$, ***$p<0.001$).

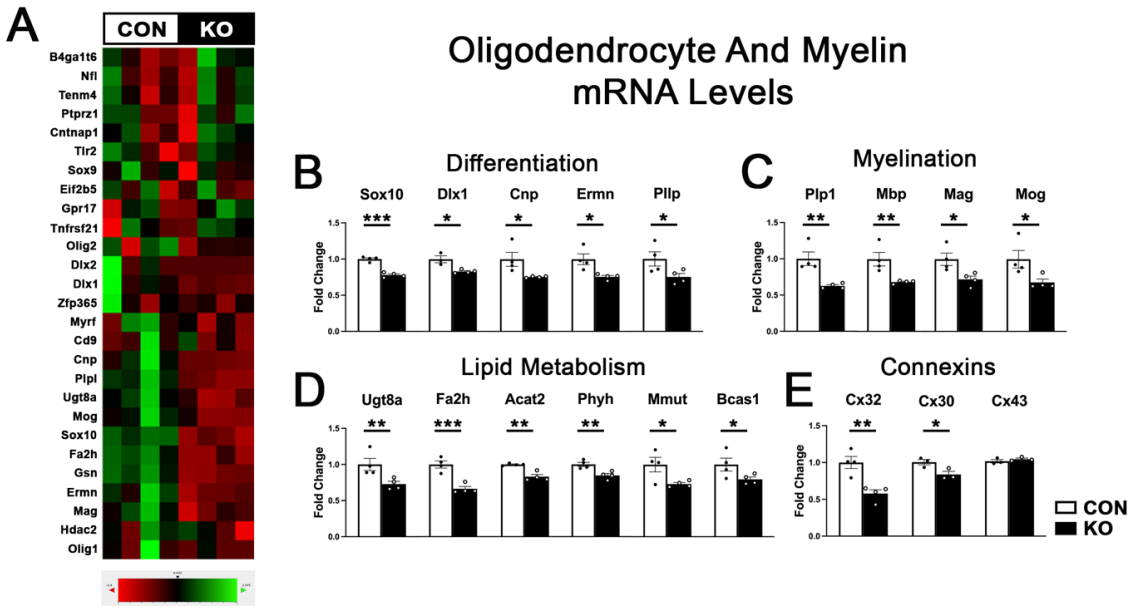


**Figure 3.2: Astrocytic ephrin-B1 KO impairs gene expression of oligodendrocyte- and myelin-associated genes. A)** Heatmap of gene expression of oligodendrocyte-associated genes in control (CON) and KO animals, generated from Nanostring gene expression analysis. **B)** Graphs show mRNA levels of genes associated with oligodendrocyte differentiation in CON and KO animals (n=3-4 mice/group, *p<0.05, ****p<0.0001). KO mice showed significant reductions in many oligodendrocyte related genes. **C)** Graphs show mRNA levels of myelin associated genes in CON and KO animals (n=4 mice/group, *p<0.05, **p<0.01). Myelin-associated gene expression was significantly reduced in KO animals. **D)** Graphs show mRNA levels of genes associated with lipid metabolism in CON and KO animals (n=4 mice/group t-test, *p<0.05, **p<0.01). Genes associated with lipid metabolism were also reduced following astrocytic ephrin-B1 KO. **E)** Graph shows mRNA expression of connexin genes, in CON and KO animals (n=3-4 mice/group t-test, **p<0.01). All data are represented as mean ± SEM.

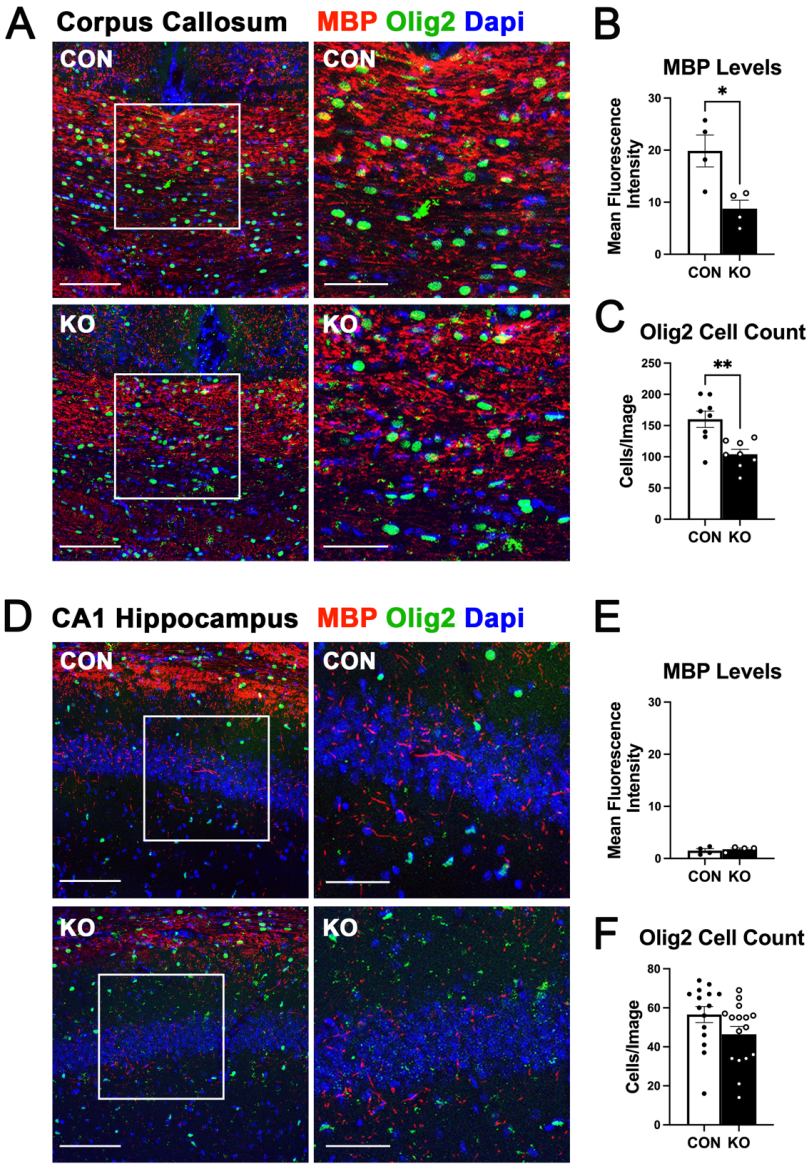
A
Corpus Callosum
MBP Olig2 Dapi
CON
CON
KO
KO
B
MBP Levels
Mean Fluorescence Intensity
30
20
10
0
*
CON KO
C
Olig2 Cell Count
Cells/Image
250
200
150
100
50
0
**
CON KO
D
CA1 Hippocampus
MBP Olig2 Dapi
CON
CON
KO
KO
E
MBP Levels
Mean Fluorescence Intensity
30
20
10
0
CON KO
F
Olig2 Cell Count
Cells/Image
80
60
40
20
0
CON KO

**Figure 3.3: Loss of astrocytic ephrin-B1 impaired myelination and reduced the number of oligodendrocytes in the corpus callosum but not the hippocampus. A)** Confocal images of brain slices showing MBP (red), Olig2 (green), and Dapi (blue) immunolabeling in the corpus callosum of CON and KO mice. Scale bar, 100 μm (left) or 50 μm (right). **B)** Graph shows the mean fluorescence intensity of MBP in the corpus callosum. KO mice showed reduced intensity of MBP compared to controls (n=4 mice per group, 8 images per group, t-test, *$p<0.05$). **C)** Graph shows the average number of Olig2+ oligodendrocytes per image of the corpus callosum of CON and KO mice. The number of Olig2+ oligodendrocytes was reduced in KO mice compared to CON (n=4 mice per group, 8 images per group, t-test, **$p<0.001$). **D)** Confocal images of brain slices depicting MBP (red), Olig2 (green), and Dapi (blue) immunolabeling in the CA1 hippocampus of CON and KO mice. Scale bar, 100 μm (left) or 50 μm (right). **E)** Graph shows the mean fluorescence intensity of MBP in the CA1 hippocampus. MBP intensity levels were unchanged in KO mice compared to controls (n=4 mice per group, 16 images per group, t-test). **F)** Graph shows the average number of Olig2+ oligodendrocytes per image of the CA1 hippocampus of CON and KO mice. There was a non-significant trend towards a reduced density of Olig2+ oligodendrocytes in KO hippocampi compared to control hippocampi (n=4 mice per group, 15-16 images per group, t-test, $p= 0.0883$). All data are represented as mean ± SEM.

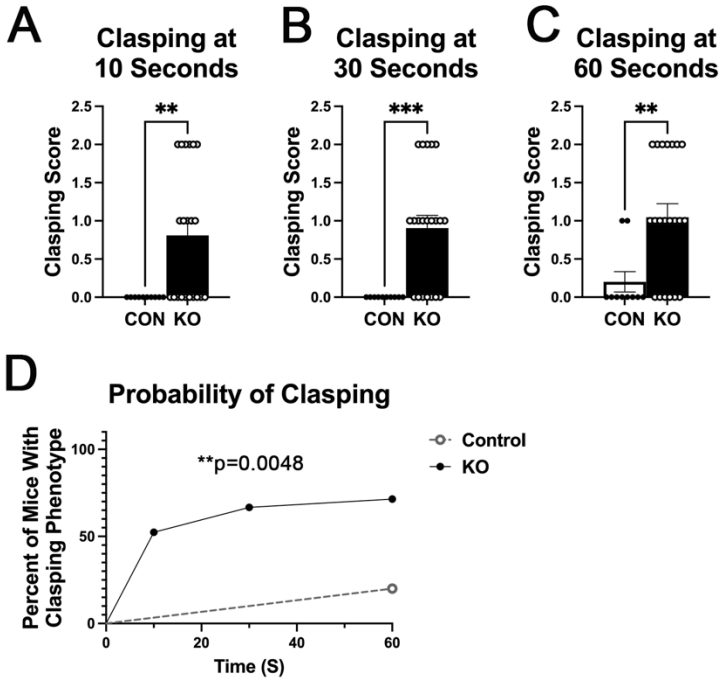


**Figure 3.4: Astrocytic ephrin-B1 KO mice show a clasping phenotype. A)** Graph shows the mean clasping score at time (t)=10 s during the clasping test (n=10-21 mice per group, Mann-Whitney test, **p<0.001). **B)** Graph shows the mean clasping score at t=30 s during the clasping test (n=10-21 mice per group, Mann-Whitney test, ***p<0.0001). **C)** Graph shows the mean clasping score at time (t)=60 s during the clasping test (n=10-21 mice per group, Mann-Whitney test, **p<0.001). KO mice exhibit a significant increase in the clasping phenotype at all three time points assessed compared to CON. **D)** Graph shows the probability of developing a clasping phenotype over the course of the test. KO mice exhibited a significantly increased chance of developing a clasping phenotype over the course of the test compared to CON mice (n=10-21 mice per group, Log-rank test, **p<0.001).

Supplemental Materials for Chapter Three

| Gene | Forward Primer | Reverse Primer |
|---|---|---|
| Connexin 43 (Gja1) | 5′-GTGCCGGCTTCACTTTCATT-3′ | 5′-CGTGGAGTAGGCTTGGACCTT-3′ |
| Connexin 30 (Gjb6) | 5′-GCAGAGGGATTTTGCAGTGACT-3′ | 5′- TGTTCACGCCACCGATGA-3′ |

**Supplemental Table S3.1: Primers sequences used for qRT-PCR analysis.**

# CHAPTER FOUR

## Conclusions and Future Directions

The work in this dissertation defines a novel mechanism by which astrocytes regulate PV inhibitory synapse development in the CA1 hippocampus and identifies EphB as a negative regulator of PV->PC connectivity during development. Additionally, a newfound role for astrocytic ephrin-B1 in oligodendrocyte development and myelination was discovered. In chapter two, I identified that astrocytic ephrin-B1 positively regulates the establishment of both structural and functional connections between PV and PC cells. Overexpression of ephrin-B1 in hippocampal astrocytes during the P14-P28 developmental period using AAV viral vector delivery approach enhanced the magnitude of the postsynaptic responses at PV->PC synapses and enhanced the number of PV presynaptic sites in the SP layer of the hippocampus. Developmental deletion of astrocytic ephrin-B1 reduced the number of structural PV presynaptic sites in the same area and analysis of PV synapse number on specific compartments of PCs revealed that perisomatic inhibitory synapses and synapses on SO dendrites were specifically reduced. Furthermore, I determined that these effects were specific to PV->PC synapses as deletion of astrocytic ephrin-B1 did not affect CCK->PC connectivity. Decreased innervation of PCs by PV interneurons led to impaired inhibition in vivo as evidenced by an increased susceptibility to PTZ induced seizure and behavioral changes in KO mice.

I determined that astrocytic ephrin-B1 controls PV->PC connectivity through regulating its receptor, EphB, in PV boutons but not in PV somata. First, I found that overexpression of astrocytic ephrin-B1 reduced the localization of EphB in PV boutons, but deletion increased the localization of the EphB receptor to PV boutons. Interestingly,

the localization of EphB within PV somata was not affected by levels of astrocytic ephrin-B1. Because the levels of EphB receptor within PV boutons seemed to be inversely correlated with levels of PV->PC innervation, I hypothesized that EphB in PV boutons negatively regulates the establishment of PV->PC connections. To confirm this hypothesis, a mouse model where EphB2 was deleted specifically in PV expressing interneurons was generated. I found that removal of EphB2 from PV boutons was indeed sufficient to boost the levels of PV->PC structural and functional connectivity. I also found that removal of EphB2 increased the expression of PV in PV interneurons, suggesting that EphB2 deletion enhanced PV interneuron maturation or activity.

To determine if astrocytic ephrin-B1 does indeed regulate PV->PC connectivity through manipulating the levels of EphB receptor in PV boutons, I overexpressed astrocytic ephrin-B1 in mice lacking EphB2 in PV interneurons, which I expected would not lead to further enhancement of PV->PC connectivity if my hypothesis was correct. In line with my hypothesis, I found that overexpression of astrocytic ephrin-B1 in mice lacking EphB2 in PV interneurons did not increase PV->PC structural or functional connectivity. Overall, the findings are consistent with my hypothesis that astrocytic ephrin-B1 facilitates the formation of PV->PC connections through negatively regulating the localization of the EphB receptor within PV boutons. Therefore, the findings reported in this dissertation elucidate a novel mechanism by which astrocytes regulate the establishment of PV->PC synapses and present a unique finding that EphB receptors are involved in establishing inhibitory connections through providing a repulsive interaction that limits inhibitory synapse number.

In this study, I analyzed PV structural synapses using PV/VGAT staining adjacent to excitatory cell somata and proximal dendrites in the SO, allowing me to quantify perisomatic structural synapses by presumed PV basket cells. I also analyzed PV presynaptic sites in the SP using PV/VGAT staining. This analysis was used to quantify perisomatic innervation but likely also captured some innervation on the axon initial segment (AIS) of PCs by PV expressing chandelier cells. Future studies should address whether astrocytic ephrin-B1 regulates both perisomatic and AIS innervation. Furthermore, PV expression is activity dependent and therefore my findings may reflect changes in the expression of PV and not necessarily changes in PV synapses. Future work may try to parse out these differences using alternative strategies to label PV interneurons or synapses such as using Syt-2 immunostaining to identify PV presynaptic sites.

In addition, our studies thus far have only investigated the effects of astrocytic ephrin-B1 on inhibitory postsynaptic responses but have not investigated the effects on PV interneuron physiology. Future studies may analyze the excitability, connectivity, and intrinsic properties of PV interneurons following overexpression of astrocytic ephrin-B1 or deletion of EphB2 in PV interneurons using whole cell recordings of PV cells to determine if these manipulations also affect PV interneuron physiology. Additionally, I observed a trend towards enhanced oeIPSC amplitudes in astrocytic ephrin-B1 OE mice lacking EphB2 in PV interneurons, which suggests that other EphB receptors besides EphB2 might play a role in PV->PC functional connectivity. Future studies should examine the role of other EphB receptors, particularly EphB1 receptor, in PV->PC

connectivity. Finally, as EphB2 has been identified as a candidate risk gene for ASD, and I observed that deletion of astrocytic ephrin-B1 increased susceptibility to seizures and resulted in behavioral phenotypes reminiscent of ASD phenotypes, future studies can address whether aberrant EphB2 signaling in PV interneurons underlies the development of pathological ASD phenotypes or drives neuronal hyperexcitability in other NDDs such as schizophrenia or epilepsy.

In chapter three, I used Nanostring gene expression analysis to analyze hippocampal gene expression changes following developmental deletion of astrocytic ephrin-B1. I identified several genes enriched in astrocytes which were dysregulated, including genes associated with calcium signaling in astrocytes, astrocyte-secreted proteins, astrocyte metabolism, transcription factors, and cell surface proteins. This was the first analysis of hippocampal gene expression changes following developmental deletion of astrocytic ephrin-B1, and therefore this screen elucidated biological processes in astrocytes which may be regulated by astrocytic ephrin-B1 signaling. My screen seems to suggest that astrocytes may sense and respond to their environment differently following loss of ephrin-B1, as genes associated with calcium signaling, cell surface proteins, and secreted proteins were affected. Future work should address whether deletion of astrocytic ephrin-B1 impairs astrocyte calcium signaling or release of secreted proteins or gliotransmitters. Furthermore, an analysis of the astrocyte specific transcriptional profile following deletion and/or overexpression of astrocytic ephrin-B1, perhaps using single cell sequencing, would improve the granularity of my study and allow us to identify astrocyte gene expression changes more specifically.

I also made the unexpected discovery that many genes associated with oligodendrocyte development, myelination, and lipid metabolism were broadly downregulated in mice lacking astrocytic ephrin-B1. Using immunofluorescence staining, I confirmed that MBP immunofluorescence intensity was reduced in the CC of KO mice. I also found that there were reduced numbers of Olig2 positive oligodendrocytes in the CC of KO mice, confirming that the gene expression changes were maintained at the protein level in vivo. However, I did not detect differences in MBP in the hippocampus, although there was a trend towards reduced numbers of oligodendrocytes in the hippocampus of KO mice. Deficiencies in myelination and oligodendrocyte development in the CC led to the development of a clasping phenotype in KO mice.

Future work should determine the mechanism leading to deficits in myelination and oligodendrocyte development in KO mice. I hypothesize that the differences are likely due to impaired astrocyte-oligodendrocyte communication as I detected reduced levels of both Cx32 and Cx30 in KO mice. Future work should test whether impairments in astrocyte-oligodendrocyte coupling exist in KO mice and if they are responsible for the observed deficits in myelination and oligodendrocyte development. Additionally, it should be tested if restoring Cx32/Cx30 levels in KO mice can rescue the observed phenotypes.

In summary, the work in this dissertation highlights the critical role of astrocytic ephrin-B1 in regulating both glial-glial and glial-neuronal interactions during development. First, I elucidated a novel mechanism by which astrocytes regulate the establishment of PV->PC connections. My work shows that EphB2 expression in PV

interneurons adversely affects inhibitory synapse development, and astrocytic ephrin-B1 positively regulates the establishment of PV->PC connections by interfering with EphB receptor signaling in PV boutons. As impaired inhibition is suggested to underlie the development of neuronal hyperactivity in NDDS and EphB2 receptor itself is also implicated in the pathogenesis of ASD, my work not only addresses critical gaps in our understanding, but also possesses clinical relevance as ephrin-B/EphB2 signaling in PV interneurons may be a promising therapeutic target to correct inhibitory circuit dysfunction in NDDs. Next, I demonstrated for the first time that astrocytes contribute to oligodendrocyte development and myelination through ephrin-B1 signaling. These findings suggest that astrocytic ephrin-B1 may be a novel therapeutic target to promote remyelination and oligodendrocyte survival in demyelinating diseases. Taken together, the role of ephrin-B1 signaling in astrocytes seems to be as diverse as the functions of astrocytes themselves, and investigation into the effects of astrocytic ephrin-B1 signaling presents exciting opportunities for developing therapeutics for a wide range of neurodevelopmental diseases.